THE CORRELATION OF ACOUSTIC EMISSION WITH FRACTURE MECHANICS PARAMETERS IN STRUCTURAL STEELS

by

DAVID MATTHEW DELONGA; ENSIGN, USN

B.S., United States Naval Academy
(1980)

SUBMITTED IN PARTIAL FULFILLMENT
OF THE REQUIREMENTS FOR THE
DEGREE OF

MASTER OF SCIENCE IN
MECHANICAL ENGINEERING

at the

MASSACHUSETTS INSTITUTE OF TECHNOLOGY

May 1981

Signature of Author . . . . . .
Department of Mechanical Engineering, May 8, 1981

Certified by. . . . . .
Thesis Supervisor

Accepted by . . . . . .
Chairman, Department Committee on Graduate Students

THE CORRELATION OF ACOUSTIC EMISSION WITH FRACTURE MECHANICS PARAMETERS IN STRUCTURAL STEELS

by

DAVID MATTHEW DELONGA; ENSIGN, USN

Submitted to the Department of Mechanical Engineering on May 8, 1981, in partial fulfillment of the requirements for the Degree of Master of Science of Mechanical Engineering.

ABSTRACT

Experimental investigations of acoustic emission (AE) in A36, A514, and A588 structural steel specimens subjected to tension-tension fatigue are conducted. Literature of previous experimental tests is reviewed and discussed. Both qualitative and quantitative observations on the relationship between acoustic emission parameters and fracture mechanics parameters are made.

Higher maximum stress intensity values result in greater values of [parameter] per loading cycle data at low crack growth rates. Shorter initial crack length results in higher values of [parameter] per loading cycle data at low crack growth rates than longer initial crack length for A514. There is no effect of crack length for A588 throughout the entire range of growth rates. A power relationship exists between crack growth rate and [parameter] per loading cycle data for all stress intensity values, initial crack lengths, and steel types. Specimens made from higher strength steels result in higher [parameter] per loading cycle values at higher stress intensity factors, whereas steel strength loses its effect at lower stress intensity factors.

Changes in maximum stress intensity factor, crack growth rate, initial crack length, or material type do not appear to significantly affect the mean [parameter] per event data. This implies that the characteristics of the events detected are independent of loading conditions and material type.

The data obtained from this investigation are not satisfactorily predicted by quantitative relationships suggested by previous experiments. Therefore, a correlating relationship of the following form is proposed:

$$\dot{N} \alpha \dot{a}^{n}$$

where $\dot{N}$ is the AE ringdown counts per loading cycle, $\dot{a}$ is the crack growth rate per loading cycle, and the exponent n is a function of the maximum stress intensity factor, the crack length and the yield strength. Recommendations are offered to assist future experimentation in the area of acoustic emission/fracture mechanics parameter correlation.

Thesis Supervisor: James H. Williams, Jr.

Title: Associate Professor of Mechanical Engineering

ACKNOWLEDGEMENTS

I dedicate this document to my parents who encourage and support me in all my endeavors.

In preparation of this document, I would like to acknowledge my appreciation to the following:

- Professor James H. Williams, Jr., my advisor, for his guidance, encouragement, and support.
- Dr. Samson S. Lee, for his humorous recommendations and technical assistance.
- My friends in the NDE lab: Hursit, Hira, Ray, Betty, Elizabeth, and Beth, for their constant encouragement and help.
- Laurie, my assistant, for her cheerful devotion.
- Bonnie, for her excellent typing of this manuscript.

Finally, the United States Navy and the National Science Foundation are gratefully acknowledged for their financial support of my graduate education at the Massachusetts Institute of Technology.

TABLE OF CONTENTS

TABLE OF CONTENTS (CONT'D)

TABLE OF CONTENTS (CONT'D)

LIST OF TABLES

LIST OF FIGURES

LIST OF FIGURES (CONT'D)

LIST OF FIGURES (CONT'D)

LIST OF FIGURES (CONT'D)

INTRODUCTION

Acoustic emission (AE) refers to the release of elastic strain energy which occurs when a material is dynamically deformed or fractured. This phenomenon has been studied with increasing interest since 1950, when the first serious investigation was made by Kaiser [1].

Current interest is centered on the use of acoustic emission as a nondestructive evaluation tool, both in metals and nonmetals. One goal of AE testing is the development of correlations between acoustic emission signal parameters and fracture mechanics parameters. A sampling of experimental correlation attempts is provided here to assess the general experimental techniques used and to illustrate the capabilities and limitations of acoustic emission in the study of fracture mechanics.

After examining the previous experimental work, an attempt is made to simplify the correlation process by selecting and comparing independent acoustic emission parameters with independent fracture mechanics parameters. Experiments are then devised to evaluate the effect of each independent fracture mechanics parameter on the acoustic emission signal obtained from a growing fatigue crack.

Compact test specimens are fabricated from plates of common structural bridge steels: A36, A514, and A588. Cyclic loads are then applied to propagate a fatigue crack at different growth rates. The resulting acoustic emission signals are detected and

processed using a state-of-the-art computerized acoustic emission system.

The acoustic emission data are then analyzed in an effort to find correlations with the known fracture mechanics parameters of each test. These correlations are discussed, followed by recommendations to guide further experimental work in this area.

CHARACTERIZATION OF THE ACOUSTIC EMISSION SIGNAL

A typical acoustic emission (AE) signal is depicted in Fig. 1. The parameters shown are often labeled in different ways in the literature. A definition for each term as used in this investigation is given below, as well as synonymous terms from other reported experimental work.

AE Event

An acoustic emission event begins with the first crossing of the voltage threshold (set by the experimenter) by the monitored acoustic emission signal. The event is completed when the signal falls below the threshold for a specified time period. This specified time is known as the "dead time" period and is set by the experimenter, within equipment limits.

AE Ringdown Counts (counts, stress wave emissions, N)

The number of ringdown counts corresponds to the number of times the individual oscillations in the monitored signal cross the voltage threshold.

Peak Amplitude

The peak amplitude is the maximum amplitude attained by the signal during an event.

Event Duration

Event duration is the time from the initial threshold crossing to the final threshold crossing of an event.

Rise Time

Rise time is the time from the beginning of an event to the peak amplitude.

Slope

Slope is the peak amplitude divided by the rise time.

These parameters are further specified by the terms "cumulative or summation of [parameter]" or "mean [parameter] per event". Cumulative or summation of ringdown counts, for example, is a total of all ringdown counts detected from the beginning of an experimental test to a specified time. Mean ringdown counts per event indicates the averaged number of ringdown counts in the events of a test.

It should be understood that the waveform shown in Fig. 1 is obtained from the output of the acoustic emission sensing device. The sensor is usually a resonant piezoelectric transducer which emits a decaying voltage signal (at its own resonant frequency) after being excited by a small physical disturbance. Thus, the actual acoustic emission signal generated within a specimen will in general be quite different from the signal displayed by the detection system.

LITERATURE REVIEW OF ACOUSTIC EMISSION-FRACTURE MECHANICS CORRELATION ATTEMPTS

Several experiments have been performed in an attempt to determine correlations between acoustic emission parameters and fracture mechanics parameters. The "cumulative ringdown counts" and "ringdown counts per loading cycle" acoustic emission parameters were the most commonly used in these correlation attempts.

This review consists of sections that each correspond to a fracture mechanics parameter. Relevant experiments are summarized and critiqued within each section. This review is limited to the acoustic emission fracture mechanical studies of metals, and as such is not concerned with AE or fracture mechanics, in general, or with the AE of nonmetallic materials.

CRACK LENGTH

Vainberg, Susedov, and Kushnir [2] sought to find a practical experimental method of using acoustic emission to characterize a growing fatigue crack. The results obtained are shown in Fig. 2. Cumulative ringdown counts appear to vary linearly with the crack length. No theoretical justification was offered for this relationship.

Bailey, Hamilton, and Pless [3] conducted experiments to attempt to correlate cumulative ringdown counts with crack length.

The results are shown in Fig. 3. Note the excellent correlation between cumulative ringdown counts and crack length. No theoretical explanations were offered in this study.

Harris and Dunegan [4] performed experiments to explore the relationship between crack length and cumulative ringdown counts. The results of this experiment for an aluminum specimen are shown in Fig. 4. There is a linear relationship between crack length and total ringdown counts, but the proportionality constant changes with the range of crack length considered. The explanation offered was that a plane stress-plane strain transition occurred which caused a change in the acoustic emission signal. The authors also mentioned that no effect of loading frequency could be detected in the acoustic emission data. A theoretical model was proposed and compared with the empirical data.

Ying [5] proposed a dislocation model as a possible mechanism for acoustic emission. This model was used to suggest a possible correlation between cumulative events and crack length in a flawed specimen, and was then applied to experimental data. Fig. 5 shows that the proposed model accurately predicted the acoustic emission data obtained at different load levels. The cumulative ringdown count is some function of crack length, rather than being directly proportional as reported in studies previously discussed. This may be due to differences in the loading characteristics, which are not clearly stated in many experimental reports.

CRACK GROWTH RATE

Morton, Harrington, and Bjeletich [6] conducted tests to investigate the relationship between crack growth rate and the resulting acoustic emission signal. The relationship obtained between the number of ringdown counts per loading cycle and crack growth rate is shown in Fig. 6. A short theoretical justification was provided that successfully predicted the outcome of the experiment.

CRACK OPENING DISPLACEMENT

Hartbower, Morais, Reuter, and Crimmins [7] conducted acoustic emission tests to assess the characteristics of crack opening displacement in fatigue cracks. The results are shown in Fig. 7. Note the good correlation between crack opening displacement and the number of ringdown counts per loading cycle. No theoretical model was proposed in this paper.

Palmer, Brindley, and Harrison [8] conducted similar experiments using the cumulative ringdown counts parameter. Fig. 8 is a plot of cumulative ringdown counts versus crack opening displacement for a single loading cycle. There appears to be an excellent correlation between these two parameters. A theoretical derivation was performed to aid in the interpretation of results.

Arii, Kashiwaya, and Yanuki [9] found a power law relationship between cumulative ringdown counts and crack opening displacement. The exponent in this power relation varied with the range of crack opening displacement considered. Fig. 9 illustrates the results for a medium strength steel specimen. No theoretical explanation was given.

STRESS INTENSITY FACTOR

A paper by Hartbower, Morais, Reuter, and Crimmins [7] sought to determine the effect of stress intensity factor on acoustic emission. A linear relationship was found between cumulative ringdown counts and the maximum stress intensity factor, as shown in Fig. 10.

Dunegan, Harris, and Tetelman [10] conducted tests which attempted to verify that the cumulative ringdown count is proportional to the stress intensity factor raised to some exponent. Fig. 11 illustrates the results obtained from plotting cumulative ringdown counts versus stress intensity factor in a log-log format. The slope of this curve thus gives the value of the exponent in the proposed equation. A theoretical model was derived which attempted to predict the value of the exponent.

RANGE OF STRESS INTENSITY FACTOR

Lindley, Palmer and Richards [11] conducted experiments to attempt to establish a correlation between the number of ringdown counts per loading cycle and the range of stress intensity factor applied to the specimen. The results for a low carbon steel specimen are shown in Fig. 12. There appears to be a power law relationship between the number of ringdown counts per loading cycle and the range of stress intensity factor. A theoretical model was also provided to explain these results.

PLASTIC ZONE SIZE

Palmer and Heald [12] suggested that the cumulative ringdown counts may be proportional to the area of the elastic-plastic boundary ahead of the crack. Their theoretical derivation which related cumulative ringdown counts to plastic zone size (via load level) predicted the empirical results quite accurately, as shown in Fig. 13.

SUMMARY OF LITERATURE REVIEW

Theoretical relationships proposed in the experimental reports discussed here have been of two general types: (1) AE ringdown counts proportional to some aspect of the plastic zone, or (2) AE ringdown counts proportional to the strain energy release that occurs during crack propagation.

Theories that cite the plastic zone usually state that the AE originates within the deformed region itself, perhaps by dislocation motion [5, 6, 8, 10, 11]. A closely related concept is that the AE originates in the elastic-plastic boundary of the plastic zone [12].

The strain energy release theories attempt to explain emissions that are thought to originate from the actual cracking of the material [4, 11]. One paper suggests that both the plastic zone and the cracking material contribute to AE [11].

Fracture mechanics relationships for plastic zone size and strain energy release rate can be used to compare the two models. Both are proportional to the square of the maximum stress intensity factor. The plastic zone size is a function of material yield strength, however, whereas the strain energy release rate is not. Empirical results have been obtained that at least partially justify each theory. Other results, however, suggest that neither of these theories applies. Future investigation into the origin

of AE should serve to clarify the present ambiguity.

Material, specimen type, sensor and filters used, couplant, sensor location, gain, threshold, acoustic emission monitoring equipment, loading apparatus, crack length measurement system, loading characteristics, noise reduction techniques, and theoretical model assumed for each experimental report covered in the literature review are given in Table 1. Note that several of the reports were incomplete in the information provided.

Table 2 is a summary of the correlation results obtained from these experiments, grouped by fracture mechanics parameters. By using fracture mechanics expressions, it is possible to condense these relationships into four independent expressions. These expressions are given in Table 3.

PROBLEMS IN THE INTERPRETATION OF ACOUSTIC EMISSION SIGNALS

The rather inconclusive and sometimes contradictory results reported in acoustic emission, in part, stem from the many problems that exist in interpreting the acoustic emission signal. Complications exist from the generation stage to the detection and display stages of the stress wave. Better theoretical models, more sophisticated equipment, and standardization of experimental reporting may someday eliminate many of the present difficulties.

Several mechanisms have been proposed to explain the sudden redistribution in stress which causes the acoustic emission signal. Crack nucleation, crack propagation, plastic deformation, and phase transformations are all possibilities [13]. There are also mechanical sources of acoustic emission such as grip noise, machine noise, fretting, crack closure, and bubble formation (in corrosion) which may mask or confuse the actual generation mechanisms. Many experimenters merely assume that the acoustic emission signal is generated from a sudden square wave. The ability to accurately describe the actual emission would aid in the interpretation of the processed signal.

Specimen characteristics can also create difficulties in acoustic emission experiments. The geometry of a body may cause multiple reflections of the stress wave before it is detected by

the transducer. A large part of the wave energy may be absorbed in mechanical resonances of the specimen [14]. The attenuation characteristics of the specimen are obviously important. Studies show that in a given material, losses due to scattering increase rapidly with increasing frequency and anisotropy. The direction of maximum stress, which is influenced by the loading arrangement inherent in the specimen design, can change the propagation characteristics [13]. It is also important to account for the strain hardening of a material as it is deformed plastically. This hardening can cause a decrease in attenuation which results in an apparent increase in acoustic emission [15]. It is apparent from the tests discussed previously that changes in heat treatment and temperature can have an effect on the generation and propagation of stress waves.

The detection of a wave by a transducer introduces more complications into the AE analysis. The acoustic emission generating mechanism creates a small displacement which must be of sufficient amplitude to deform the crystal element in the transducer. Because of resonances within the crystal element itself, waves of equal stress but different frequency may produce signals of different amplitude within the transducer. Various methods of applying a white noise source to a specimen and monitoring the resulting transducer output are currently being tested to better

understand the energy transfer between the specimen and the transducer. The physical dimensions of the transducer may actually tend to attenuate or accentuate certain frequencies in the detected signal [14]. The couplant (usually a viscous liquid) used to acoustically join the transducer to the specimen can also create difficulties. Although the thickness of the couplant film may be only a small fraction of a wave length, phase shifts and reflections from both faces of the film can distort the acoustic emission signal being transmitted [13].

The final signal of the acoustic emission event is an amplified and filtered voltage which is processed and displayed in various ways. From this resultant voltage, details about the generating mechanism are desired [16]. This task is made difficult because of the distortion that each electronic component contributes to the signal as it is processed. Transfer function determination of each component is therefore necessary to deduce the characteristics of the actual incoming signal. The frequency limitations of various components further detract from the ability of the AE system to accurately analyze the input waveform. The current use of sophisticated minicomputers in acoustic emission systems has made the task of data reduction much easier than in the past. The computer is helpful in providing software that can graphically display the data as well as acoustically isolate sections of the specimen via geometric discrimination to reduce spurious noise.

EXPERIMENTS

OBJECTIVES

The objectives of the experiments are to determine correlations between fracture mechanics parameters and acoustic emission parameters. As has been illustrated in the literature review section, there is a large number of parameters that can potentially be correlated. Because many parameters are interrelated, however, it is possible to simplify the correlation experiments by attempting to relate only independent fracture mechanics and independent acoustic emission parameters.

Possible fracture mechanics parameters include crack length (a), crack growth rate ($\dot{a}$), maximum stress intensity factor (K_{max}), range in stress intensity factor (ΔK), plastic zone size (r_p), crack opening displacement (COD), and strain energy release rate (G). Using relationships between these parameters as given in Table 4, however, it is possible to extract three independent parameters which can be used to define all the other possible parameters. In this investigation, the three independent parameters are chosen to be crack length (a), crack growth rate ($\dot{a}$), and maximum stress intensity factor (K_{max}).

In an analagous manner, there are many possible acoustic emission parameters such as events, event duration, peak amplitude, ringdown counts, rise time, and slope. The use of a resonant

transducer, however, implies that event duration is equal to the number of ringdown counts divided by the resonant frequency of the transducer. Thus, it is possible to eliminate either event duration or ringdown counts from the possible parameters listed. The definition of slope can also be used to eliminate either rise time or peak amplitude from the remaining parameters.

The experiments are therefore devised to vary the independent fracture mechanics parameters of crack length, crack growth rate, and maximum stress intensity factor during fatigue tests while the independent acoustic emission parameters events, peak amplitude, ringdown counts, and slope are monitored.

The acoustic emission data are analyzed in two forms: "[parameter] per loading cycle" and "mean [parameter] per event" (the data reduction procedure is given in Appendix F). The [parameter] per loading cycle data are clearly a function of the number of events detected per unit time, as well as the characteristics of each event. The mean [parameter] per event data, however, are only a function of the event characteristics, independent of the number of events detected. Thus, provisions are made to determine whether the changes in acoustic emission from each growth rate are due to a different number of events or from changes in the characteristics of the individual events.

PROCEDURES

A series of experiments was devised to determine the effect of initial crack length, crack growth rate, maximum stress intensity factor, and material type on the acoustic emission parameters. Details of the experimental test matrix are given in Appendix E.

The effect of crack length was determined by testing specimens using an initial crack length of either 22.5 or 27.5 mm. All the specimens were machined with a 17.5 mm long crack-initiating notch, and thus required the growth of a pre-fatigue crack of either 5 or 10 mm.

Crack growth rates were selected in the range from 5.1×10^{-5} to 1.5×10^{-3} mm/cycle, which fell within the mid-range fatigue region for all steel types.

The tests were conducted at one of three maximum stress intensity factors: 49.5, 60.4, or 71.4 $MN/m^{3/2}$. These values were selected so that the K_{IC} value for each steel would not be exceeded, as well as to permit the use of the necessary ΔK values to achieve the desired crack growth rates using tension-tension fatigue cycling. The use of a constant K_{max} for different growth rates was advantageous in that it maintained the plastic zone at a relatively constant size.

The usual procedure in acoustic emission/fatigue experiments has been to maintain a constant load ratio (R) for each growth

rate which causes K_{max} (and thus the plastic zone size) to increase with increasing growth rates. By maintaining K_{max} constant, therefore, the effect of the changing plastic zone size is removed from the effect of changing growth rates. This is necessary to determine whether acoustic emission is better correlated by changing plastic zone size or by actual crack growth.

The experiments were performed using three types of steels: A36, A514, and A588. These were selected in order to assess the effect of a range of material characteristics on the acoustic emission signals. See Appendix A for details on material characteristics. Compact test specimens were machined from plates of the three steels in the T-L orientation. Details on specimen geometry are given in Appendix B.

Each specimen was fatigued on an Instron electro-servohydraulic testing machine at 50 Hz to extend a fatigue crack from the starter notch an additional 5 or 10 mm, as required. The electric potential method was used to determine the crack length during this phase, as the empirical crack growth rate curve does not accurately predict crack initiation from a machined notch.

The specimens were then loaded into a Materials Testing System (MTS) servohydraulic testing machine and fatigued at 0.1 Hz for 500 cycles while being acoustically monitored. (Details of the acoustic emission monitoring system are given in Appendix C.) Each specimen was tested in this way, at a constant maximum stress

intensity factor, at each crack growth rate, starting with the lowest rate. Load level was set as necessary to maintin a constant maximum stress intensity factor and provide the correct ΔK to produce the desired crack growth rate as predicted by the empirical crack growth rate curve. Because of the low growth rates and relatively low number of loading cycles used for the tests, initial crack length was assumed to remain relatively constant at either 22.5 or 27.5 mm. The fatigue testing system is described in Appendix D, and a detailed description of the experimental procedure is provided in Appendix E.

RESULTS AND DISCUSSION

The results can be discussed in both qualitative and quantitative terms. The data reduction procedure is described in Appendix F.

QUALITATIVE ANALYSIS

It was found that the [parameter] per loading cycle plots were all fairly similar to one another for a given set of loading conditions. Similarly, the mean [parameter] per event data were also found to exhibit the same behavior for a given set of loading conditions regardless of the particular acoustic emission parameter considered. In order to facilitate the presentation of the data, therefore, ringdown counts per loading cycle will be the only parameter per loading cycle and mean slope per event will be the only mean parameter per event plots illustrated, and should be interpreted as typical of the remaining parameters in each type of plot. All curves are drawn using linear regression. All logarithms are common logs to the base 10.

[Parameter] Per Loading Cycle Data

The effect of the maximum stress intensity factor (K_{max}) is illustrated in Figs. 14, 15, and 16. For clarity, only the smallest and the largest K_{max} (49.5 and 71.4 $MN/m^{3/2}$, respectively) are shown. For A514 and A588, a higher K_{max} value results in a greater

number of ringdown counts per loading cycle than a lower K_{max} value at low growth rates. K_{max} does not seem to have a large effect at any growth rate for A36. This may be due, however, to the problem discussed in Appendix G concerning the plastic zone/region of acceptance interaction. Figs. 15 and 16 suggest that at high growth rates, the K_{max} curves intersect and (or) may merge to one curve. Thus, [parameter] per loading cycle data appear to be relatively insensitive to K_{max} at high growth rates.

The effect of the initial crack length (a_o) is shown in Figs. 17 and 18 for A514 and A588, respectively, with K_{max} = 71.4 $MN/m^{3/2}$. In the case of the A514, the ringdown counts per loading cycle is higher at low growth rates with the shorter initial crack length. As the growth rate increases, however, the number of ringdown counts per loading cycle with the longer initial crack length eventually equals that of the shorter crack length specimen. The possibility that there is no significant effect of a_o at any growth rates is suggested by the A588 data, in which the different a_o curves are quite close over the entire range of growth rates considered.

The effect of the crack growth rate ($\dot{a}$) on parameter per loading cycle data is immediately apparent from any of the plots already presented in Figs. 14 through 18. In all cases regardless of K_{max}, a_o, or material type, increasing $\dot{a}$ resulted in a higher number of ringdown counts per loading cycle. Additionally, the

relationship between $\dot{a}$ and ringdown counts per loading cycle data appears to be approximately linear on the log-log plots presented, thus implying that a power relationship exists between these two parameters.

The material effects on the data observed are illustrated in Fig. 19 for K_{max} = 49.5 MN/m$^{3/2}$, and in Fig. 20 for K_{max} = 71.4 MN/m$^{3/2}$ (both with a_o = 22.5 mm). Notice that at the lowest K_{max} value, Fig. 19, ringdown counts per loading cycle does not appear to vary significantly with steel type. However, at the highest K_{max} value shown in Fig. 20, the ringdown counts tend to increase for increasing steel strength. The lowest strength steel (A36) results in the lowest number of ringdown counts throughout the range of crack growth rates. A possible conclusion is that higher strength steels are more active emitters at high values of K_{max}. However, the observed effect may simply be due to the plastic zone/region of acceptance interaction problem explained in Appendix G.

Fig. 21 is also provided to examine the possible effect of material type on emissions from specimens with long initial crack lengths. Data from tests with A514 and A588 are shown, with K_{max} = 71.4 MN/m$^{3/2}$ and a_o = 27.5 mm. The results appear similar to those illustrated in Fig. 20, which are for the same K_{max} value but with a_o = 22.5 mm. As before, the higher strength steel is a more active emitter. Therefore, stronger materials appear to emit a higher number of ringdown counts per loading cycle

regardless of crack length (at this particular K_{max} value of 71.4 $MN/m^{3/2}$).

Mean [Parameter] Per Event Data

Mean slope per event results are taken here to be representative of all mean [parameter] per event data. In general, it was found that the characteristics of the individual events were independent of the entire set of variables tested. It should be mentioned, though, that the data reduction of these acoustic emission parameters was very difficult because of a wide variability in results, especially at low growth rates. It is nevertheless interesting that the chracteristics of the events did not significantly change as loading conditions or materials were varied.

Figs. 22, 23, and 24 show mean slope per event for A36, A514, and A588, respectively. All data from tests with both a_o = 22.5 and 27.5 mm are presented. Note that varying K_{max}, a_o, or $\dot{a}$ does not significantly affect the results.

Fig. 25 is presented to determine if material type has an effect on mean slope per event. There does not appear to be a significant difference between the three steels in the data of this parameter. This lends support to the possible conclusion that mean [parameter] per event data are independent of loading conditions and material type.

QUANTITATIVE ANALYSIS

The results were quantitatively analyzed by first attempting to apply the correlation results found in the literature review. These results are summarized in Table 2. By using fracture mechanics relationships, the results can be condensed into four expressions, each utilizing ringdown counts per loading cycle as the acoustic emission parameter. These condensed relationships are given in Table 3.

The first relationship, $\dot{N} \alpha \dot{a}^j$, implies that the ringdown counts per loading cycle is a function of the crack growth rate only. Table 5 gives the values of the exponent j for the various test conditions of this investigation. For example, the value of j for A36 with K_{max} = 49.5 $MN/m^{3/2}$ and a_o = 22.5 mm is equal to 1.47. Note that j varies with material, maximum stress intensity factor, and crack length; which, of course, is not predicted by the relationship $\dot{N} \alpha \dot{a}^j$.

The results of applying the second relationship, $\dot{N} \alpha K_{max}^{\ k}$, are shown in Table 6, which gives values of the exponent R for the experimental data. For example, for A36 and $\dot{a}$ = 5.1 x 10^{-5} mm/cycle, K is equal to 2.25. The exponent is seen to vary with both crack growth rate and material yield strength, whereas the given relationship suggests that K_{max} is the only relevant variable.

The third relationship, $\dot{N} \alpha (K_{max}/Y)^{\ell}$, and the fourth relationship, $\dot{N} \alpha (K_{max}{}^2/Y)^m$, imply that crack growth rate and initial crack length do not affect the number of ringdown counts per loading cycle. Tables 7 and 8, however, show that the value of the exponent in both these relationships changes with growth rate and crack length.

Because the four relationships obtained from the literature review failed to satisfactorily explain the effects of all the variables on the acoustic emission data, a new relationship is proposed. This relationship is of the form

$$\dot{N} \alpha \dot{a}^n$$

where

$\dot{N}$ = ringdown counts per loading cycle

$\dot{a}$ = crack growth rate

$n = f(K_{max}, a_o, Y)$

K_{max} = maximum stress intensity factor

a_o = initial crack length

Y = material yield strength

The exponent n is assumed to be a linear function of K_{max}, a_o, and Y; that is, $n = C_1 K_{max} + C_2 a_o + C_3 Y + C_4$. Appendix H provides details of the procedure that is used to develop the proposed equation, as well as the values of the constants in the expression

for n.

The results of applying the proposed equation that attempts to explain changes in maximum stress intensity factor and initial crack length for all steel types are given in Table 9. The accuracy of this equation in predicting the value of the exponent n in the proposed relationship can be assessed by comparing these values to the corresponding values in Table 5, which gives the known values of n for different loading and material conditions. It is obvious that there is considerable error in some values.

In order to reduce this error, a relationship can be sought that only explains the effect of maximum stress intensity factor and initial crack length on ringdown counts per loading cycle for a given material. An equation of this type for A588 is developed in Appendix H. The results obtained for the exponent n in this proposed equation are given in Table 10. Comparison with the known values of n for A588 (given in Table 5) show this simpler equation can better predict n than if the material yield strength variable is included. Of course, this results in an equation which is material-specific, rather than a general equation which applies to all materials.

Thus, it is possible to develop a relationship which can explain (although inaccurately) the effects of fracture mechanics variables on acoustic emission parameters. Perhaps a more sophisticated relationship can be developed to obtain a better correlation than

the proposed equation presented here.

CONCLUSIONS AND RECOMMENDATIONS

CONCLUSIONS

The following conclusions can be inferred from the results obtained from these experiments:

(1) A reasonable number of events must be detected during a test for effective data reduction. This is especially necessary considering the statistical nature of acoustic emission.

(2) Low crack growth rates usually result in a relatively low number of events being detected, whereas the opposite is true for higher growth rates.

(3) Meaningful comparisons between results obtained from different steel types are difficult to make if, in fact, it is not certain that the entire plastic zone is detected by the acoustic emission system. Thus, it is also uncertain as to whether or not the plastic zone size is significant in affecting acoustic emission.

(4) High maximum stress intensity values result in greater values of [parameter] per loading cycle data than low maximum stress intensity values at low crack growth rates. It appears that this effect becomes less significant at high growth rates.

(5) Shorter initial crack length specimens result in higher

values of parameter per loading cycle data at low crack growth rates than longer initial crack length specimens. This does not appear to be the case at high growth rates. Some results indicate that there may be no effect of crack length throughout the entire growth rate range tested for some materials (A588).

(6) A power relationship exists between crack growth rate and [parameter] per loading cycle data for all stress intensity values, initial crack length values, and material types.

(7) Specimens made from higher strength steels result in higher [parameter] per loading cycle values at high stress intensity factors, whereas steel strength loses its effect at low stress intensity factors. This behavior is exhibited regardless of initial crack length, and implies that there might be a coupling effect between maximum stress intensity factor and yield strength which influences [parameter] per loading cycle data.

(8) Changes in maximum stress intensity factor, crack growth rate, initial crack length, or material type do not appear to significantly affect mean [parameter] per event data. This implies that the characteristics of the events detected are actually independent of loading conditions and material type. Thus, all events resulting

from fatigue crack growth may be nearly identical, with different loading conditions and material types simply affecting the number of events produced.

(9) The data obtained from this investigation are not satisfactorily predicted by quantitative relationships developed in past experimentation.

(10) A quantitative relationship can be developed to correlate [parameter] per loading cycle data with loading conditions and material type. Although the proposed equation presented here is likely to be altered by additional testing, it provides a starting point for further quantitative work.

RECOMMENDATIONS

Based on the experience gained in this research effort, several recommendations can be offered to assist future experimentation in this area:

(1) Tests conducted under similar conditions should be repeated several times to assess the variability of acoustic emission results, as well as to permit the averaging of data. This is particularly important when performing fatigue experiments which typically result in data with a significant degree of scatter.

(2) The electric potential method should be used to continuously monitor crack length during acoustic emission experiments. The use of load levels that are obtained from the empirical crack growth rate data to produce a specified growth rate is not certain to result in that growth rate under all conditions. The large scatter in the empirical growth rate data is another reason why a more accurate method to determine crack length is required. The electric potential method allows for a high degree of precision in measuring crack length, and thus makes it suitable for detecting the actual crack growth rate that occurs due to a certain load level.

(3) The tests should be carried out using at least several thousand loading cycles, especially at low growth rates ($\simeq 10^{-5}$ mm/cycle). This is necessary because of the sometimes sporadic nature of fatigue crack growth, especially at low growth rates. To facilitate performing high loading cycle experiments, the test machine/specimen grip system must be able to accurately apply the desired loads at a practical cyclic loading frequency (> 1 Hz). This is difficult when the grips contain very compliant material, such as rubber, which makes load control impractical except at very low

loading frequencies.

(4) The test specimens should be longer (measured along the dimension between the two loading pins) than the specimens used in this investigation. The spatial discrimination feature of the acoustic emission monitoring system works best when the two transducers are as far apart as possible; hence, longer specimens permit better spatial discrimination. The specified region that was selected for these experiments had to be small due to the proximity of the loading pins to the fatigue crack, thus introducing an additional complication. The K_{max} values that were used produced a plastic zone size that was sometimes greater than the region of acceptance; this was particularly true with the A36 specimens and sometimes with the A588 specimens. A longer specimen would permit the use of a larger acceptance region that would include all plastic zones caused by the loading conditions and materials used, and thus would ensure that this possible origin of acoustic emission (that is, the volume or the elastic-plastic boundary of the plastic zone) would not be excluded from detection, and thus as a potential correlating parameter.

(5) It is apparent that a large number of data points is necessary to obtain a meaningful quantitative

relationship between acoustic emission parameters and fracture mechanics parameters. Therefore, a wide range of crack growth rates, initial crack lengths, and maximum stress intensity factors should be used to assess the effect of each variable.

(6) Separate specimens should be used for each crack growth rate desired. That is, the same specimen should not be subjected to different loads and used to generate acoustic emission data for several different crack growth rates. This precaution should be taken because of the subtle effects such as crack arrest or acceleration that can take place during a fatigue experiment because of prior loading effects that are not well understood.

REFERENCES

[1] J. Kaiser, "Untersuchungen uber das Auftreten von Gerauschen beim Zugversuch", Dr. Ing. Thesis, Technische Hochschule, Munich, 1950.

[2] V.E. Vainberg, V.N. Sosedov, and A.M. Kushnir, "Acoustic Emission Study of Crack Growth". Soviet Journal of Non-destructive Testing, Vol. 11, No. 3, 1975, pp. 374-376.

[3] C.D. Bailey, J.M. Hamilton, and W.M. Pless, "AE Monitoring of Rapid Crack Growth in a Production-size Wing Fatigue Test Article". NDT International, Dec. 1976, pp. 298-304.

[4] D.O. Harris and H.L. Dunegan, "Continuous Monitoring of Fatigue Crack Growth by Acoustic Emission Techniques". Experimental Mechanics, Vol. 14, No. 2, Feb. 1974, pp. 71-81.

[5] S.P. Ying, "Effect of Crack Size on Acoustic Emission Related to Moving Dislocations". Journal of Applied Physics, Vol. 46, No. 7, July 1975, pp. 2882-2888.

[6] T.M. Morton, R.M. Harrington, and J.G. Bjeletich, "Acoustic Emissions of Fatigue Crack Growth". Engineering Fracture Mechanics, Vol. 5, 1973, pp. 691-697.

[7] C.E. Hartbower, C.F. Morais, W.G. Reuter, and P.P. Crimmins, "Acoustic Emission from Low-Cycle High-Stress-Intensity Fatigue". Engineering Fracture Mechanics, Vol. 5, 1973, pp. 765-789.

[8] I.G. Palmer, B.J. Brindley, and R.P. Harrison, "The Relationship Between Acoustic Emission and Crack Opening Displacement Measurement". Materials Science and Engineering, Vol. 14, 1974, pp. 3-6.

[9] M. Arii, H. Kashiwaya, and T. Yanuki, "Slow Crack Growth and Acoustic Emission Characteristics in COD Test". Engineering Fracture Mechanics, Vol. 7, 1975, pp. 551-556.

[10] H.L. Dunegan, D.O. Harris, and A.S. Tetelman, "Detection of Fatigue Crack Growth by Acoustic Emission Techniques". Materials Evaluation, Oct. 1970, pp. 221-227.

REFERENCES (CONT'D)

[11] T.C. Lindley, I.G. Palmer, and C.E. Richards, "Acoustic Emission Monitoring of Fatigue Crack Growth". Materials Science and Engineering, Vol. 32, 1968, pp. 1-15.

[12] I.G. Palmer and P.T. Heald, "The Application of Acoustic Emission Measurements to Fracture Mechanics". Materials Science and Engineering, Vol. 11, 1973, pp. 181-184.

[13] C. Spanner, Acoustic Emission Techniques and Applications. Intex Publishing Company, Evanston, Ill., 1974.

[14] D.E.W. Stone and P.F. Dingwall, "Acoustic Emission Parameters and their Interpretation". NDT International, Vol. 10, No. 2, Apr. 1977, pp. 51-62.

[15] W.F. Hartman, "Correlation of Mechanical and Metallurgical Parameters with the Acoustic Emission during Tensile Deformation of Several Metals and Alloys". Prepared for the U.S. Energy Research and Development Administration, NTIS C00-2204-14.

[16] N.N. Hsu, J.A. Simmons, and S.C. Hardy, "An Approach to Acoustic Emission Signal Analysis-Theory and Experiment". Materials Evaluation, Oct. 1977, pp. 100-106.

[17] D. Broek, Elementary Engineering Fracture Mechanics. Sijthoff and Noordhoff International Publishers B.V., Alphen aan den Rijn, The Netherlands, 1978.

[18] R. Roberts, J.M. Barsom, J.W. Fisher, S.T. Rolfe, "Fracture Mechanics for Bridge Design". Prepared for the Federal Highway Administration, U.S. Department of Transportation, P.O. No. 5-3-0209.

[19] J.E. Srawley, "Wide Range Stress Intensity Factor Expressions for ASTM E399 Standard Fracture Toughness Specimens". International Journal of Fracture, Vol. 12, No. 3, 1976, p. 475.

[20] R.O. Ritchie, "Crack Growth Monitoring: Some Considerations of the Electrical Potential Method", Department of Materials Science Report, University of Cambridge, Jan. 1972.

TABLE I Summary of Correlation Experiment Reporting[a].

Ref.	Material	Specimen type	Sensor and filters	Couplant	Sensor location specified?	Gain (dB)	Threshold	Acoustic emission monitoring system	Loading apparatus and crack length measurement system	Loading characteristics	Noise reduction techniques	Basis for theoretical model[b]
[2]	D16T aluminum alloy	600mmx100mm rectangular, thickness 2.5-20mm	400-800kHz broadband transducer with 200kHz high pass filter	transformer oil	no	100	1.0v	AF-20 (amplifier and counter)	GRM-60 hydraulic pulser with microscope	Fixed nominal stress range from 50-90% of yield stress with 10Hz loading frequency	—	—
[3]	7075-T6511 aluminum alloy	production-size aircraft wing	700-800kHz resonant transducer with 350kHz high pass filter	acrylic adhesive	yes	70	1.0v	Dunegan Model 1032	hydraulic jacks with telescope	constant amplitude loads	—	—
[4]	7075-T6 aluminum and 4140 steel	22mmx75mmx1mm rectangular single edge notched	150kHz and 1.5MHz resonant transducers, with, respectively, 100-300kHz and 1-2MHz bandpass filters	viscous resin (V-9)	no	60, 80, 95	1.0v	amplifier and counter with voltage-controlled gate	MTS model 811 with 10x microscope	2 or 1yHz loading frequency	universal joints and aluminum-steel interface in load train	H&C
[5]	A212 carbon steel	cylindrical pressure vessel 2m high, 50cm O.D., 25mm thickness	100-300kHz bandpass filters	—[c]	no	88	—[c]	6 channel computerized location determining system[c]	internal hydraulic pressurization	cyclic loading from 0 to 17 MPa	—	H or r_p
[6]	2024 aluminum alloy	60mmx60mmx12mm compact test specimen	Dunegan 155kHz resonant transducer with 145-155kHz bandpass filter	—	yes	80	20mv above background noise	voltage controlled gate	25xmicroscope with scribed graduations on specimen surface	constant ΔK and load ratio with 4Hz loading frequency	aluminum-steel interfaces in load train	H or r_p
[7]	D6aC steel, 6Al-4V titanium, and 7075-T6 aluminum	30.5cmx7.5cm rectangular single-edge notched, thickness 2.5-7.5mm	400-1000kHz bandpass filter	quartz wax	no	100	a "few" mv above background noise	amplifier and counter	MTS model 301.02 with specimen-mounted crack opening gage	0.1Hz loading frequency	teflon tape used on all threaded connections in load train	—
[8]	carbon-manganese nuclear reactor pressure vessel steel	25mm thick compact test specimen[c]	—[c]	—[c]	no	—[c]	—[c]	—[c]	Instron tensile testing machine[c]	—[c]	—	H or r_p
[9]	mild, quenched and tempered, and precipitation hardened steel	25mm thick x 50cm rectangular single edge notched	220kHz resonant transducer	—	yes	66	0.5v	amplifier and counter	hydraulic ram	—	pre-stress of specimens around loading pins	—
[10]	"trip" steel	40mmx45mmx5mm wedge opening load	150kHz resonant transducer with 120-170kHz bandpass filter	viscous resin	no	—	—	amplifier and counter	—	constant load cycling between 0 and 5720N	—	H or r_p
[11]	Ducol W30B, 12C, EN30B, C5n, Fv520B steel, and 7075-T651 alum.	compact test specimen	Dunegan 750kHz resonant transducer with 300-1000kHz bandpass filter	—[c]	no	94	—[c]	amplifier and counter with voltage-controlled gate	telescope with scribed graduations on specimen surface, or electric potential method	tension-tension fatigue using constant ΔK at 3Hz	coated steel loading pins to minimize metal-to-metal contact	H or r_p and H&C
[12]	carbon-manganese steel	25mm thick compact test specimen	140kHz resonant transducer	—	no	97	0.8v	Dunegan Research Corporation	—	—	—	No area of elastic-plastic boundary

(a) Vendor of equipment is quoted if given in reference. A "—" indicates that the information is not reported.

(b) H = AE ringdown counts.
G = strain energy release rate.
r_p = plastic zone size.

(c) Details are referenced to other papers.

TABLE 2 Summary of Correlation Results.

Parameter	Relationship*	Reference(s)
Crack length (a)	$N \alpha a$	[2]
	$N \alpha a$ (depends on range of a)	[3], [4]
	$N \alpha f(a)$ (depends on load)	[5]
Crack growth rate ($\dot{a}$)	$\dot{N} \alpha \dot{a}^n$	[6]
Crack opening displacement (COD)	$\dot{N} \alpha COD$	[7]
	$N \alpha (COD)^n$	[8]
	$N \alpha (COD)^n$ (depends on COD range)	[9]
Stress intensity factor (K)	$N \alpha K$	[7]
	$N \alpha K^n$	[10]
Range of stress intensity factor (ΔK)	$\dot{N} \alpha \Delta K^n$	[11]
Plastic zone size (r_p)	$N \alpha r_p$	[12]

* "α" means "is proportional to".

N = cumulative ringdown counts.

$\dot{N}$ = ringdown counts per loading cycle.

TABLE 3 Condensation of Correlation Results Using Fracture Mechanics Relationships.

Relationship*	Reference(s)
$\dot{N} \alpha \dot{a}^{j}$	[2], [3], [4], [5], [6], [11]
$\dot{N} \alpha K_{max}^{k}$	[7], [10]
$\dot{N} \alpha (K_{max}/Y)^{\ell}$	[12]
$\dot{N} \alpha (K_{max}^{2}/Y)^{m}$	[7], [8], [9]

* "α" means "is proportional to".

TABLE 4 Fracture Mechanics Relationships.

Relationship	Reference
$\dot{a} = A(\Delta K)^n$ for mid-range fatigue	[17]
$K = A\sigma\sqrt{\pi a} = Pf(a)$	(by definition)
$\Delta K = K_{max} - K_{min}$	(by definition)
$R = K_{min}/K_{max}$	(by definition)
$r_p = 1/2\pi(K_{max}/Y)^2$ for plane stress	[18]
$r_p = 1/6\pi(K_{max}/Y)^2$ for plane strain	[18]
$COD = 4/\pi\ K^2_{max}/YE$	[17]
$G = K^2_{max}/E$ for plane stress	[17]
$G = 1/(1 - \nu)^2\ K^2_{max}/E$ for plane strain	[17]

where:

a = crack length
$\dot{a}$ = crack growth rate
A = constant
COD = crack opening displacement
E = Young's modulus
G = strain energy release rate
K = stress intensity factor
ΔK = range in stress intensity factor
n = constant
P = load
r_p = plastic zone size
R = load ratio
ν = Poisson's ratio
σ = applied nominal stress
Y = yield strength

TABLE 5 Value of Exponent "j" in Relationship $\dot{N} \alpha \dot{a}^{j}$.

	Maximum stress intensity factor ($MN/m^{3/2}$)		
	49.5	71.4	
Material yield strength (MPa)	Initial crack length=22.5 mm	Initial crack length=22.5 mm	Initial crack length=27.5 mm
248 (A36)	1.47	1.25	--
690 (A514)	2.47	0.33	1.18
345 (A588)	3.31	1.57	1.37

TABLE 6 Value of Exponent "k" in Relationship $\dot{N} \alpha K_{max}^{k}$.

Material yield strength (MPa)		Crack growth rate (mm/cycle)		
		5.1×10^{-5}	1.8×10^{-4}	5.1×10^{-4}
248	(A36)	2.25	-5.25	-4.31
690	(A514)	16.38	10.75	1.25
345	(A588)	9.75	7.38	-5.31

TABLE 7 Value of Exponent "ℓ" in Relationship $\dot{N} \alpha \left(\frac{K_{max}}{Y}\right)^{\ell}$.

	Crack growth rate (mm/cycle)		
Initial crack length (mm)	5.1×10^{-5}	1.8×10^{-4}	5.1×10^{-4}
22.5	.859	-.609	-1.147
27.5	-1.412	-1.129	-3.968

TABLE 8 Value of Exponent "m" in Relatiohship $\dot{N}\alpha\left(\frac{K_{max}^2}{Y}\right)^m$.

	Crack growth rate (mm/cycle)		
Initial crack length (mm)	5.1×10^{-5}	1.8×10^{-4}	5.1×10^{-4}
22.5	1.655	.082	-1.082
27.5	1.454	-1.167	-4.100

TABLE 9 Values of Exponent "n" obtained using Proposed Equation for all Tests.

	Maximum stress intensity factor ($MN/m^{3/2}$)		
	49.5	71.4	
Material yield strength (MPa)	Initial crack length=22.5 mm	Initial crack length=22.5 mm	Initial crack length=22.5 mm
248 (A36)	2.71	1.44	0.98
690 (A514)	2.32	1.05	0.59
345 (A588)	2.63	1.36	0.90

TABLE 10 Values of Exponent "n" obtained using Proposed Equation for A588.

	Maximum stress intensity factor ($MN/m^{3/2}$)	
Initial crack length (mm)	49.5	71.4
22.5	3.67	1.83
27.5	--	0.76

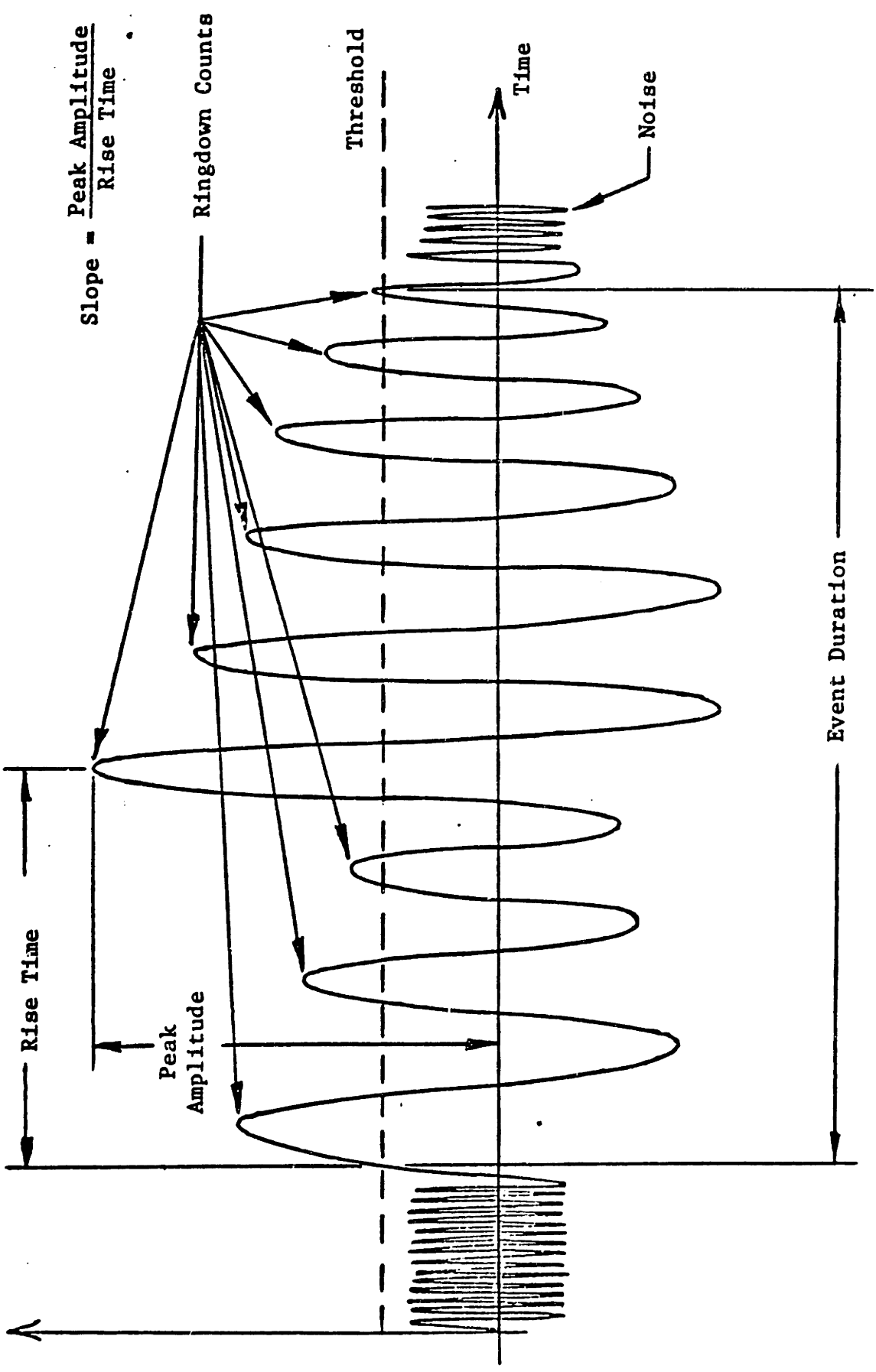

Fig. 1 Schematic of acoustic emission parameters.

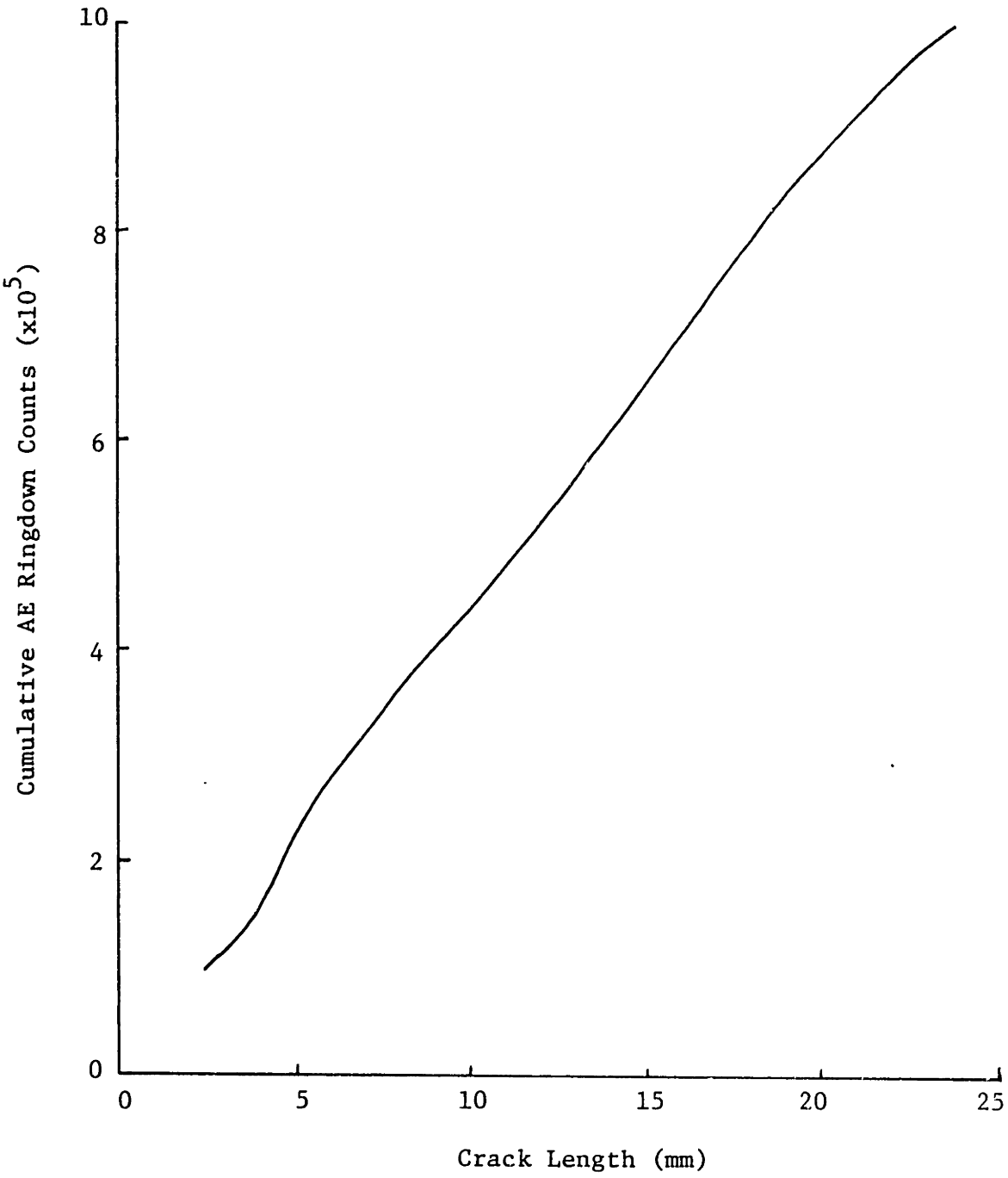

Fig. 2 Cumulative AE ringdown counts versus crack length [2].

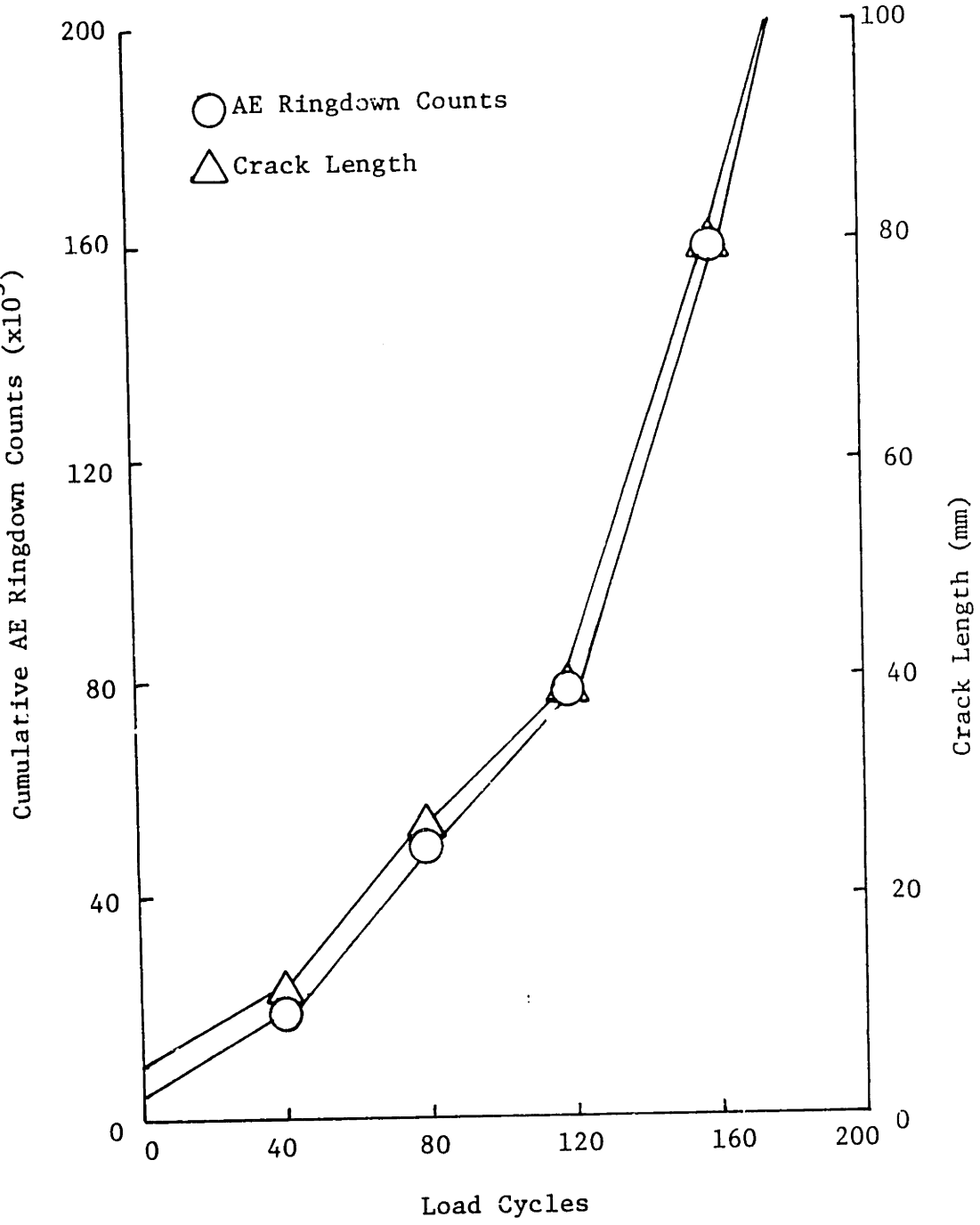

Fig. 3 Cumulative AE ringdown counts and crack length versus load cycles [3].

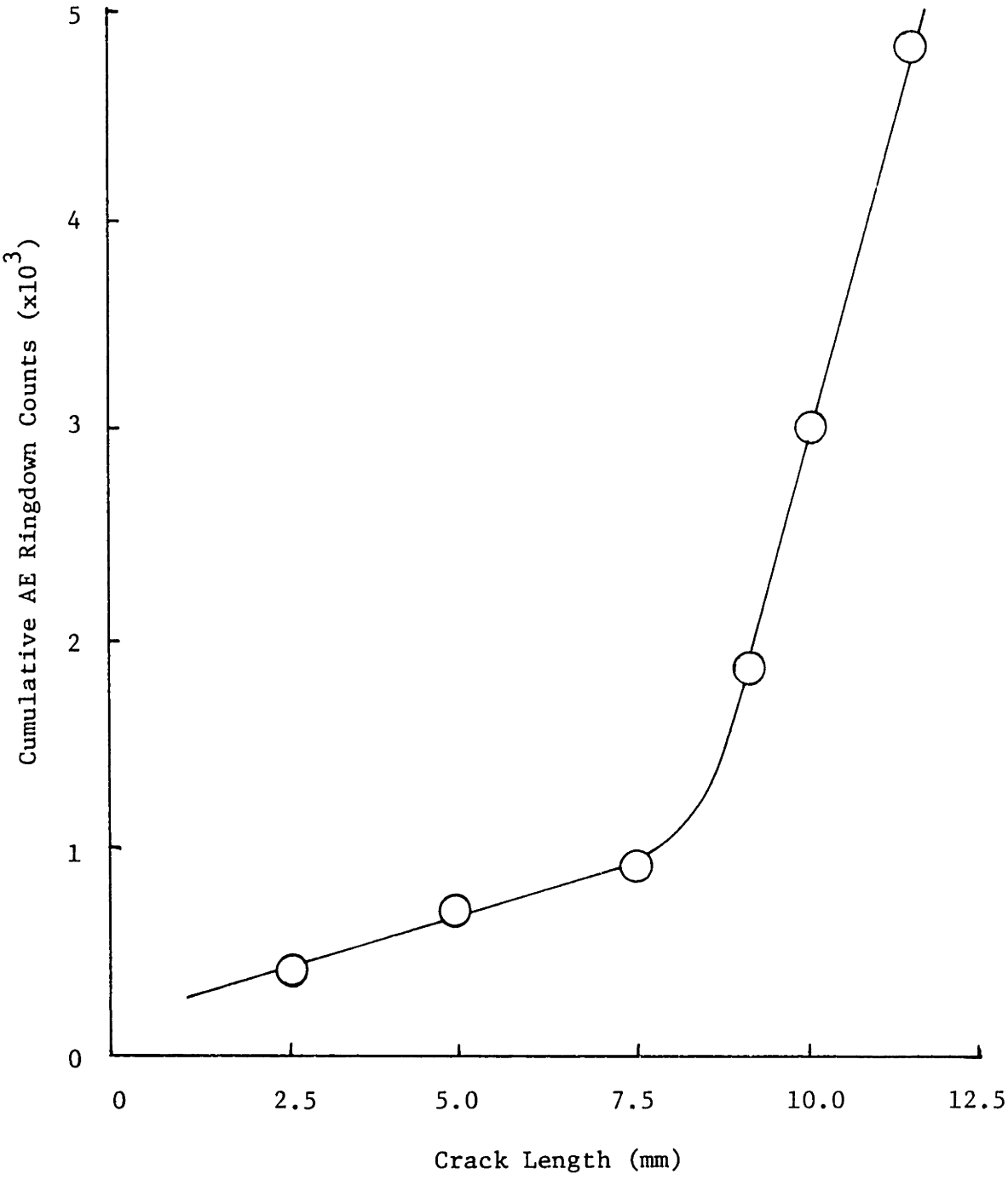

Fig. 4 Cumulative AE ringdown counts versus crack length [4].

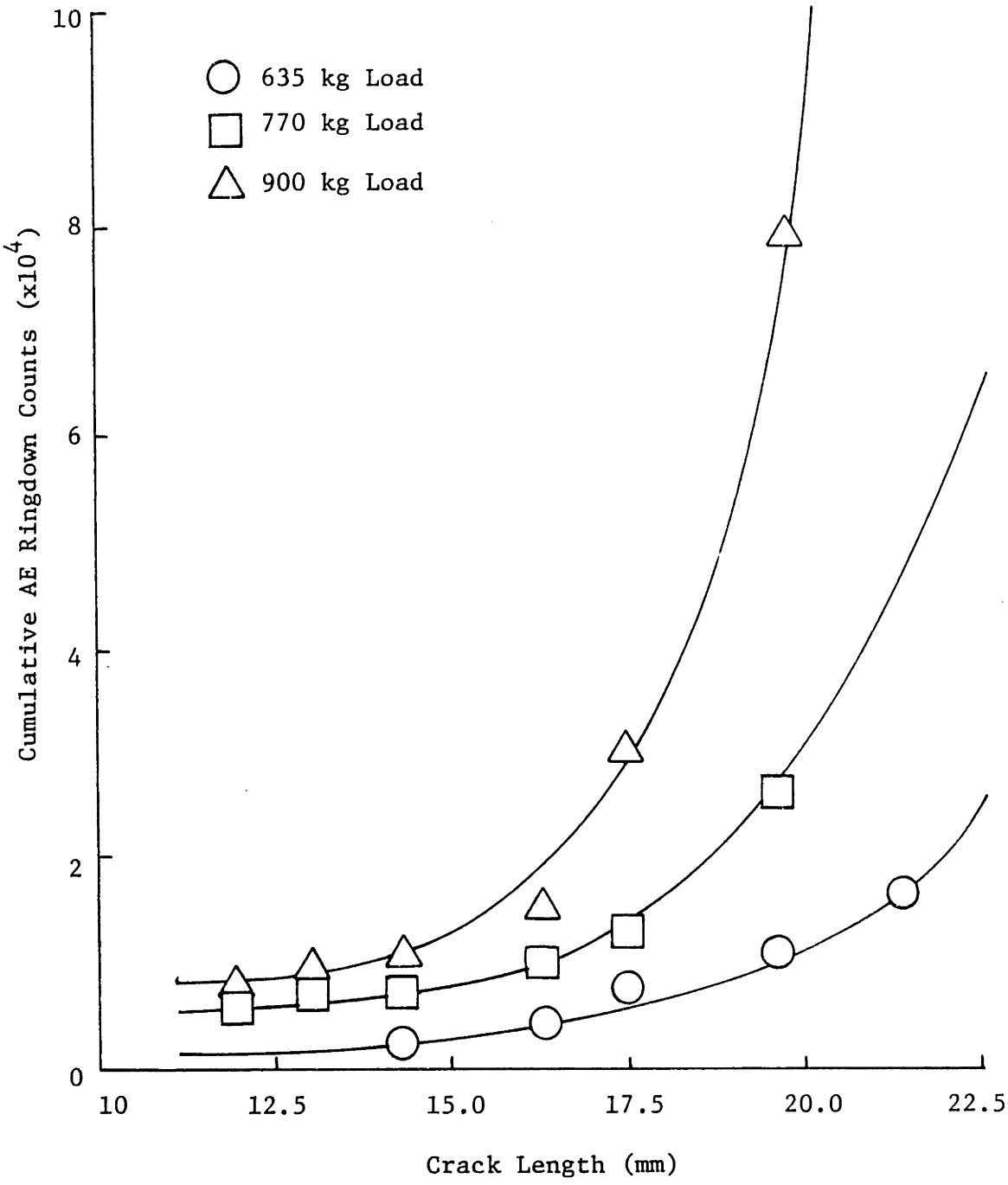

Fig. 5 Cumulative AE ringdown counts versus crack length [5].

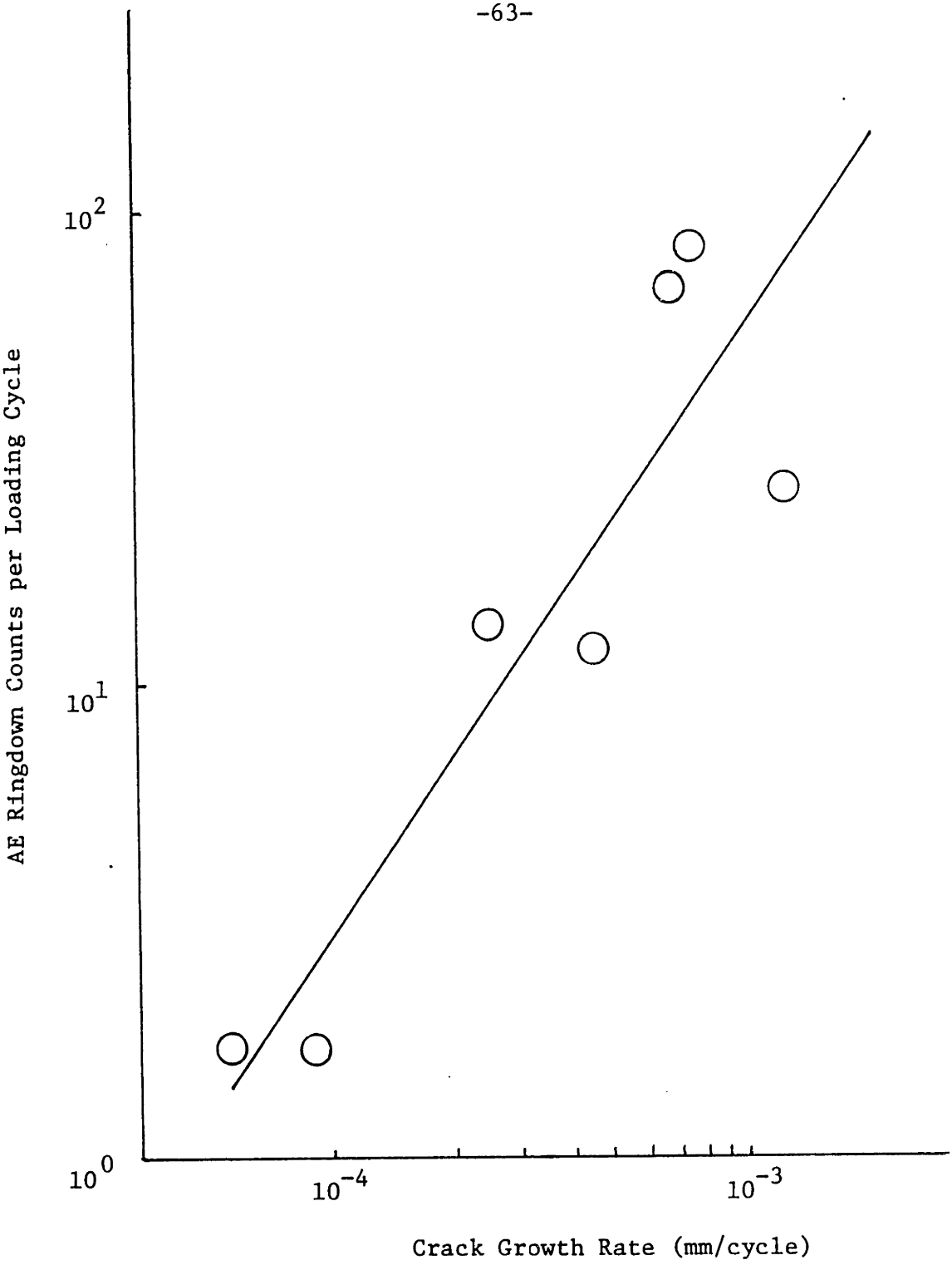

Fig. 6 AE ringdown counts per loading cycle versus crack growth rate [6].

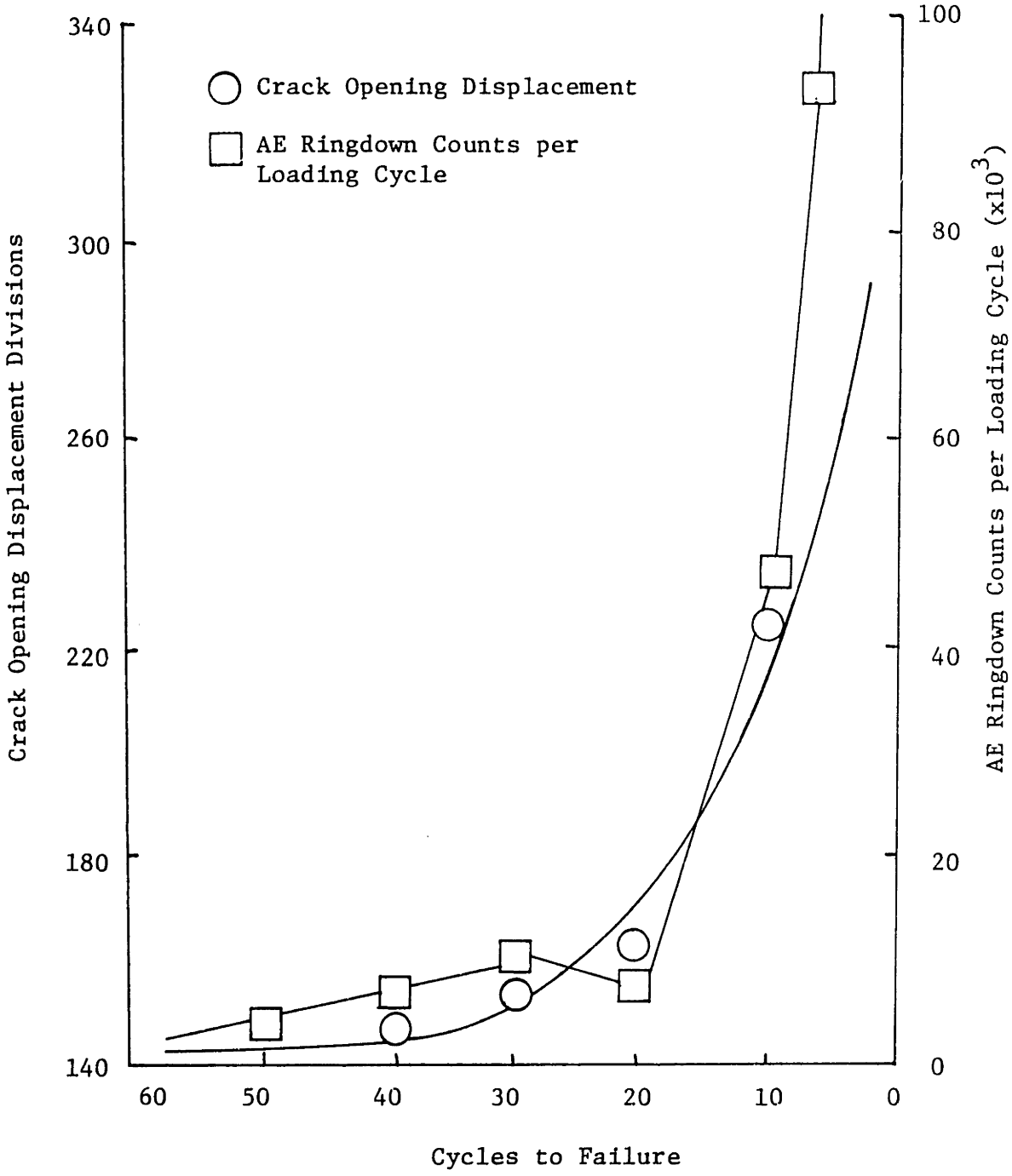

Fig. 7 AE ringdown counts per loading cycle and crack opening displacement versus cycles to failure [7].

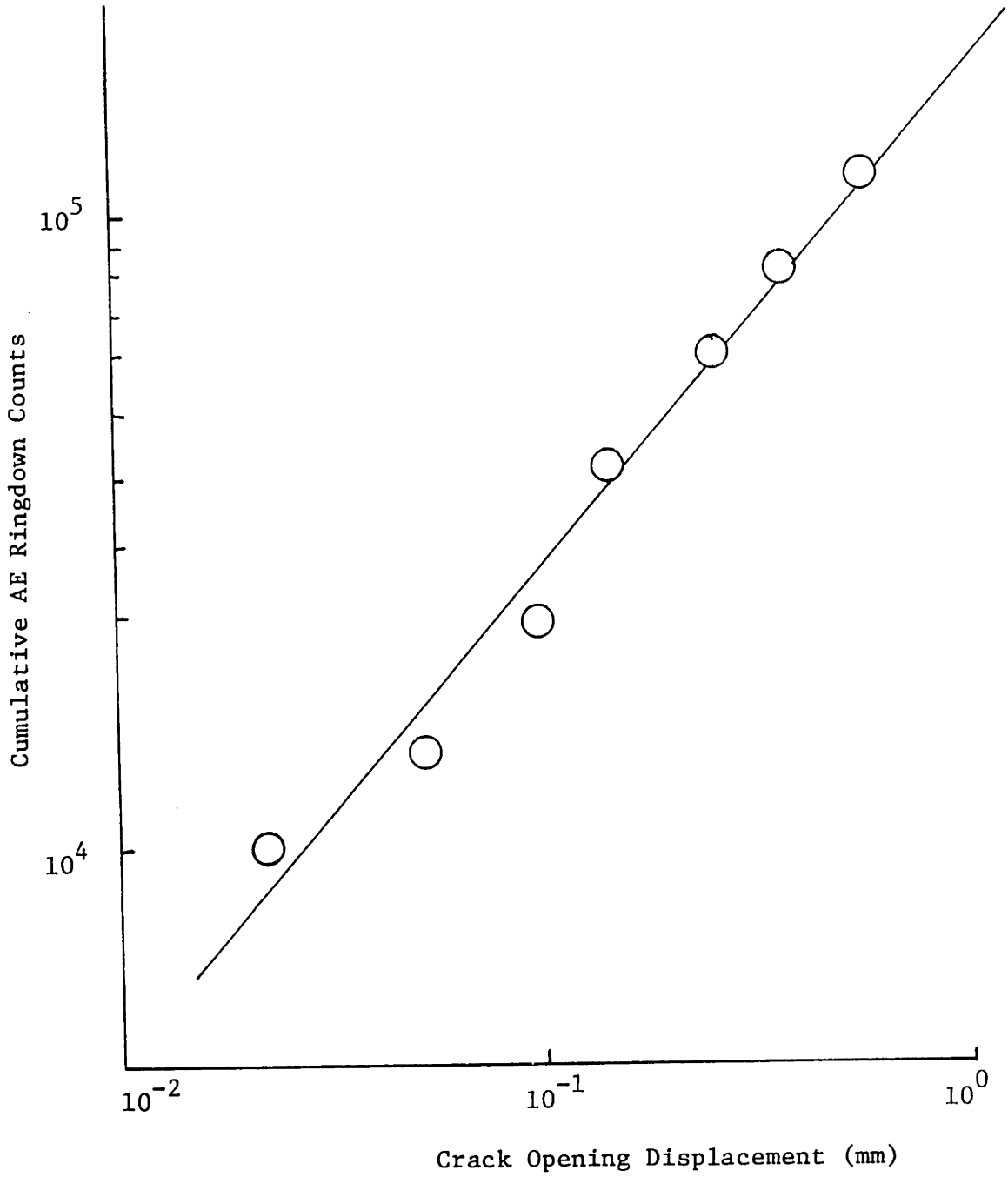

Fig. 8 Cumulative AE ringdown counts versus crack opening displacement [8].

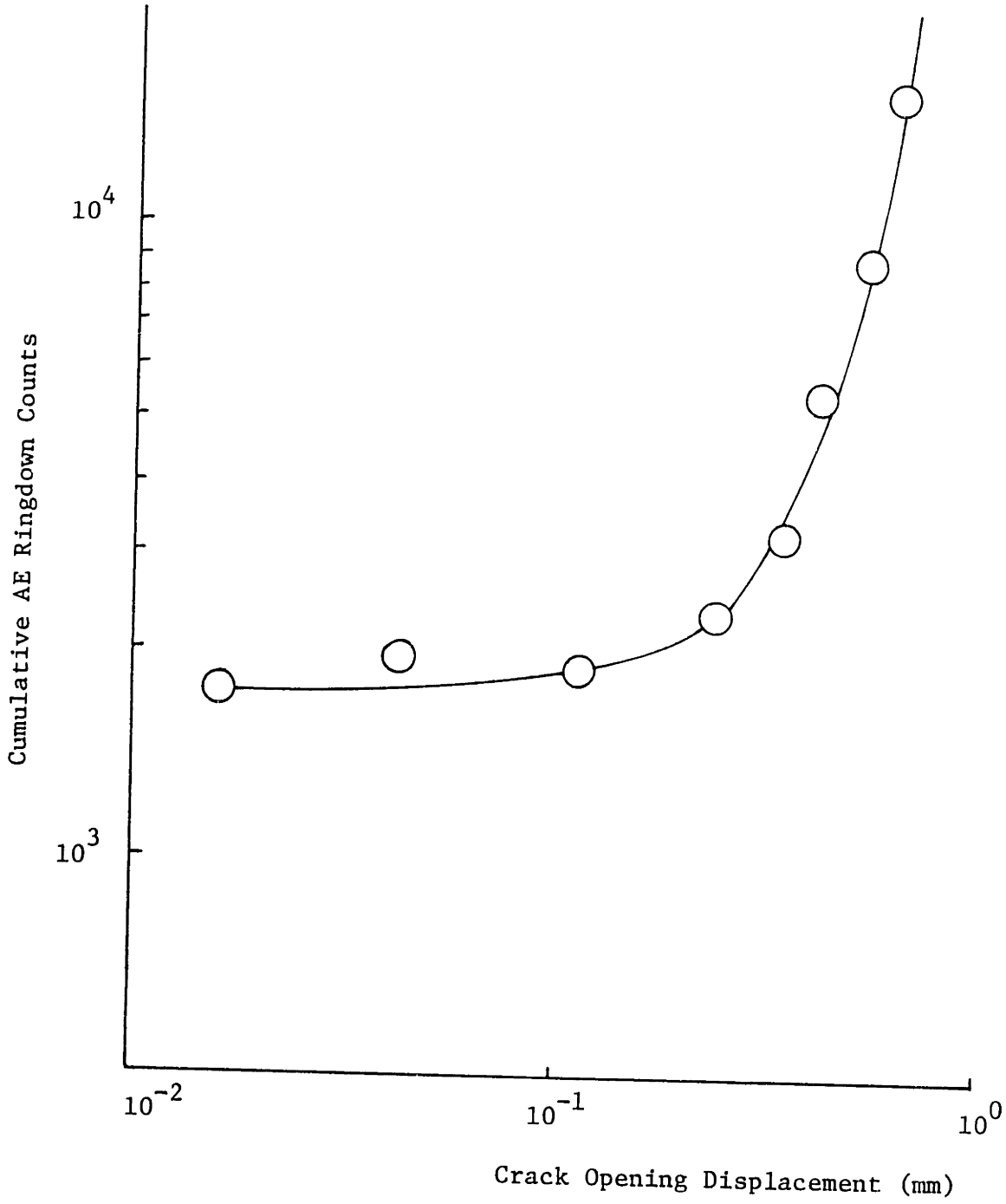

Fig. 9 Cumulative AE ringdown counts versus crack opening displacement [9].

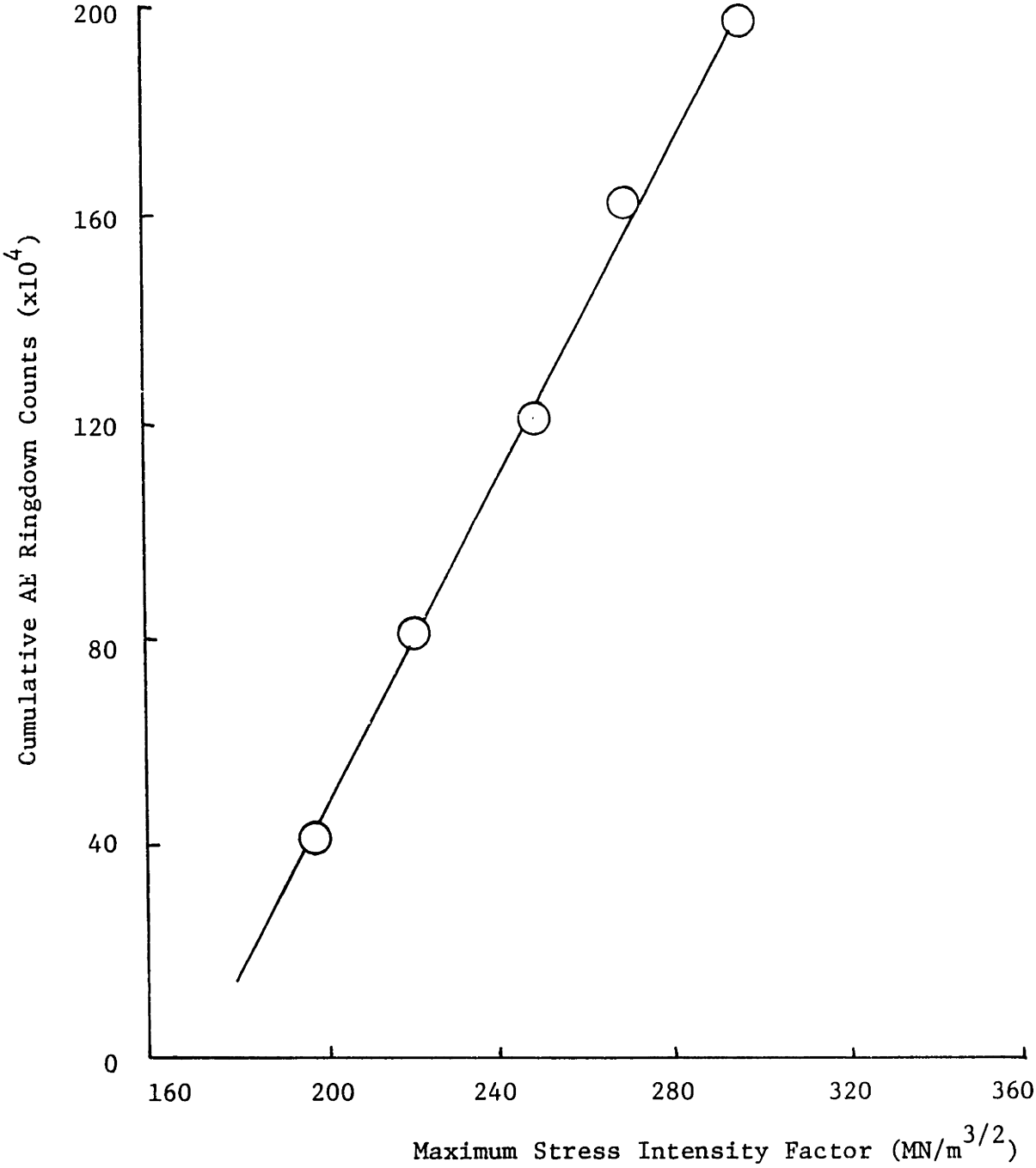

Fig. 10 Cumulative AE ringdown counts versus maximum stress intensity factor [7].

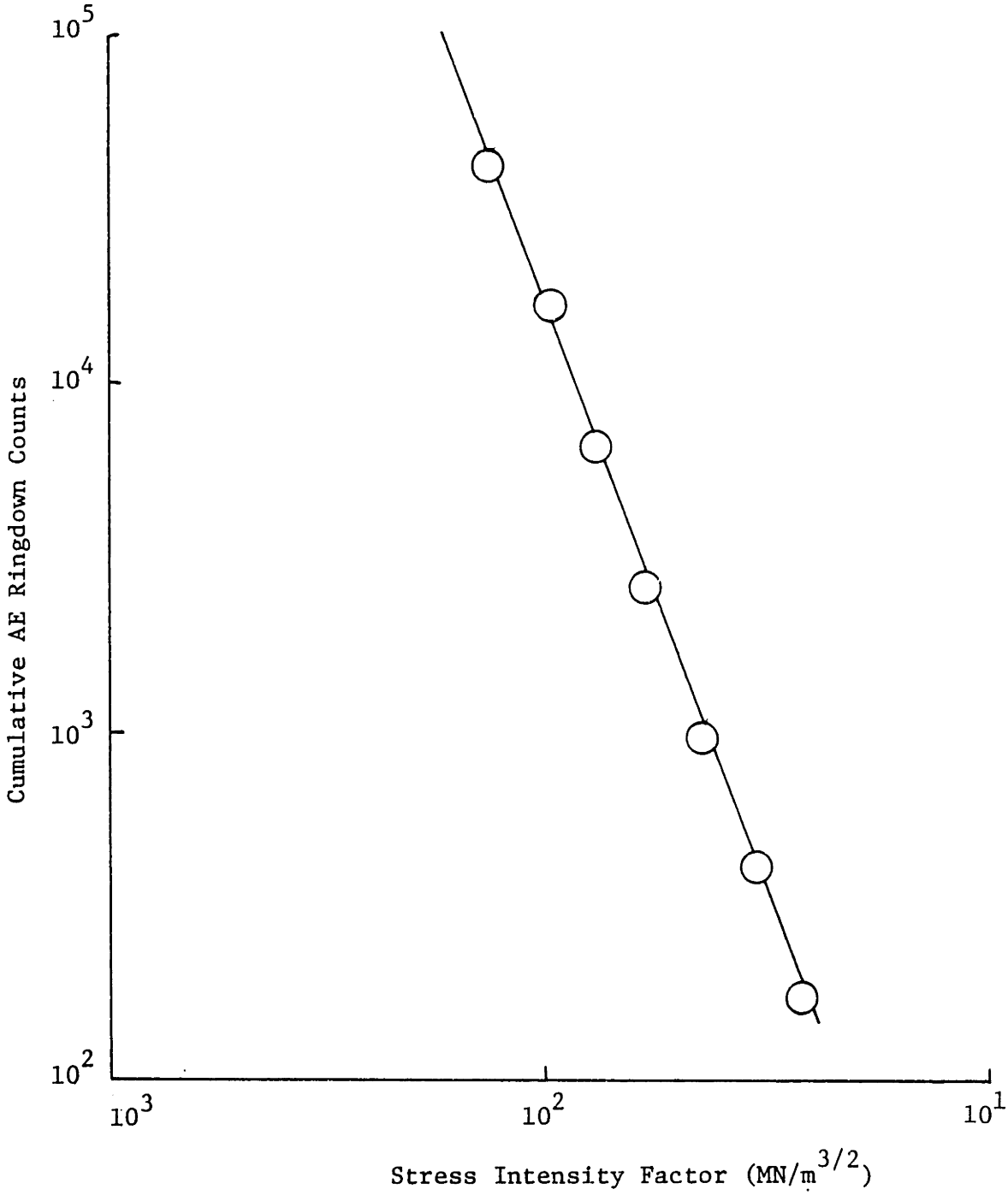

Fig. 11 Cumulative AE ringdown counts versus stress intensity factor [10].

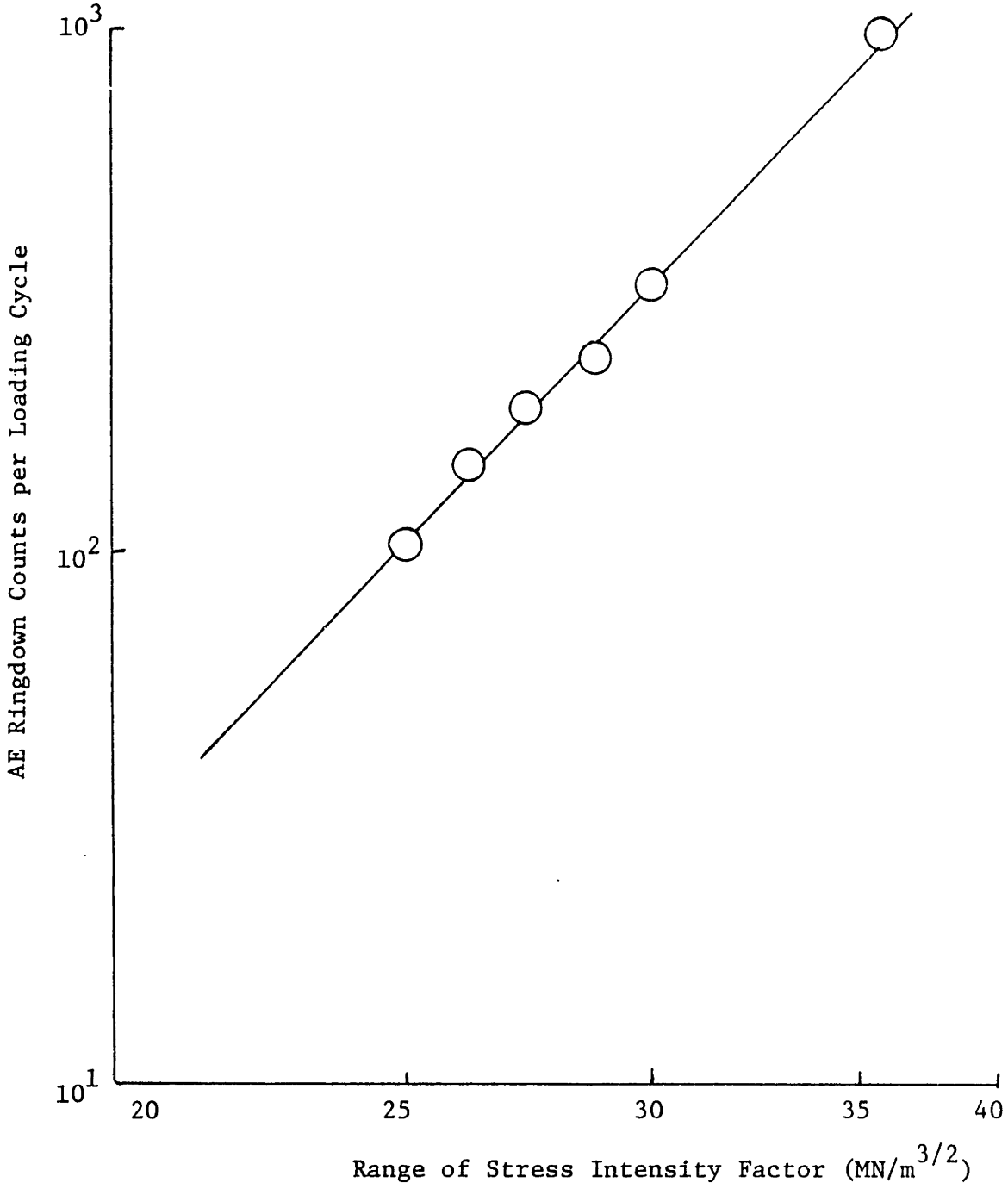

Fig. 12 AE ringdown counts per loading cycle versus range of stress intensity factor [11].

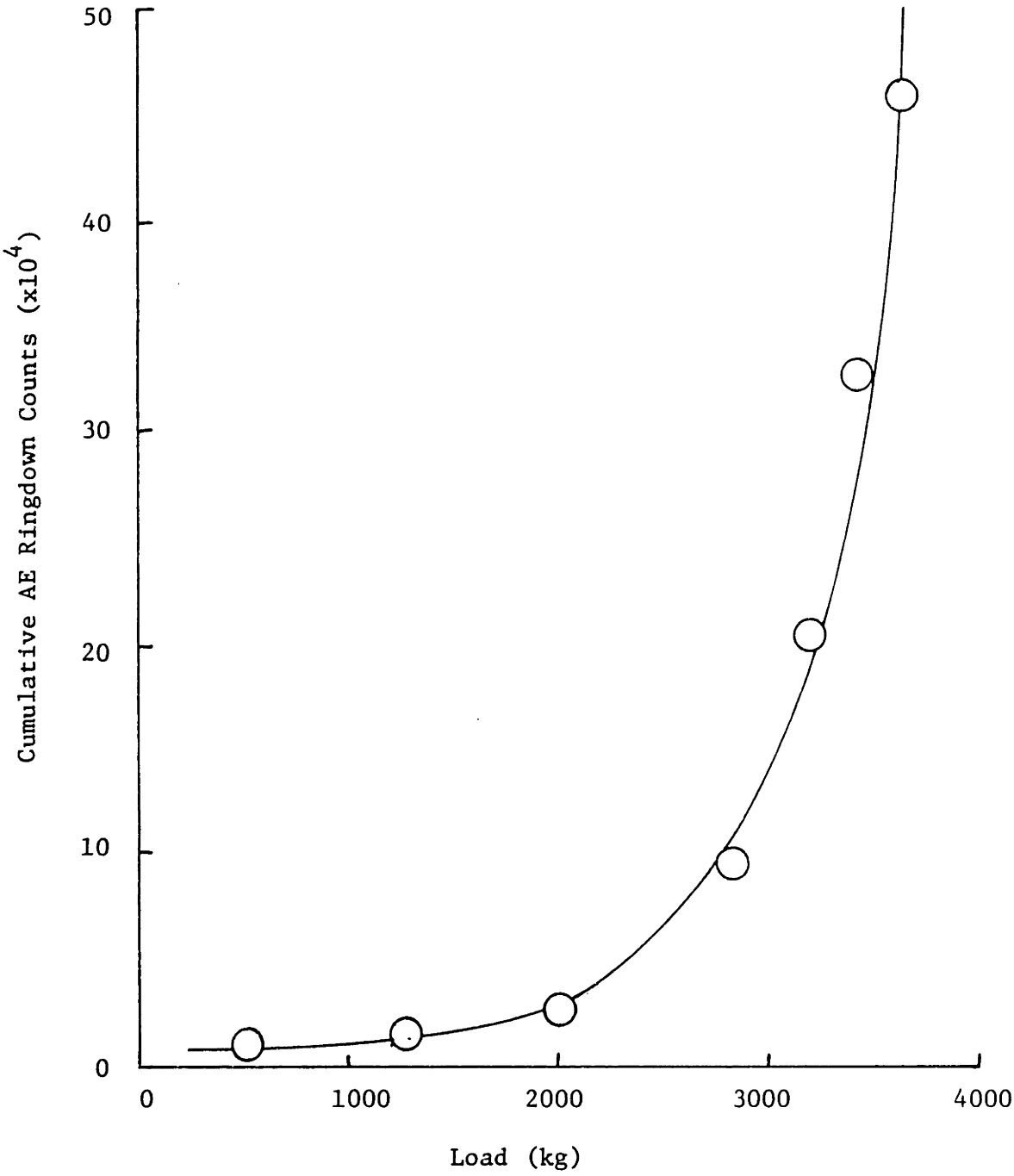

Fig. 13 Cumulative AE ringdown counts versus load [12].

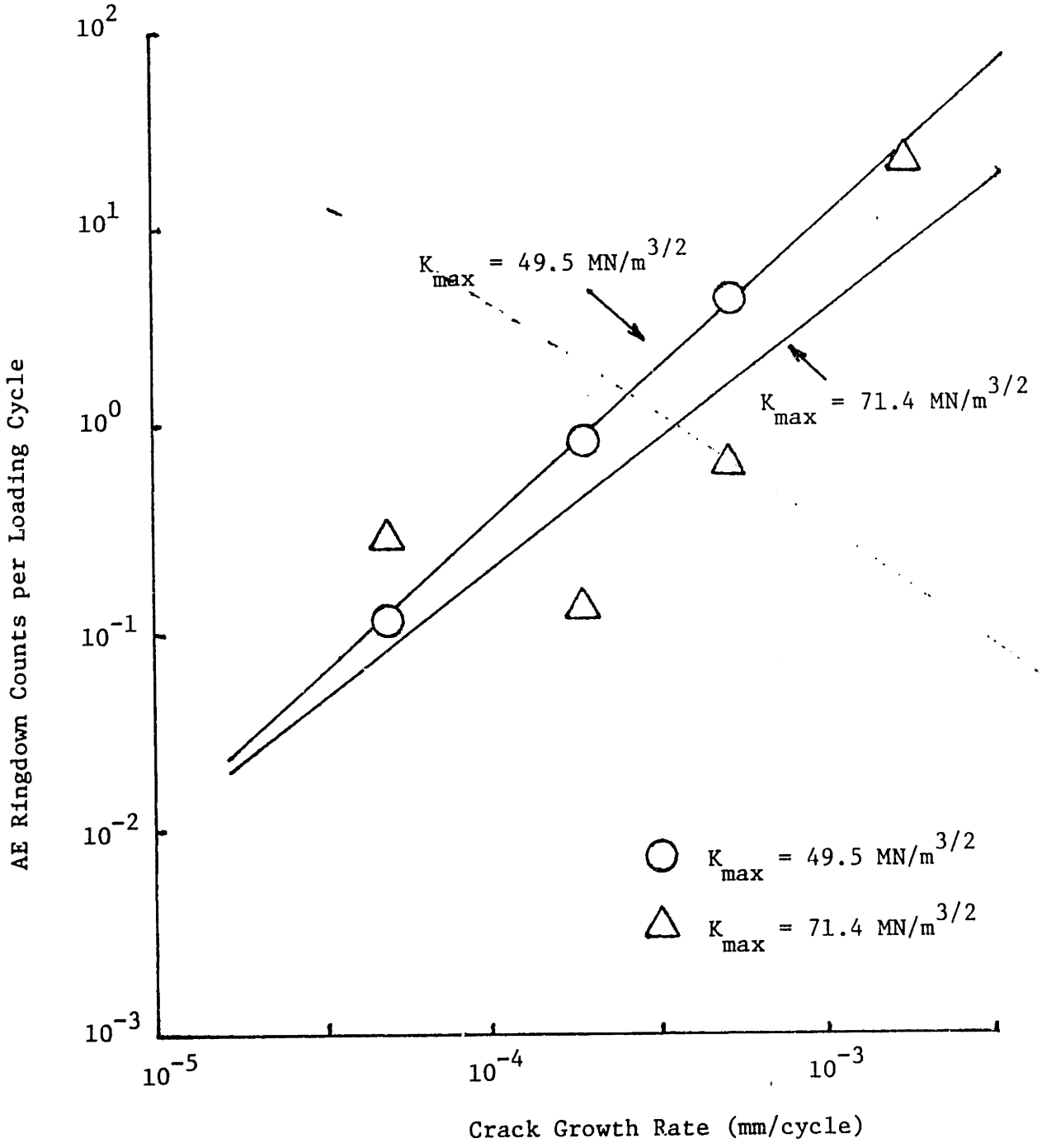

Fig. 14 AE ringdown counts per loading cycle versus crack crowth rate for A36 with initial crack length of 22.5 mm.

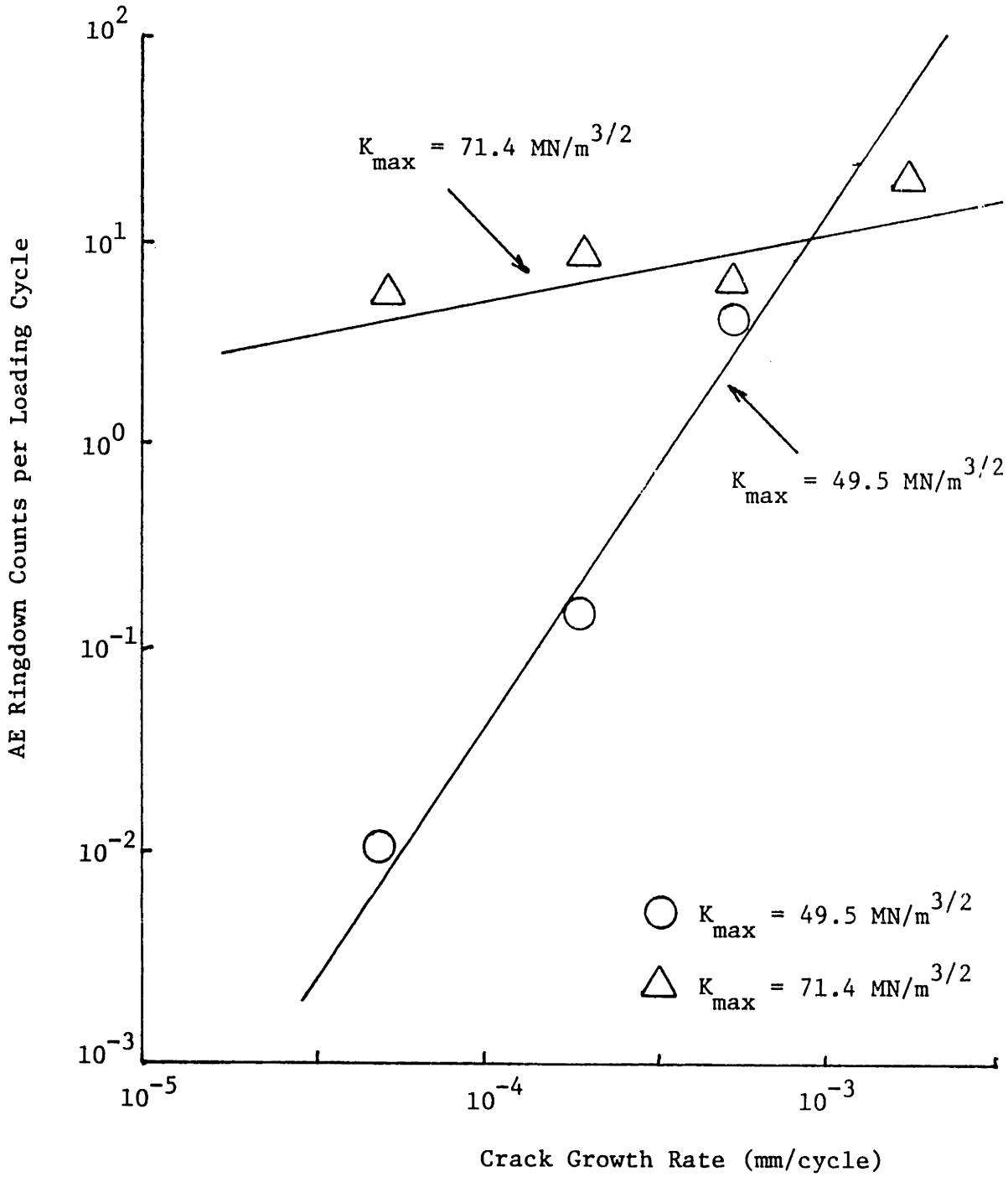

Fig. 15 AE ringdown counts per loading cycle versus crack growth rate fo: A514 with initial crack length of 22.5 mm.

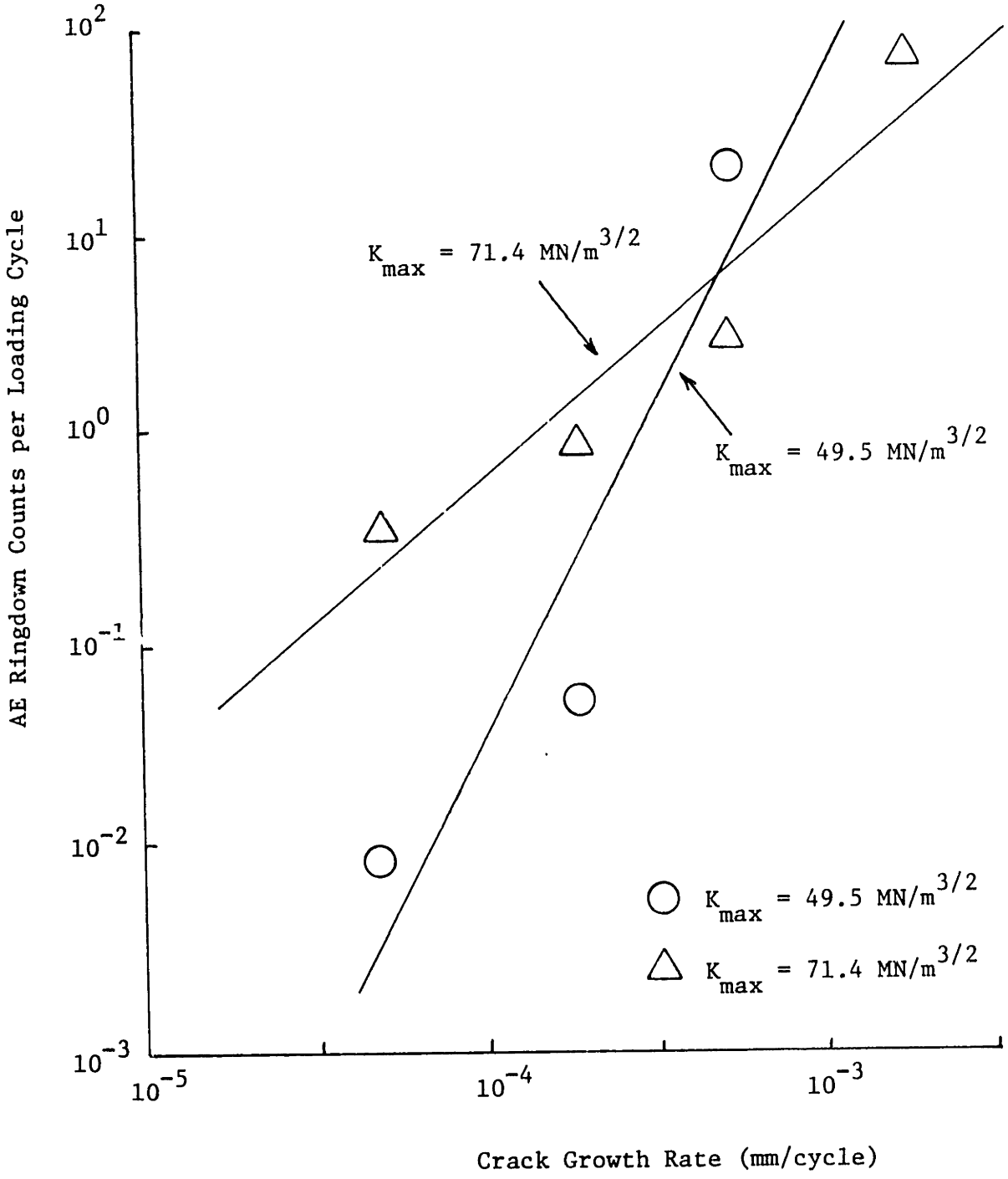

Fig. 16 AE ringdown counts per loading cycle versus crack growth rate for A588 with initial crack length of 22.5 mm.

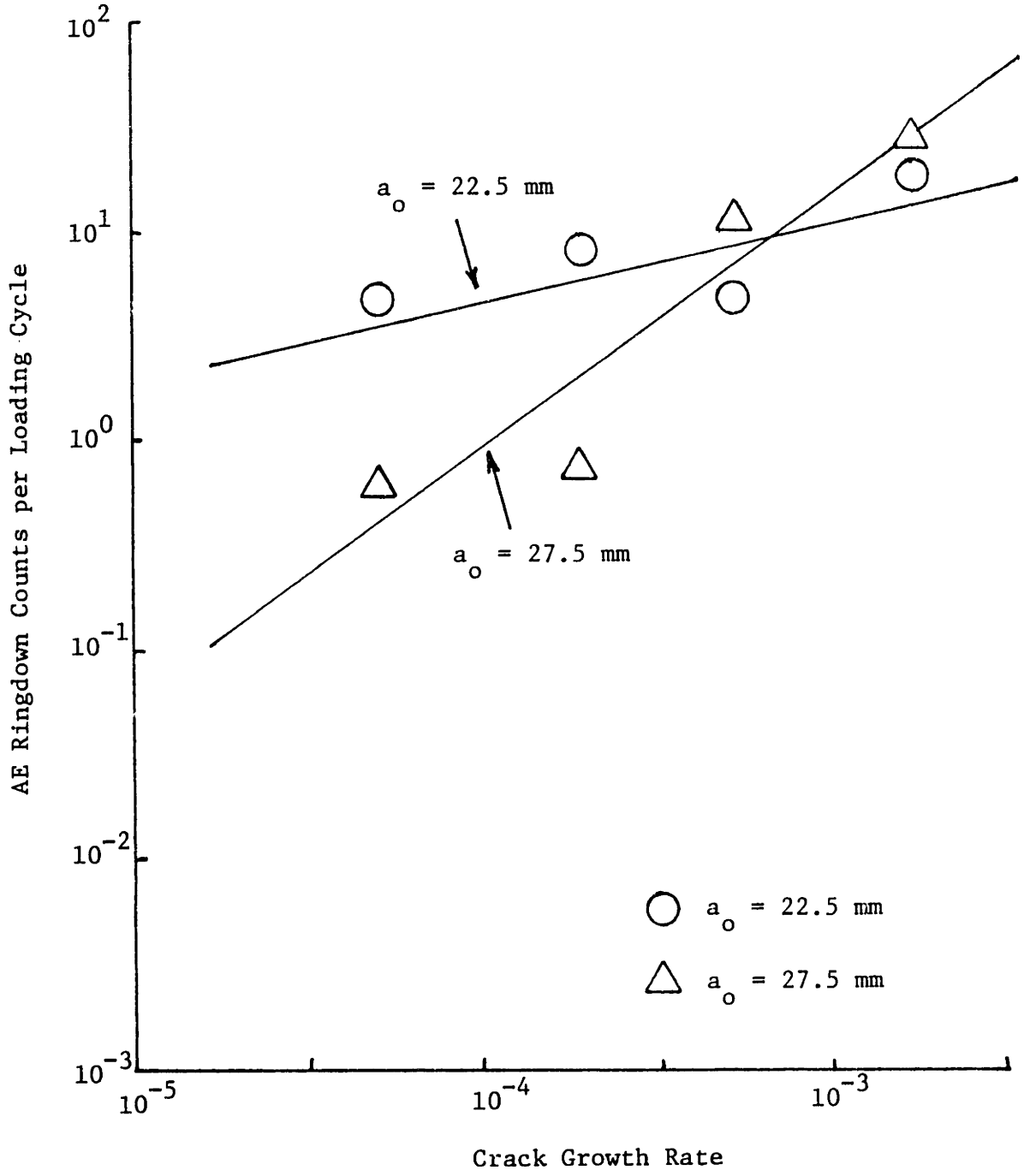

Fig. 17 AE ringdown counts per loading cycle versus crack growth rate for A514 with maximum stress intensity factor of 71.4 MN/m $^{3/2}$.

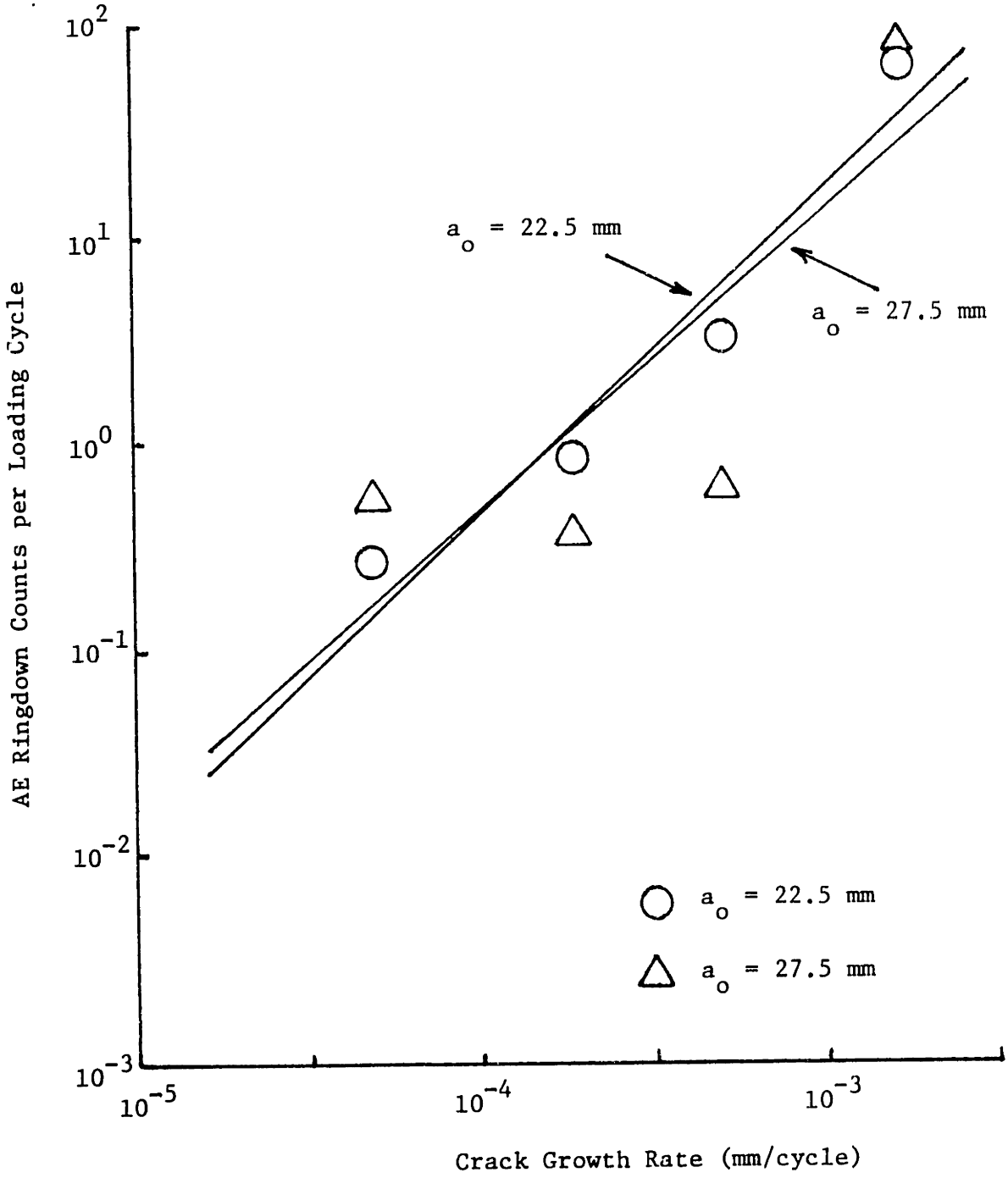

Fig. 18 AE ringdown counts per loading cycle versus crack growth rate for A588 with maximum stress intensity factor of 71.4 $MN/m^{3/2}$.

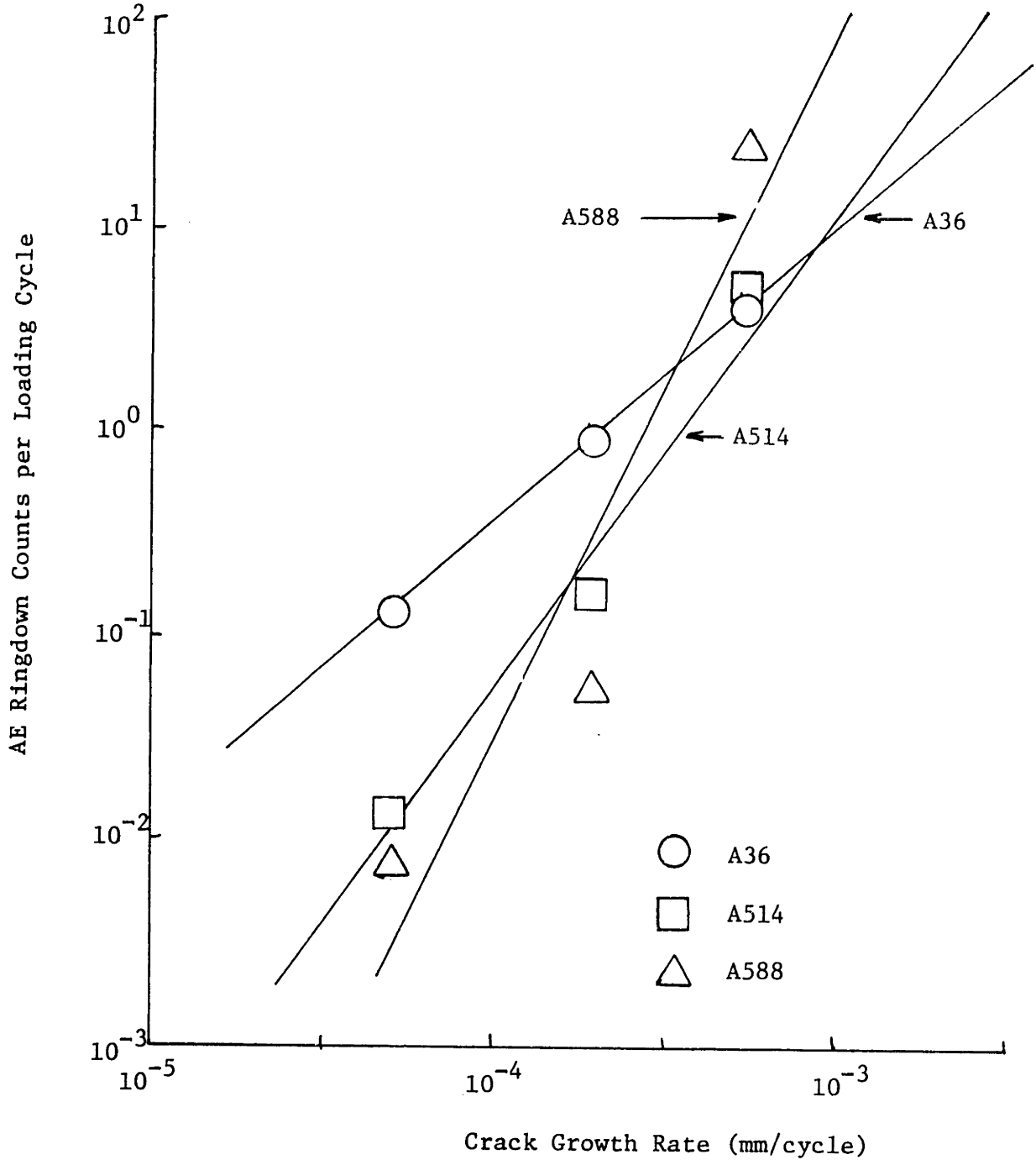

Fig. 19 AE ringdown counts per loading cycle versus crack growth rate for maximum stress intensity factor of 49.5 $MN/m^{3/2}$ and initial crack length of 22.5 mm.

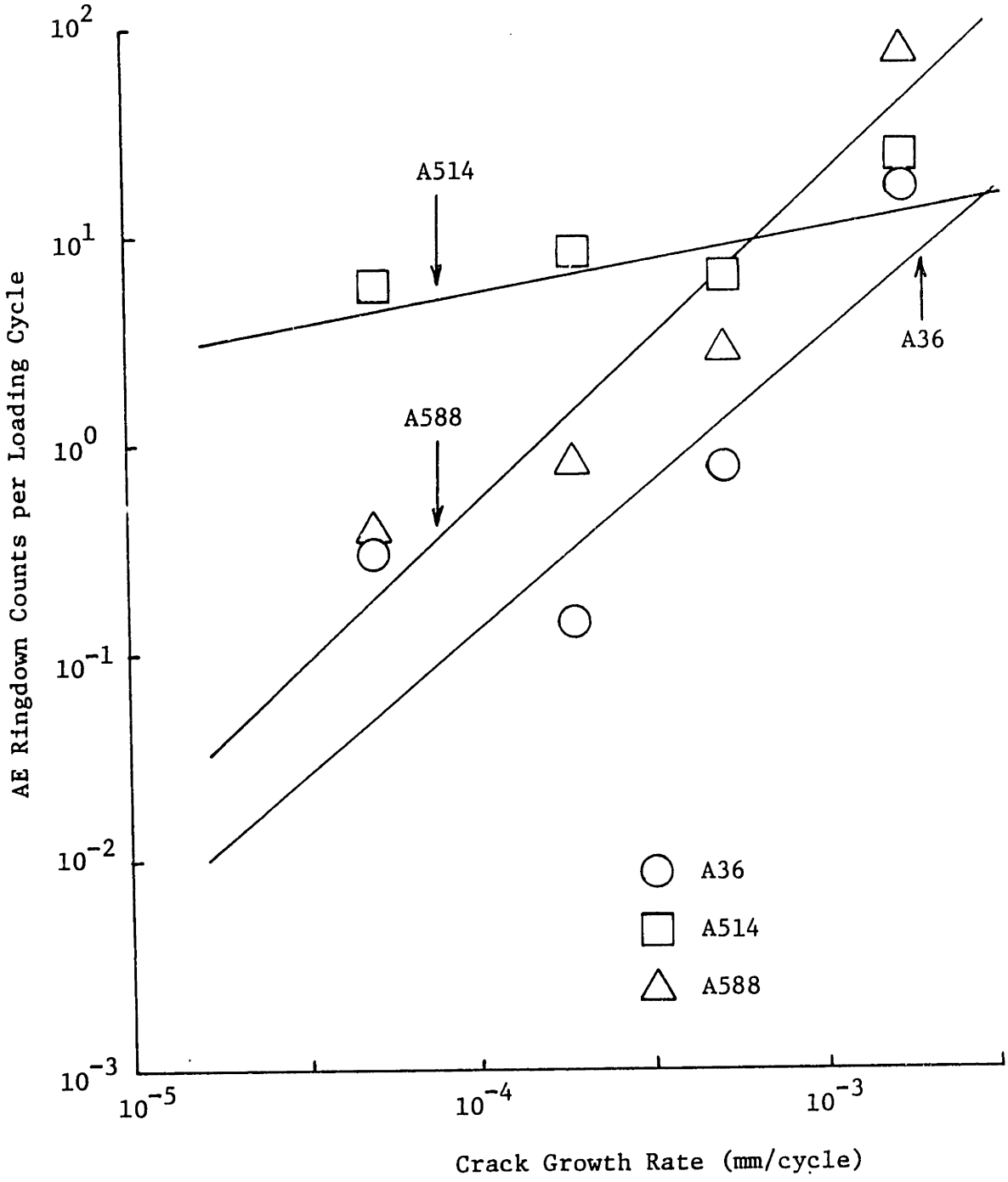

Fig. 20 AE ringdown counts per loading cycle versus crack growth rate for maximum stress intensity factor of 71.4 $MN/m^{3/2}$ and initial crack length of 22.5 mm.

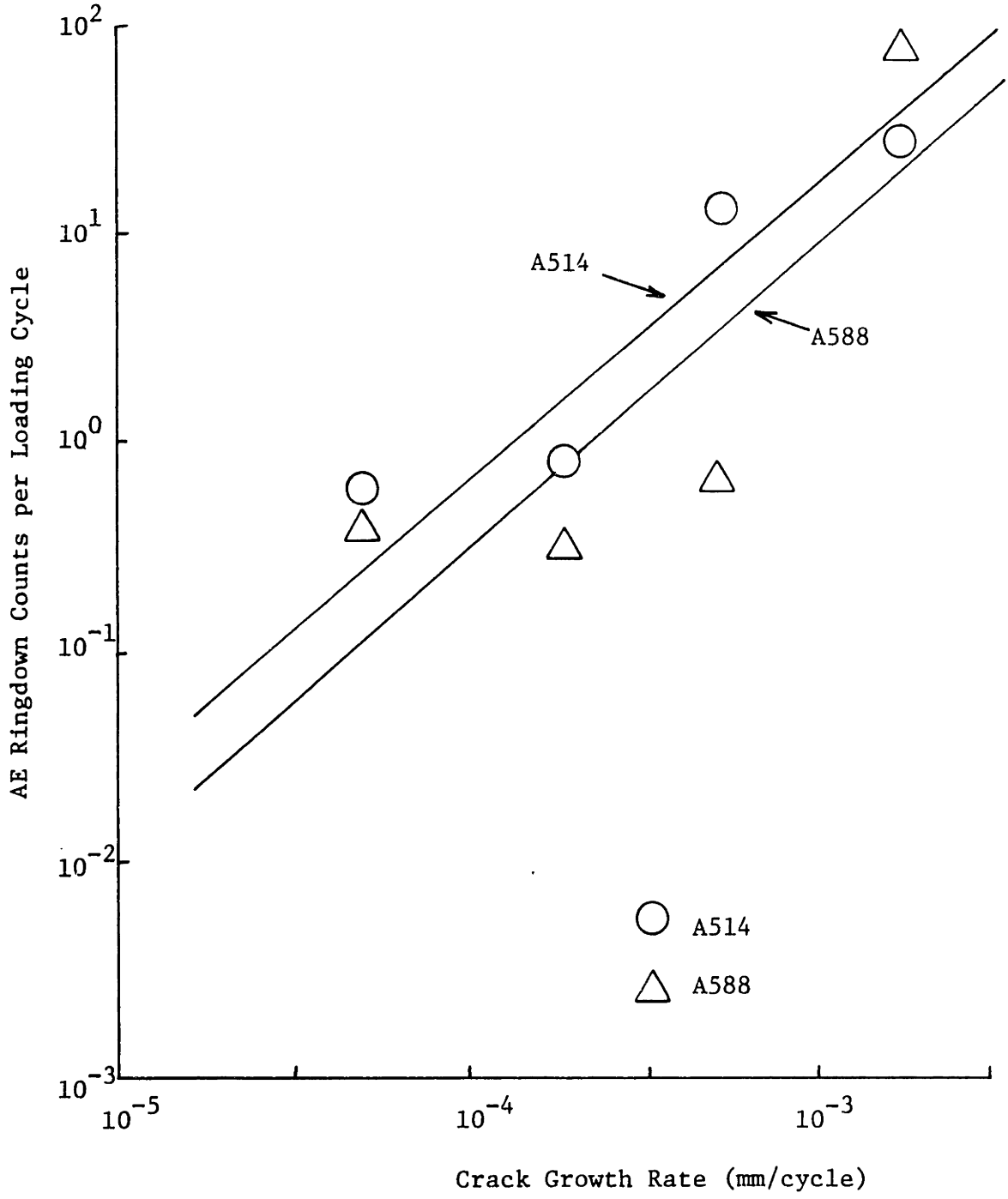

Fig. 21 AE ringdown counts per loading cycle versus crack growth rate for maximum stress intensity factor of 71.4 $MN/m^{3/2}$ and initial crack length of 27.5 mm.

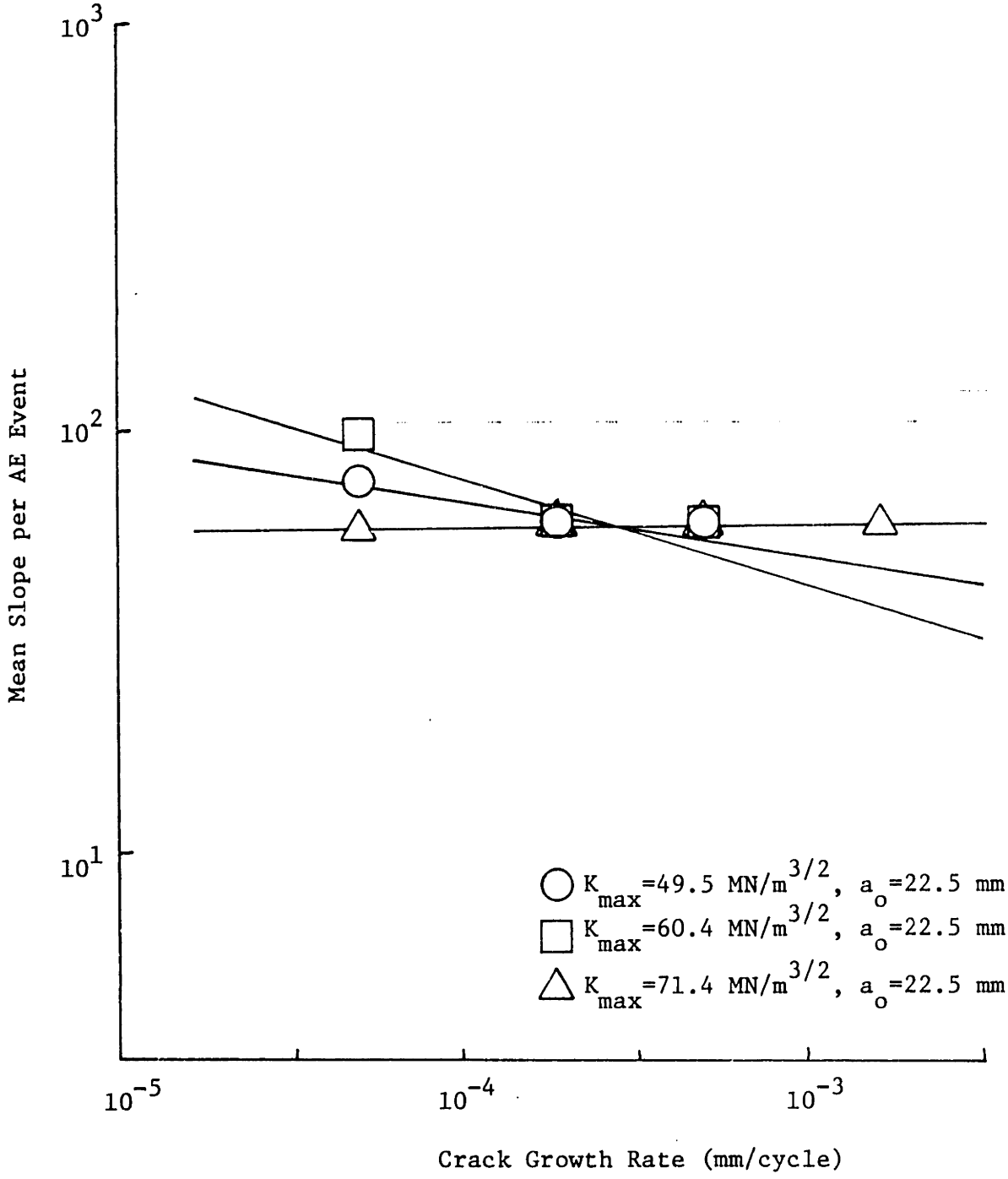

Fig. 22 Mean slope per AE event versus crack growth rate for A36.

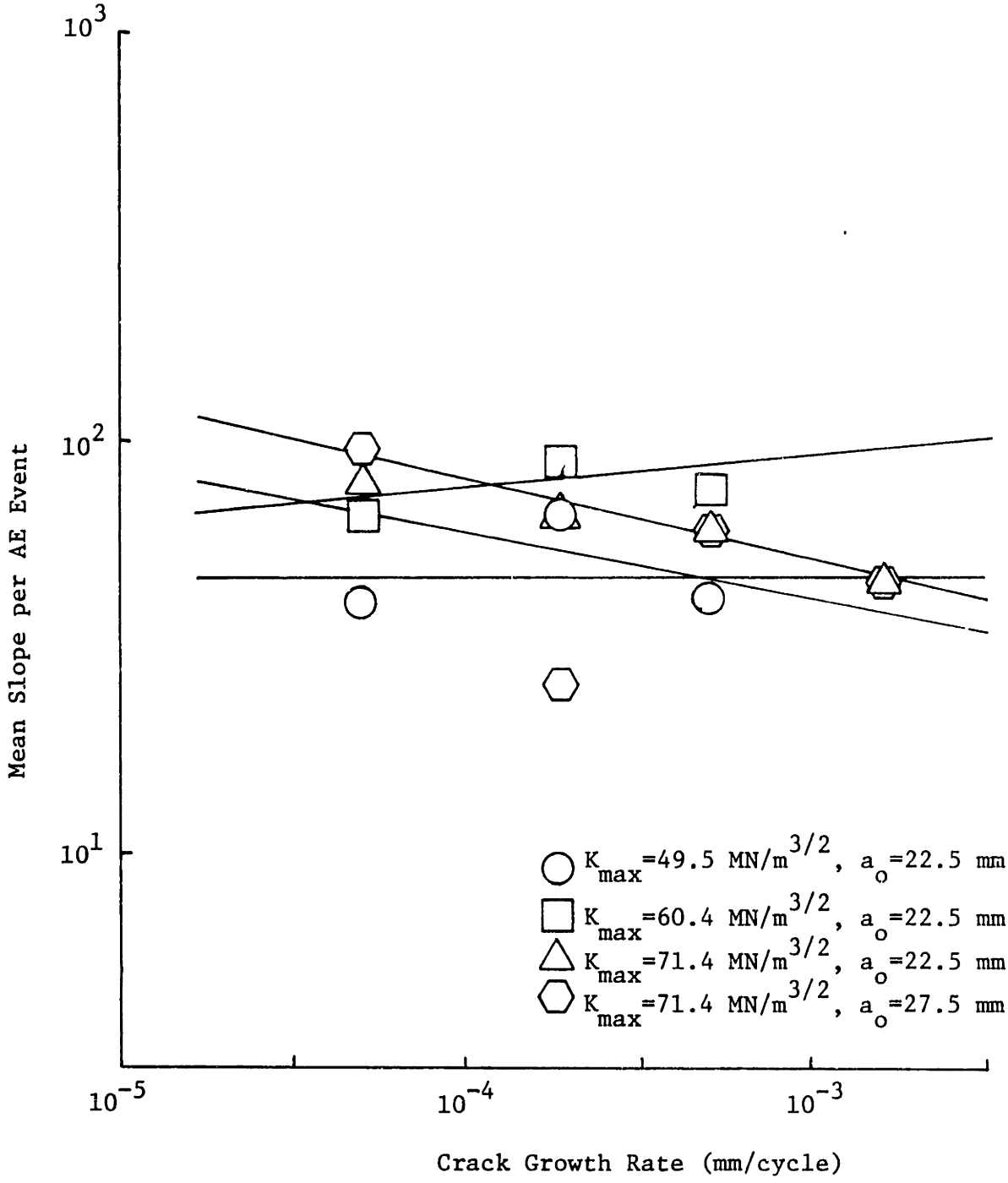

Fig. 23 Mean slope per AE event versus crack growth rate for A514.

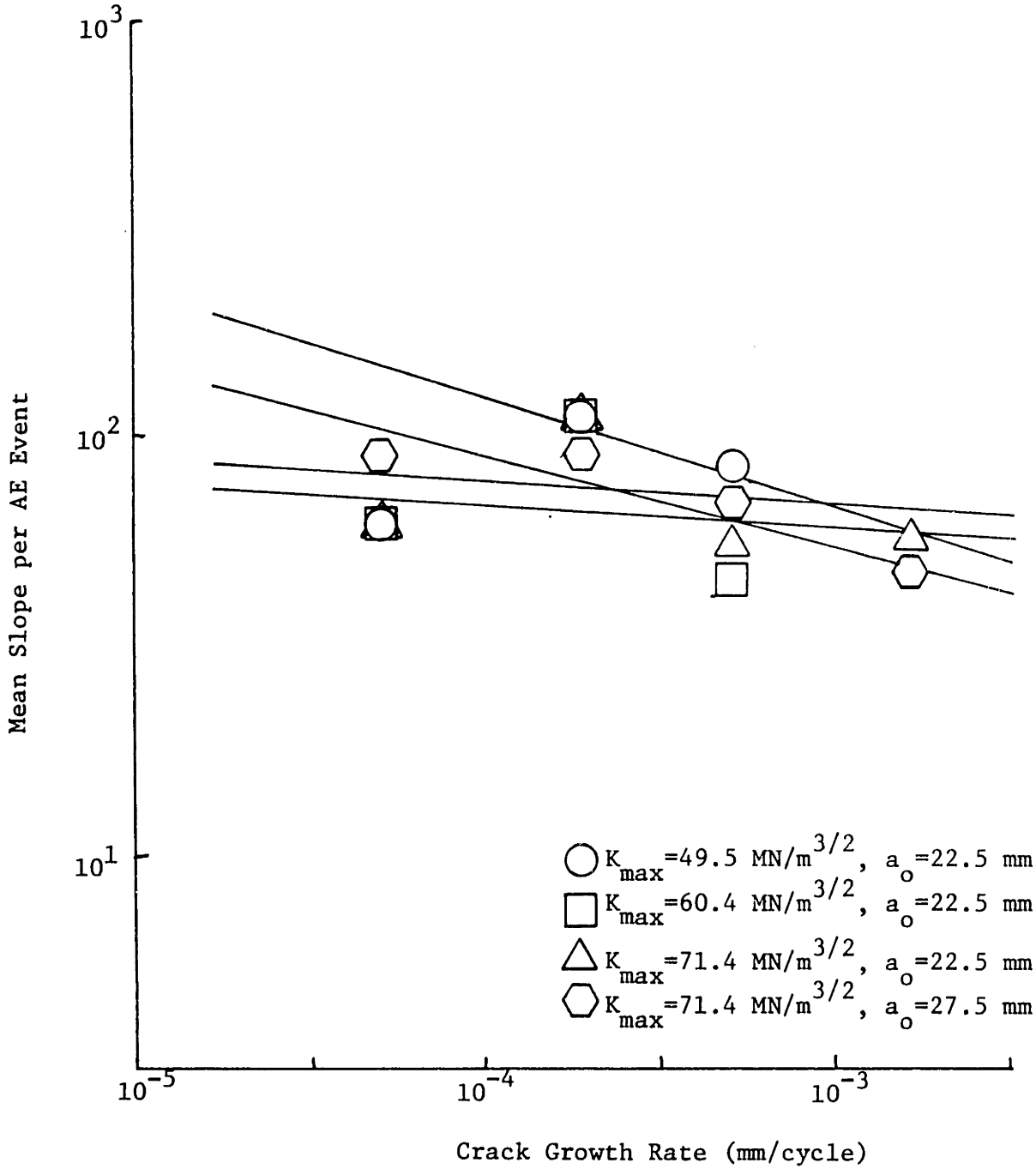

Fig. 24 Mean slope per AE event versus crack growth rate for A588.

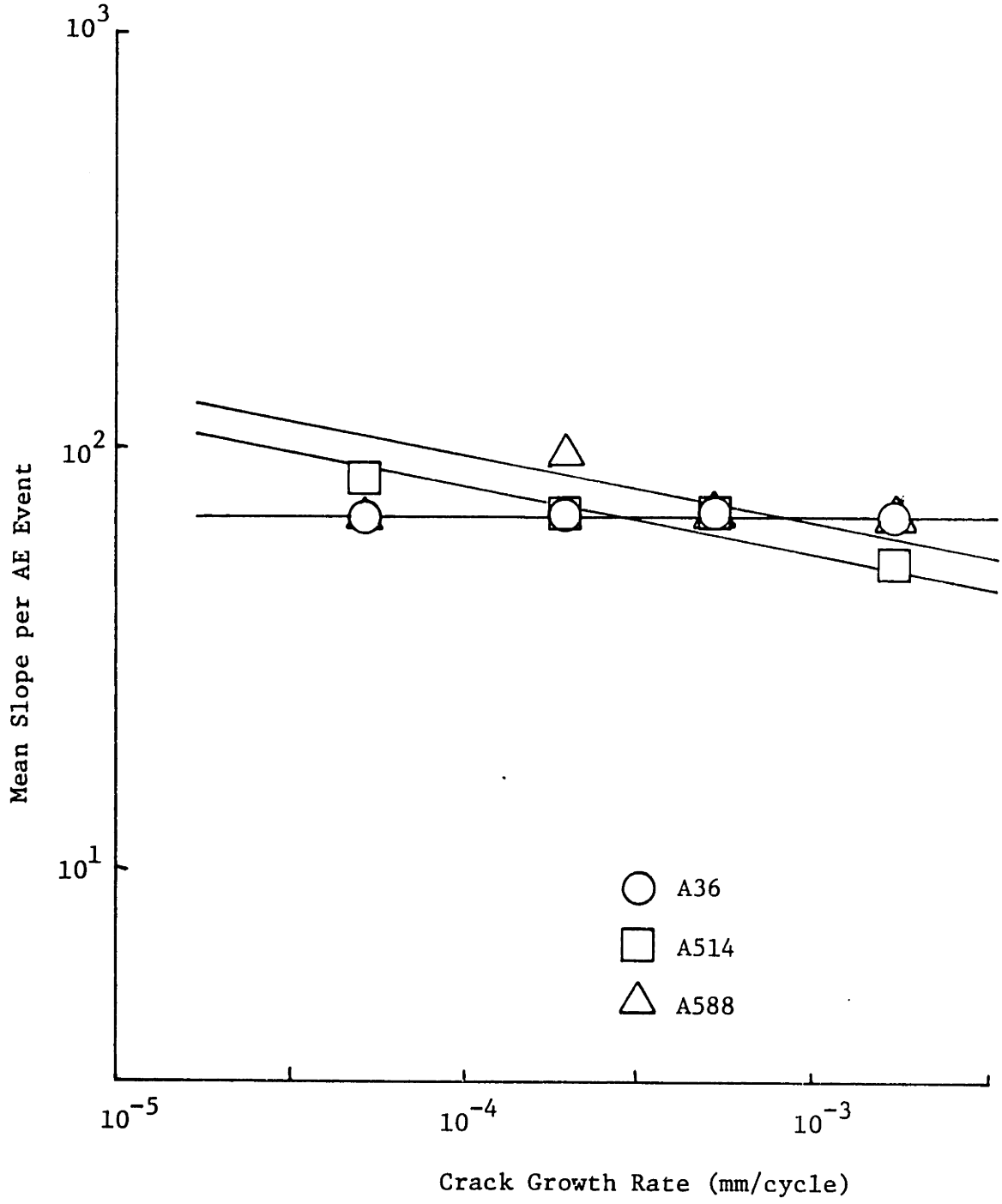

Fig. 25 Mean slope per AE event versus crack growth rate for maximum stress intensity factor of 71.4 $MN/m^{3/2}$ and initial crack length of 22.5 mm.

APPENDIX A

MATERIAL PROPERTIES

The specimens were machined from plates of three common structural steels: A36, A514, and A588. The steel was purchased from a branch of the U.S. Steel Company located in Boston, Massachusetts.

Basically, A36 is a low-strength carbon steel, A514 is a high-strength alloy steel, and A588 is a high-strength low-alloy steel. The characteristics of each material type are presented in Table A-1. A36 and A588, both being ferrite-pearlite steels, have an identical empirical fatigue growth rate curve which is shown in Fig. A-1. A514, which is a martensitic steel, has a slightly different crack growth rate curve which is illustrated in Fig. A-2. Grain size for these materials is on the order of 30×10^{-6} m.

TABLE A-1 Steel Characteristics.

		Material		
		A36	A514	A588
Yield strength (MPa)		248	690	345
Ultimate tensile strength (MPa)		517	827	483
Critical stress intensity factor ($MN/m^{3/2}$)		99	143	143
% Composition	Carbon	0.25	0.15-0.21	0.19
	Manganese	0.80-1.20	0.80-1.10	0.80-1.25
	Phosphorus	0.04	0.035	0.04
	Sulfur	0.05	0.04	0.05
	Silicon	--	0.40-0.80	0.30-0.65
	Nickel	--	--	0.40
	Chromium	--	0.50-0.80	0.40-0.65
	Molybdenum	--	0.18-0.28	--
	Vanadium	--	--	0.02-0.10
	Zirconium	--	0.05-0.15	--
	Copper	0.20	--	0.25-0.40
	Boron	--	0.0025	--

"-" indicates a negligible constituent.

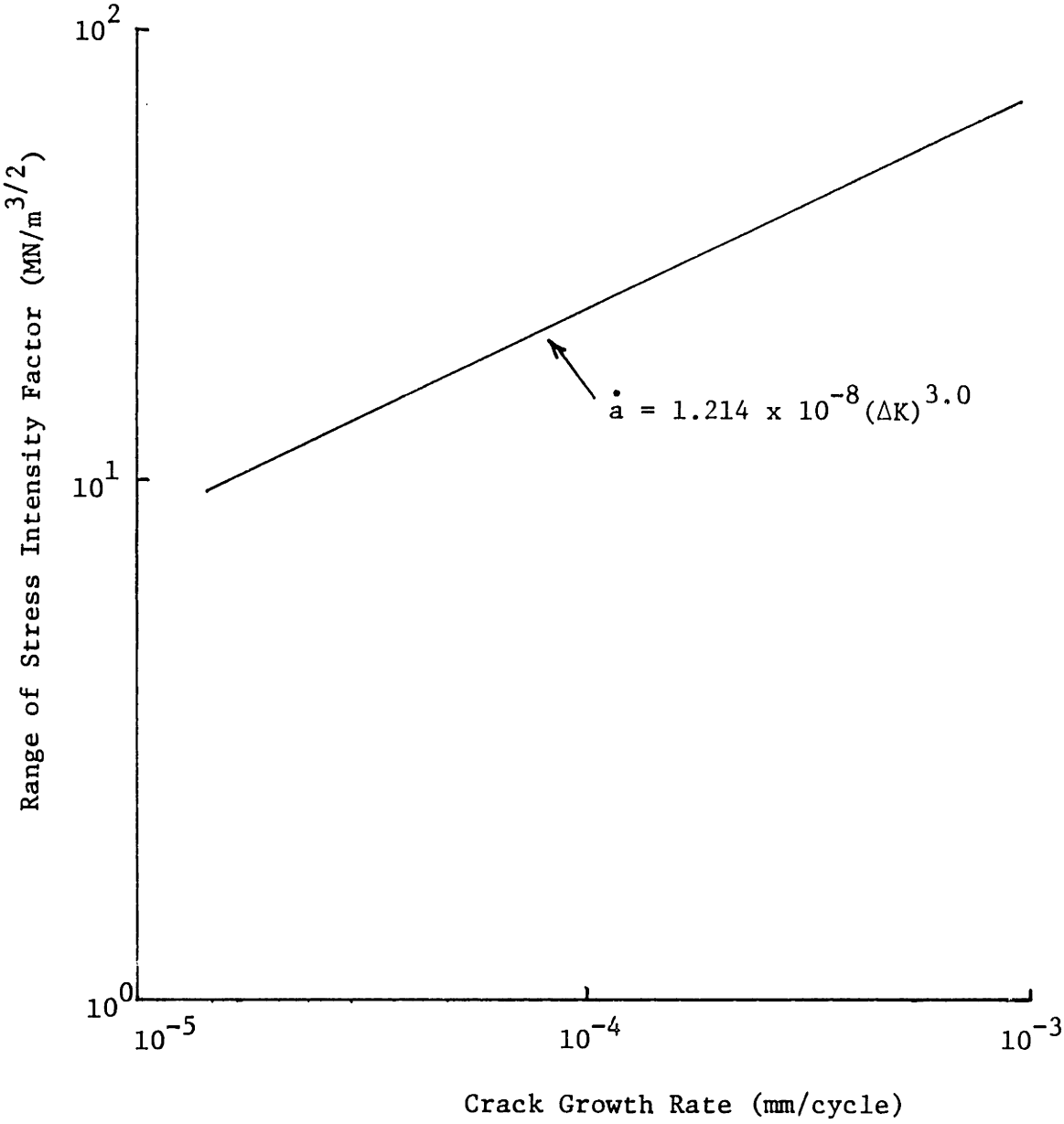

Fig. A-1 Empirical fatigue crack growth rate curve for A36 and A588 ferrite-pearlite steel [18].

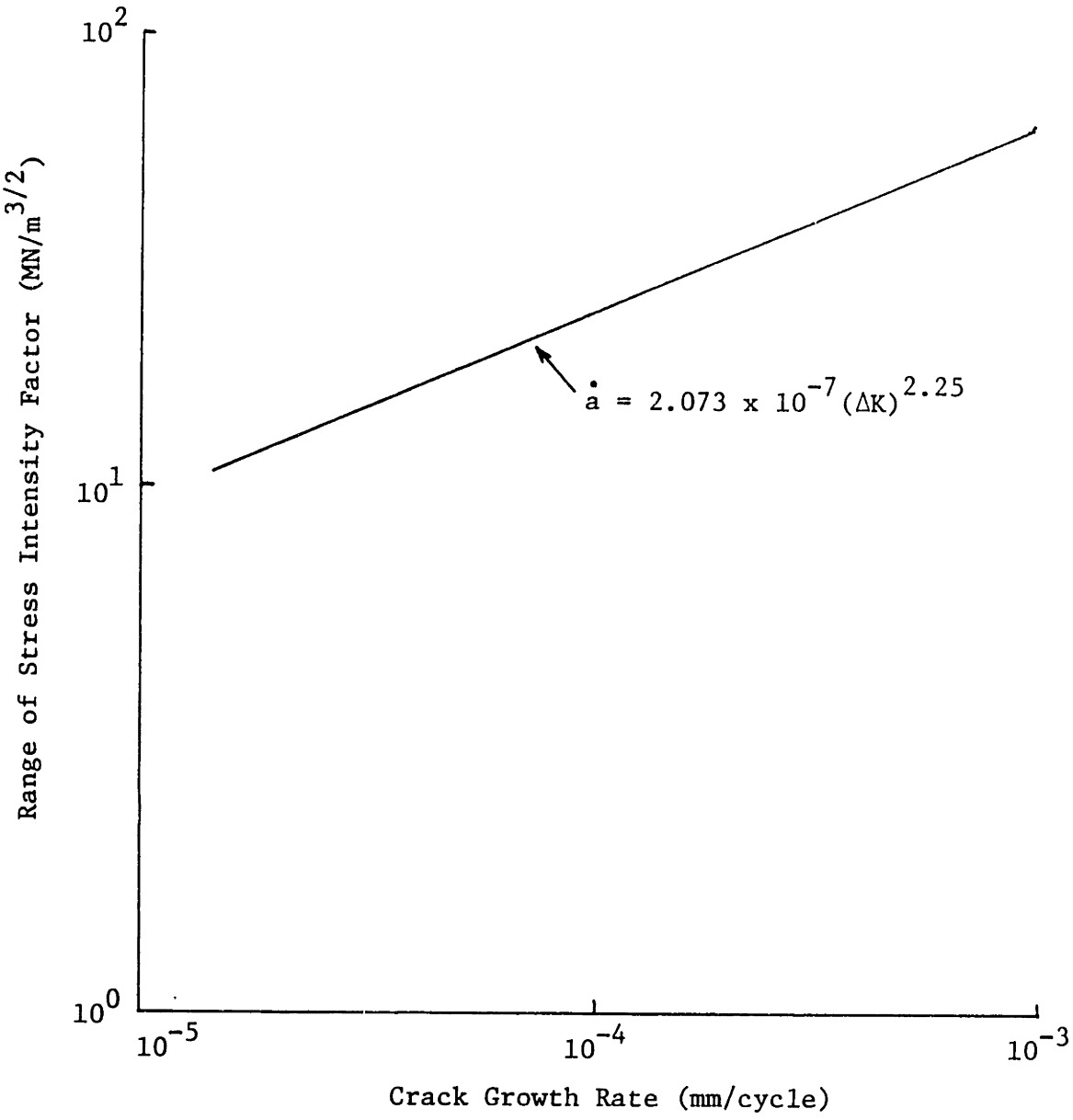

Fig. A-2 Empirical fatigue crack growth rate curve for A514 martensitic steel [18].

APPENDIX B

SPECIMEN CHARACTERISTICS

Fig. B-1 gives the dimensions of the compact test specimens. The function used to determine the stress intensity factor is [19]:

$$K = \frac{P}{B \cdot W^{1/2}} \frac{(2 + \alpha)(.886 + 4.64\alpha - 13.32\alpha^2 + 14.72\alpha^3 - 5.6\alpha^4)}{(1 - \alpha)^{3/2}} \quad \text{(B1)}$$

where:

K = Stress intensity factor ($MN/m^{3/2}$)

P = Applied load (N)

B = Specimen thickness (0.0127 m)

W = Specimen width (0.050 m)

α = a/W, with a = crack length (m)

Notice that the crack length, a, was measured from the center-line of the loading pins. The initial crack length due to the machined fatigue-initiating notch, therefore, was 17.5 mm.

Note also that the rolling direction of the steel was parallel to the axis of the machined fatigue-initiating notch. Specimens prepared in this manner are designated as being in the "T-L orientation".

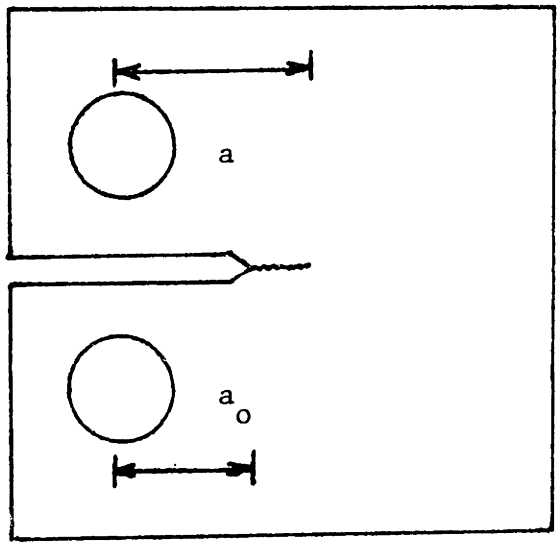

Thickness = 12.7 mm

1 cm

Fig. B-1 Compact test specimen.

APPENDIX C

ACOUSTIC EMISSION MONITORING SYSTEM

An Acoustic Emission Technology AET-5000 acoustic emission system was used for all tests. The AET-5000 is a computer based system which detects, analyzes, and stores processed acoustic emission data from up to four signal channels. Graphic data displays are provided in real time as well as after the completion of the test.

The AET-5000 is based on a 16-bit LS 14/10 micro processor located within a bench-top mainframe of approximately 71 cm x 46 cm x 28 cm. Within the mainframe is a time clock, input/output interface, 36k words of memory for data and display, 16k words of memory for program storage, and various plug in modules for data processing.

The time clock has a basic clock rate of 125 nsec. This clock rate is equivalent to a sampling frequency of 8 MHz. The event duration, rise time, and location clocks have rates which are multiples of the time clock rate. The output displays for event duration and rise time are in terms of clock pulses which can be easily converted to seconds, knowing the particular clock rate.

Acoustic emission signals are detected by up to four sensors. Each sensor output is preamplified 60 dB and frequency filtered before it is fed into the computer. Adjustable postamplification

is available on each channel up to an additional 40 dB.

The AET-5000 calculates the location of an event by comparing the times-of-arrival at two different sensors. A simple algorithm is used to compute from what point the event originated within the specimen. To utilize this algorithm, it is first necessary to determine the acoustic wave propagation speed within the specimen. An acoustic pulser simulates an event which can be used to calculate this velocity. Another method used to simulate an event is the breaking of a small diameter pencil lead adjacent to one of the transducers. This produces a sharp, high-amplitude pulse which is desirable for accurate wave velocity calibration.

A vital feature of the AET-5000 is its capability of signal and/or noise discrimination. The system can be set to accept data from only preselected spatial regions, as well as from ranges of ringdown counts per event, peak amplitude, rise time, slope, or external signal level. The spatial discrimination feature is especially well suited to eliminating grip or loading pin noise while allowing emissions from the particular region of interest to be processed.

Data can be processed and displayed in a large variety of formats. As summarized in Fig. C-1, any parameter (such as ringdown counts), mean parameter per event (such as mean ringdown counts per event), and cumulative parameter (such as cumulative

ringdown counts) can be displayed versus time or an external analog parameter. The distribution (and cumulative distribution) of events by spatial location and other parameters can also be displayed. All plots are presented using linear or logarithmic scales, as desired. Any display can be requested in real time or after the completion of the test, provided the memory space has been allocated for the display prior to the initiation of the test.

Communications with the computer are accomplished through the separate graphic display terminal. Simple keyboard commands control the system, with test parameters such as threshold value set through the terminal. Data displays are presented on a 30.5 cm (diagonally measured) screen on the graphic display terminal. All displays can be further annotated by the user before the hard copy is obtained from the separate hard copy unit. A video printer provides a hard copy on a 12.7 cm wide electrosensitive paper roll.

To facilitate future experimentation in this area, the AET-5000 parameter settings used in these tests are provided in Table C-1.

TABLE C-1 AET-5000 Test Parameter Settings.

Parameter	Setting
Gain	100 dB
Threshold	1.0 v.(fixed)
Interval for time plots	50 sec.
Number of time plot intervals	150
Number of sensors	2
Location of sensors	0, 100
Number of regions	3
Location of regions	0-44, 45-55, 56-100
Event duration clock rate	500 nsec.
Rise time clock rate	250 nsec.
Location clock rate	125 nsec.
Acoustic reset time	0 nsec.
Maximum "Delta Time (DT)"	70 location clock pulses

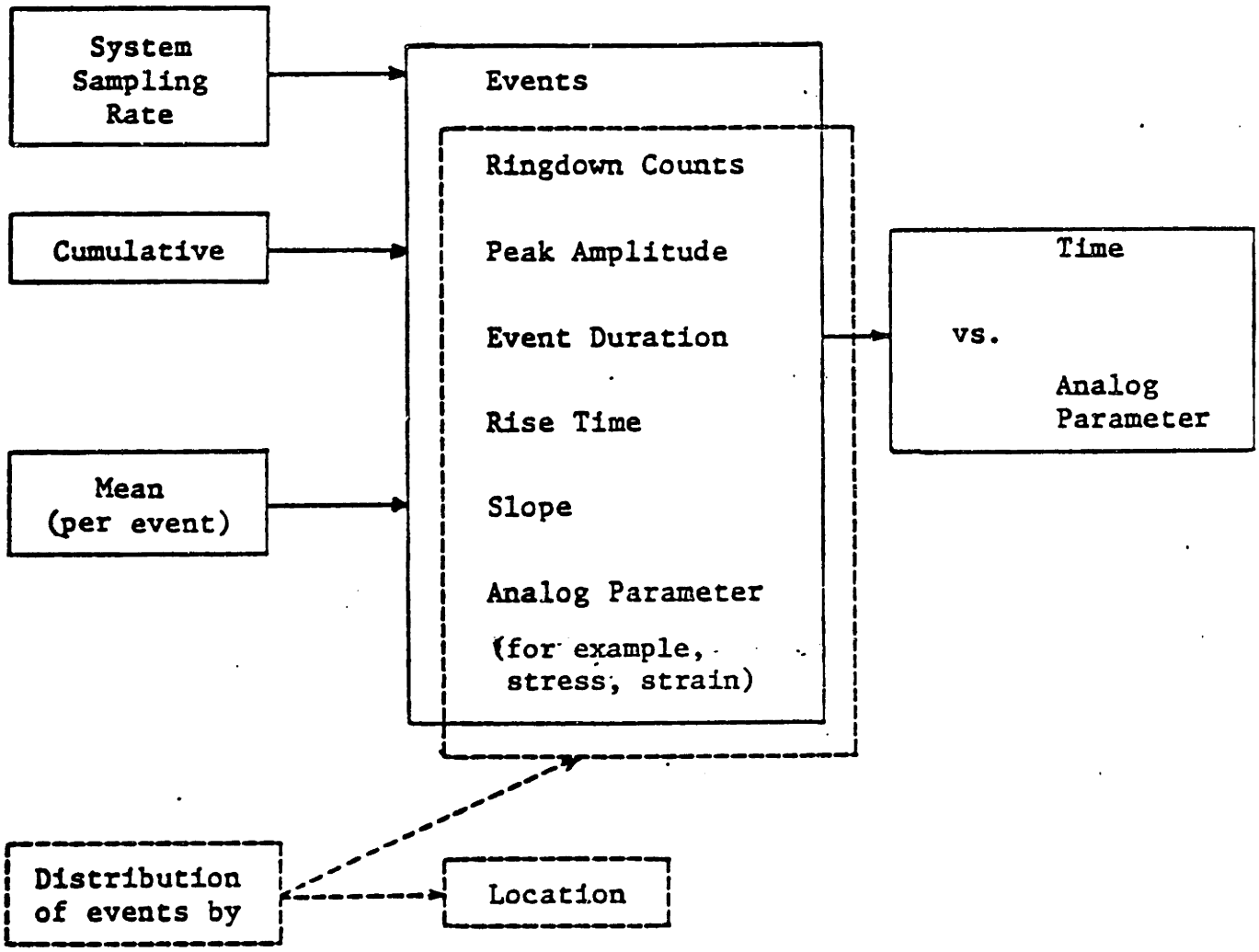

Approximate Number of Displays = 4 x 7 x 2 = 56

Fig. C-1 Schematic of available data displays on AET-5000.

APPENDIX D

FATIGUE TEST SYSTEM

Two fatigue test systems were used for these experiments: an Instron model 1350-10 with electric potential crack length monitoring system for pre-cracking the specimens, and a Materials Testing System model 810.14A for fatiguing the specimens during acoustic emission monitoring.

The Instron model 1350-10 is a servo-hydraulic fatigue system with a fatigue load rating of ± 44kN. A separate controller is provided for load, stroke, and strain control. A function generator is used to generate waveforms with a loading frequency up to 100 Hz. The electric potential crack length monitoring system operates by passing a constant current of about 40 amp through the specimen, and measuring the resulting potential difference across the crack. As the crack extends, the uncracked cross-sectional area of the specimen decreases, thus increasing the electrical resistance and the potential difference across the crack. The use of suitable calibration curves enables the crack length to be determined from this potential difference. The system has been found to be capable of measuring absolute crack length to within 0.1 mm, and to detect changes in crack length of 0.01 mm [20].

A Materials Testing System (MTS) model 810.14A was used to load the specimens during the acoustic emission experiments. The MTS is

a hydraulically operated axial test machine equipped with a Digital Equipment PDP 11/05 computer for automatic control and data acquisition. Fatigue tests under load, stroke, or strain control are possible using the 50 metric ton load frame and the control console for manual operation.

The primary machine controls are a MTS 413 Master Control Panel which houses the main power switch and hydraulic pump controls, and a MTS 442 Controller which has potentiometers to set the mean level and oscillating amplitude of the load, stroke, or strain. An inner panel on the controller is used to set load, stroke, and strain calibration and their maximum allowable ranges. Finally, a MTS 417 Counter Panel totals the number of load cycles applied during the fatigue test.

A MTS 410 Digital Function Generator supplies input signals of the desired waveform to drive the hydraulic ram. A Tektronix D11 double beam storage oscilliscope (with two 5A15N amplifiers and a 5B10N time base) is used to display both the signal from the function generator and the response signal from the hydraulic ram or load cell. A MTS 430 Digital Indicator and a MTS 431.12 x-y recorder are used to read and record these input and response signals.

The load frame, shown in Fig. D-1, accommodates a load train (specimen and grips) up to 127 cm in length. The actuator or ram, which is housed in the frame platform, has a 15.2 cm maximum stroke

and a 13.7 cm diameter. A MTS 661.23A-02 load cell is mounted within the crosshead. It detects load via strain gauges and has a capacity of 50 metric tons. The practical accuracy of the load measurement is limited by the load cell to within 110 N. The practical accuracy of the stroke measurement is to within 0.1 mm.

Fatigue cycling can be accomplished between 35 metric tons tension and 35 metric tons compression. The maximum possible loading frequency for a given load depends on the stiffness of the load train. The mean and amplitude levels of the deflection sine wave signal are set on the MTS 442 Controller. The "set point" potentiometer assigns the mean value and the "span 1" potentiometer sets the oscillating amplitude for the fatigue test.

It was found that when using standard steel grips to load the specimen, excessive noise was transmitted from the hydraulic ram through the load train which made acoustic emission detection impossible. Special grips therefore had to be fabricated to acoustically isolate the specimen from the test machine.

A diagram of the grips designed and utilized in the experiments is given in Fig. D-2. 10 cm lengths of 15 cm square steel tubing with a thickness of 1 cm formed the foundation for the grips. Two 2.5 cm thick nylon blocks, insulated from each other with 4 mm thick rubber sheets, were placed within the square tubing. The shaft leading to the specimen passed through a large hole drilled into the middle of the nylon and rubber. The resulting arrangement

did not allow any metal-to-metal contact between the test machine and the specimen, and was found to completely eliminate noise. Nylon and rubber were selected because of the relatively high attenuation they offer to acoustic wave propagation. Fig. D-3 is a photograph of the grips in place for a typical experiment.

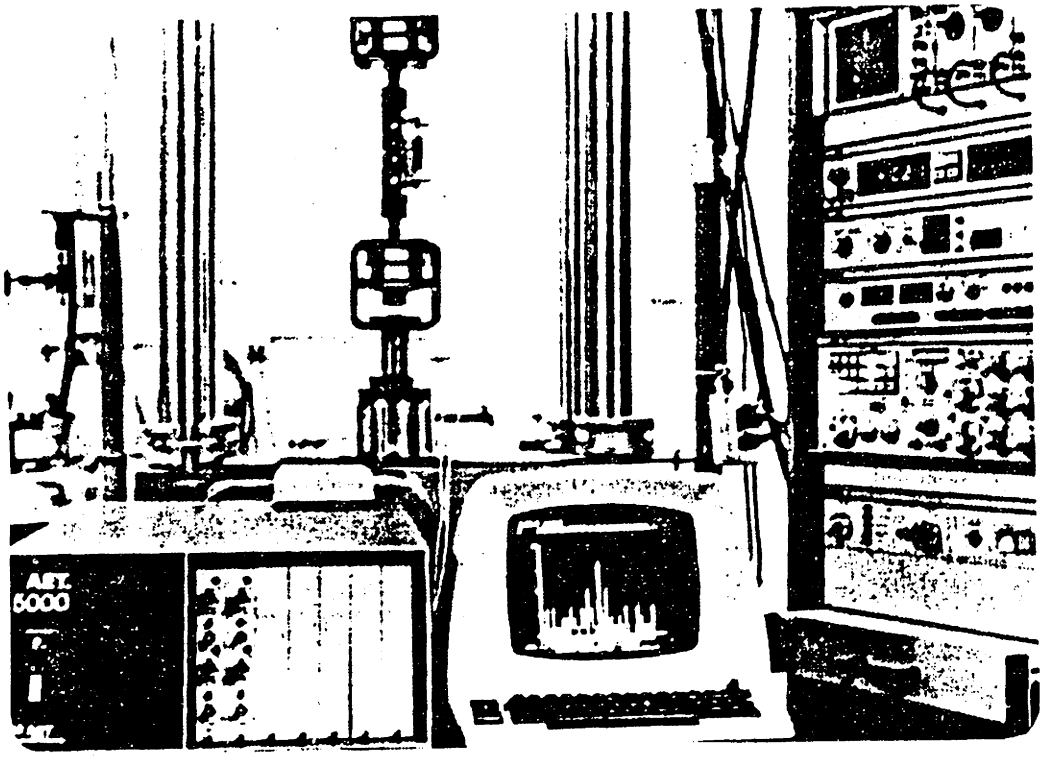

Fig. D-1 Photograph of fatigue testing system.

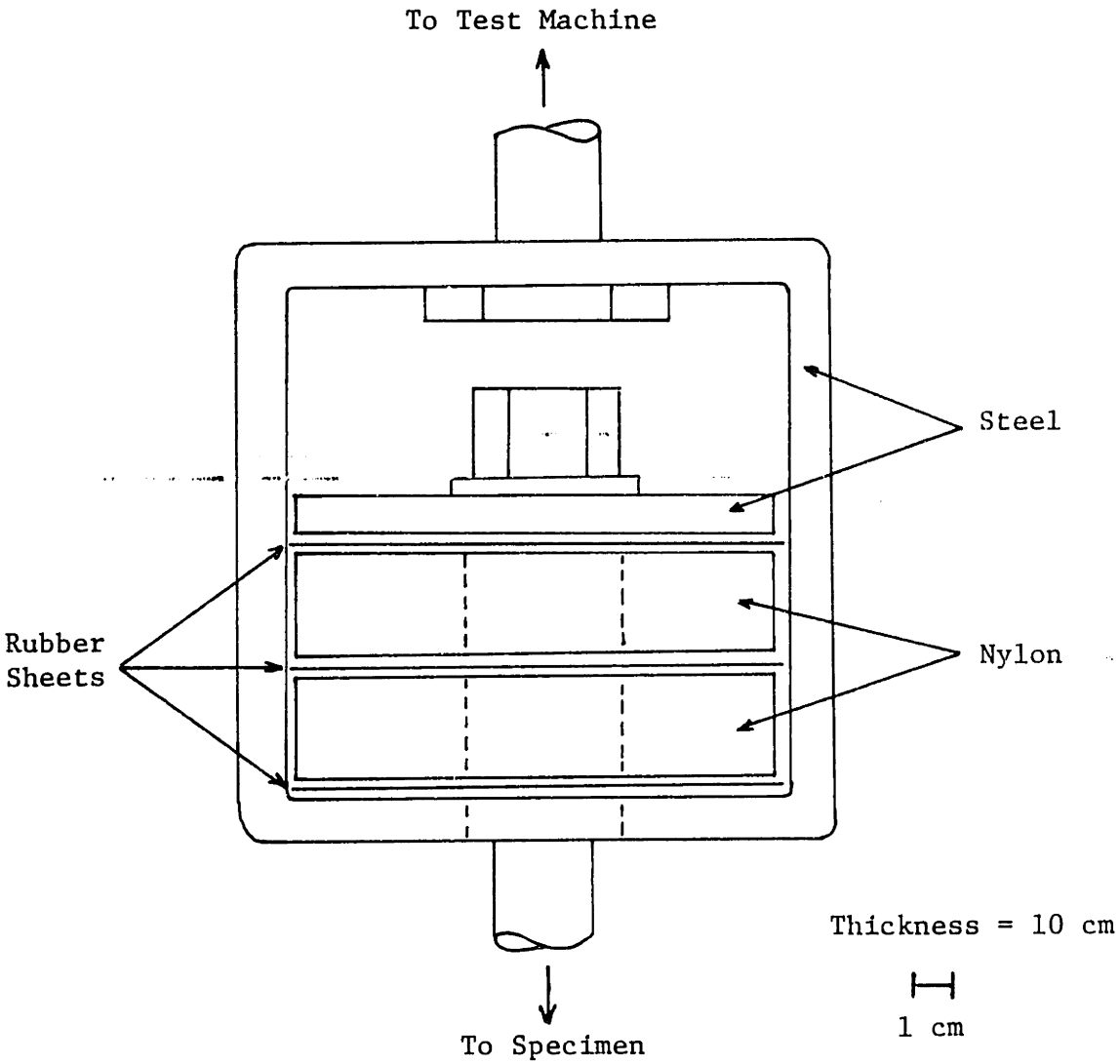

Fig. D-2 Sound isolating grip arrangement.

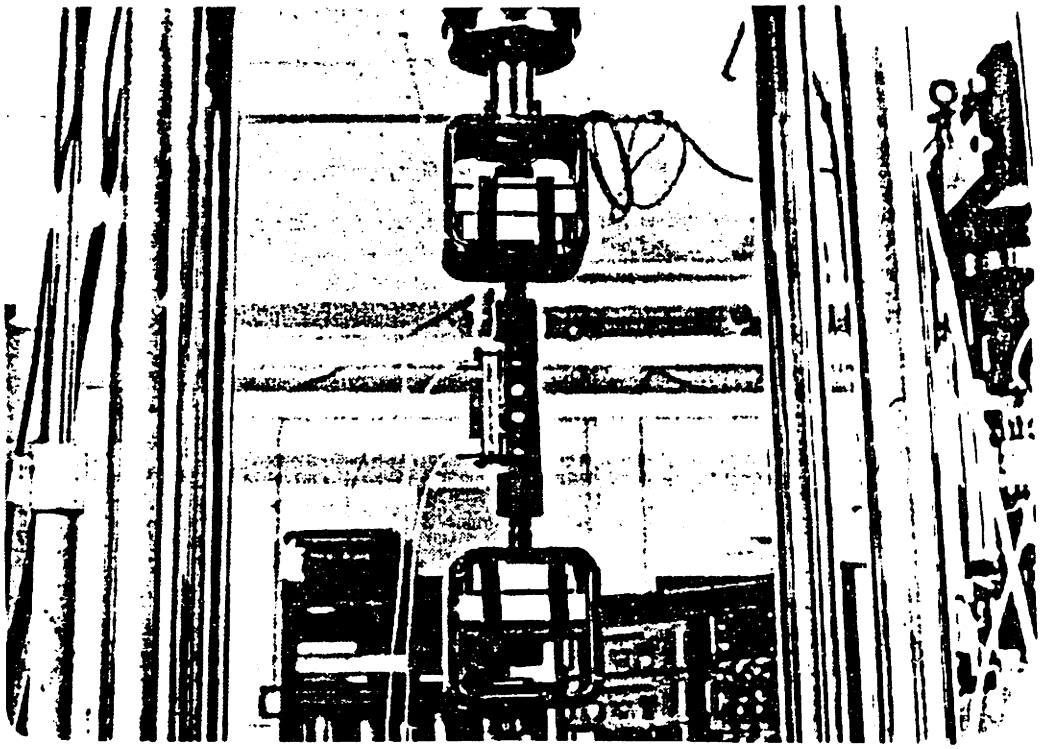

Fig. D-3 Photograph of sound isolating grips.

APPENDIX E

EXPERIMENTAL PROCEDURE

Specimen Preparation

The specimens, as delivered after production, were unsuitable for immediate fatigue testing due to the effects of machining at the crack-initiating notch. A fatigue crack therefore had to be propagated for a distance of at least several millimeters before it would follow the empirical crack growth rate curve. Pre-cracking was also necessary to obtain the different initial crack lengths that were variables in the experimental test matrix.

Pre-cracking was performed on an Instron fatigue testing system which was equipped with an electric potential crack length monitoring apparatus. The specimen was placed in the grips using insulated connectors, and the appropriate current and potential leads were attached to the electric potential system.

The pre-crack had to extend for either 5 or 10 mm, depending on the particular test for which the specimen was to be used. This resulted in an initial crack length of 22.5 or 27.5 mm for the acoustic emission tests. Note that the machined notch gave a starting crack length of 17.5 mm. A minimum and a maximum load were desired for the pre-cracking which would result in a fast-growing crack, but at the same time not create a plastic zone in the specimen that would exceed the plastic zone to be used during the

acoustic emission experiments. This precaution was necessary because of the possibility of crack arrest due to previous overloads. Since plastic zone size was determined by the maximum stress intensity factor, K_{max} (which is a function of load and crack length), it was necessary to limit the maximum load applied so that at the longest pre-crack length the K_{max} would be below the values that would be used during the experiments.

It was determined that if a maximum load of 15.4 kN and a minimum load of 0.9 kN were used for pre-cracking, the resultant K_{max} would be 46.2 and 62.0 $MN/m^{3/2}$ at crack lengths of 22.5 and 27.5 mm, respectively. The lowest K_{max} value planned in the tests for a specimen with a_o = 22.5 mm was 49.5 $MN/m^{3/2}$, and the lowest K_{max} value planned in the tests for a specimen with a_o = 27.5 mm was 71.4 $MN/m^{3/2}$. Therefore, the loads could remain constant as the crack grew and not result in any specimen damage that would affect future tests.

The specimens were fatigued at these loads until the crack length monitoring system indicated that the crack had propagated for the desired distance. The actual time needed to propagate the pre-crack was typically less than 10 minutes for all steel types.

Acoustic Emission Monitoring of Fatigue Crack Growth

After pre-cracking had been accomplished, the specimens were ready for acoustic emission testing. The MTS fatigue system was

used for this phase of the experiments.

The experimental test matrix is shown in Table E-1. One specimen from each steel type was used in each test. The empirical crack growth rate curves were used to calculate the necessary range in stress intensity values that would result in the desired growth rates. The range in stress intensity values was then converted into a range of load levels. For this purpose, the crack length was assumed to remain constant at the initial crack length because of the low growth rates and number of loading cycles to be applied. Finally, the K_{max} values were converted to maximum loads. Knowing the maximum load and the range in loads desired made it possible to calculate the mean and oscillating amplitude load for each test.

Several preparations were necessary before conducting an experiment. First, the AET-5000 system was set with its test parameters. The specimen was then mounted in the grips and the sensors attached. Acoustic Emission Technology AC-375 (375 kHz) resonant transducers were used with AET SC-6 acoustic couplant. The transducers were held on the specimen using a common hose clamp with rubber insultators to prevent metal-to-metal contact. A photograph of the specimen ready for testing is shown in Fig. E-1.

The calculated load levels were then set on the MTS Fatigue machine. The load range was selected in which a 10 volt signal from the controller would correspond to a load level of 48.4 kN. The mean and amplitude levels were thus converted into a voltage

reading, which was then entered into the "set point" and "span 1" controls, respectively. The frequency of loading was set at 0.1 Hz due to the excessive compliance in the grips which made operation under load control at higher frequencies difficult.

The test was then started simultaneously on the AET-5000 and the MTS. Each test was run for 500 cycles, which took about 83 minutes at 0.1 Hz. At that time, the function generator was stopped and the acoustic emission test terminated. The data plots were then recalled from the AET-5000 memory, from which a hard copy was made on the printer.

The load level was then changed to the necessary values for the next crack growth rate. Note that each specimen was tested at several crack growth rates, starting with the lowest rate. No external provision was made to measure crack length or growth rate, as the specimen was assumed to follow the empirical growth curve. Additionally, a record was kept of the load levels and number of loading cycles that each specimen underwent during the testing. A photograph of the complete testing sysem is shown in Fig. E-2.

TABLE E-1 Experimental Test Matrix.

Test No.	Initial crack length (mm)	Stress intensity factor ($MN/m^{3/2}$)	Crack growth rate (mm/cycle)
1	22.5	49.5	5.1×10^{-5}, 1.8×10^{-4}, 5.1×10^{-4}
2	22.5	60.4	5.1×10^{-5}, 1.8×10^{-4}, 5.1×10^{-4}
3	22.5	71.4	5.1×10^{-5}, 1.8×10^{-4}, 5.1×10^{-4}, 1.5×10^{-3}
4	27.5	71.4	5.1×10^{-5}, 1.8×10^{-4}, 5.1×10^{-4}, 1.5×10^{-3}

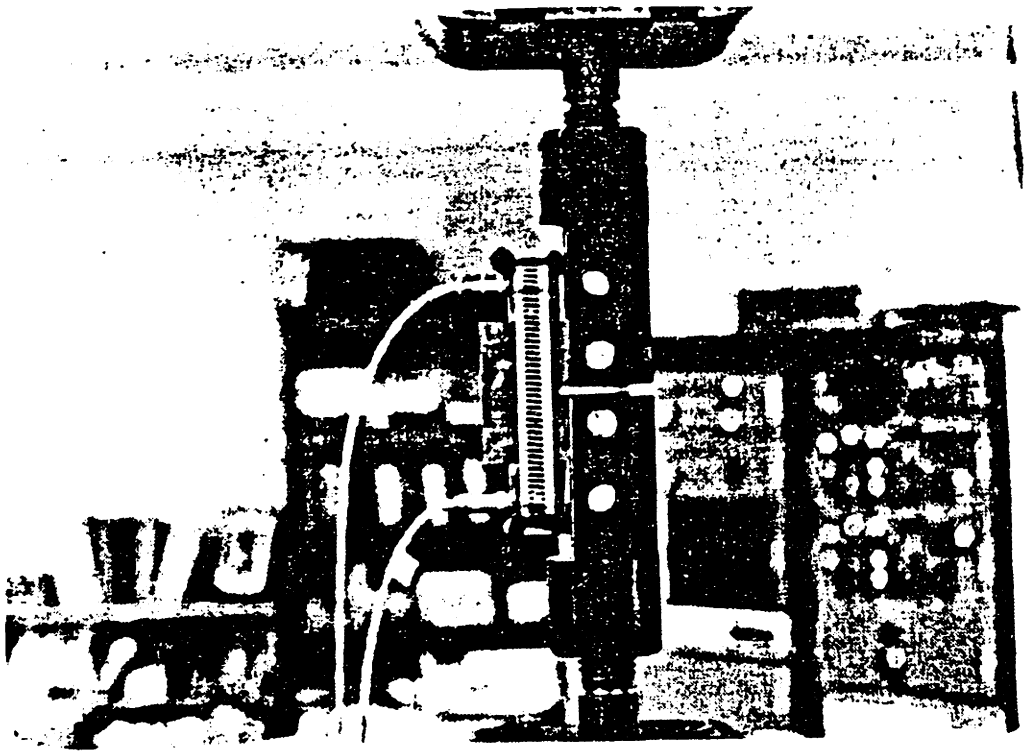

Fig. E-1 Photograph of specimen mounting.

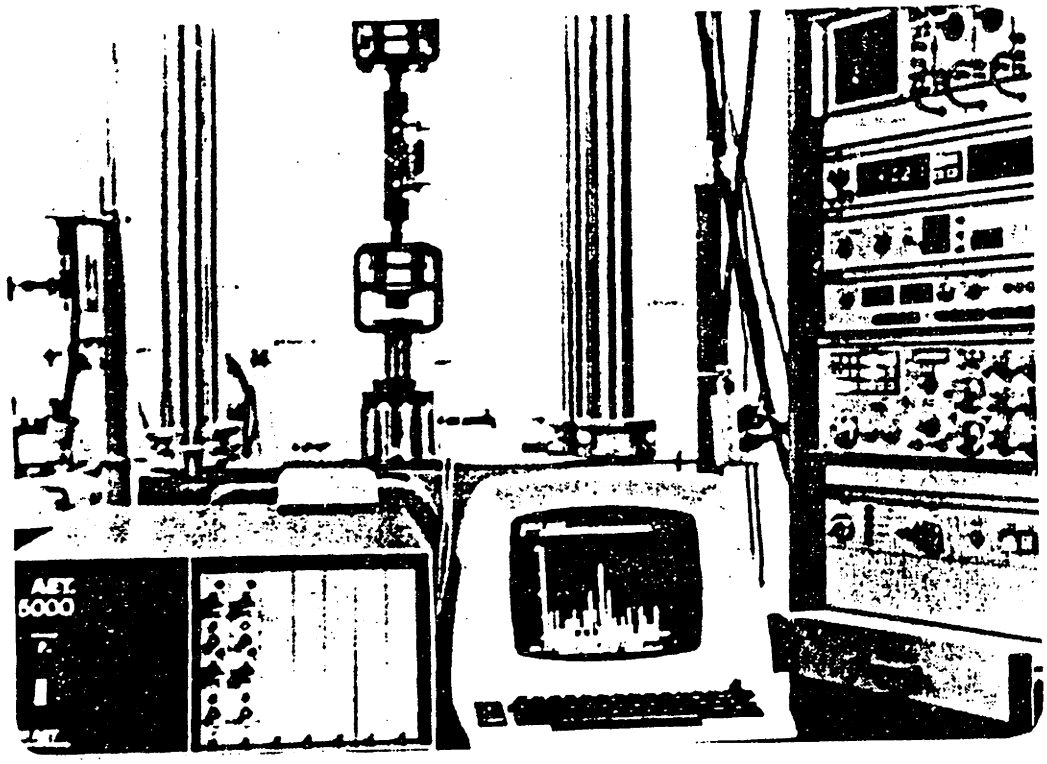

Fig. E-2 Photograph of complete testing system.

APPENDIX F

DATA REDUCTION PROCEDURE

The acoustic emission data collected from the experiments ranged from statistically too few events to quite consistent results. The major difficulty with the data was the low level of AE from the growing fatigue cracks in the specimens. This was particularly a problem at low growth rates where there may have been fewer than ten events detected during an entire experiment. Generally, though, experiments performed at high growth rates resulted in a statistically adequate number of events being detected.

The acoustic emission parameters of events, peak amplitude, ringdown counts, and slope were plotted by the AET-5000 in the form of "cumulative [parameter] versus time" for each test. Since the tests were conducted at a fixed loading frequency, the slopes of these plots were capable of being converted into "[parameter] per loading cycle" data. The parameters of peak amplitude, ringdown counts, and slope were also presented by the AET-5000 in the form of "mean [parameter] per event versus time". The average values of these plots were taken as the "mean [parameter] per event" for that particular experiment.

The low number of events detected at low crack growth rates is clearly illustrated in Fig. F-1, which shows the number of events received from different locations within an A588 specimen,

with $\dot{a} = 5.1 \times 10^{-5}$ mm/cycle, $a_o = 22.5$ mm, and $K_{max} = 49.5$ MN/m$^{3/2}$. The bottom of the specimen corresponds to the leftmost location on the abcissa, and the top of the specimen corresponds to the extreme right. The fatigue crack is located approximately at the middle. Note the absence of any significant acoustic emission activity from the cracking region of the specimen. This, combined with the fact that not more than one event was detected at any one location in the specimen, leads to the probability that no significant emission was in fact observed as the events shown are probably due to noise or electrical transients.

Fig. F-2 shows the distribution of events by location for a test in which a high growth rate was used. This specimen was made of A514, with $\dot{a} = 1.5 \times 10^{-3}$ mm/cycle, $a_o = 22.5$ mm, and $K_{max} = 71.4$ MN/m$^{3/2}$. Note the significant peak and large number of events detected from the fatigue crack location which implies that this is a valid acoustic emission test.

The data reduction problem can be illustrated by presenting typical plots of cumulative ringdown counts versus loading cycles (as representative of all cumulative [parameter] versus loading cycle plots) and mean slope per event versus loading cycle (as representative of all mean [parameter] per event versus loading cycle plots) for both a low and a high growth rate test. Figs. F-3 and F-4 illustrate these plots for an A588 specimen, with $\dot{a} = 5.1 \times 10^{-5}$ mm/cycle, $a_o = 22.5$ mm, and $K_{max} = 49.5$ MN/m$^{3/2}$.

The slope of the cumulative ringdown counts versus time curve was used to obtain ringdown counts per loading cycle; note how the slope is difficult to determine accurately due to the low number of events (2) that occurred during the entire test. The average value of the mean slope per event versus loading cycle graph is used to define the mean slope per event for a particular test condition. The presence of only one data point on Fig. F-4 demonstrates the difficulty of obtaining this information when there are few events detected during an experiment.

Figs. F-5 and F-6 illustrates cumulative ringdown counts versus loading cycle and mean slope per event versus loading cycle, respectively, for A514 with $\dot{a} = 1.5 \times 10^{-3}$ mm/cycle, $a_o = 22.5$ mm, and $K_{max} = 71.4$ MN/m$^{3/2}$. Notice the ease of determining an accurate ringdown counts per loading cycle value from the slope of the cumulative ringdown counts versus loading cycle curve in Fig. F-5. The mean slope per event versus loading cycle is also determined fairly easily from the average value of the curve presented in Fig. F-6.

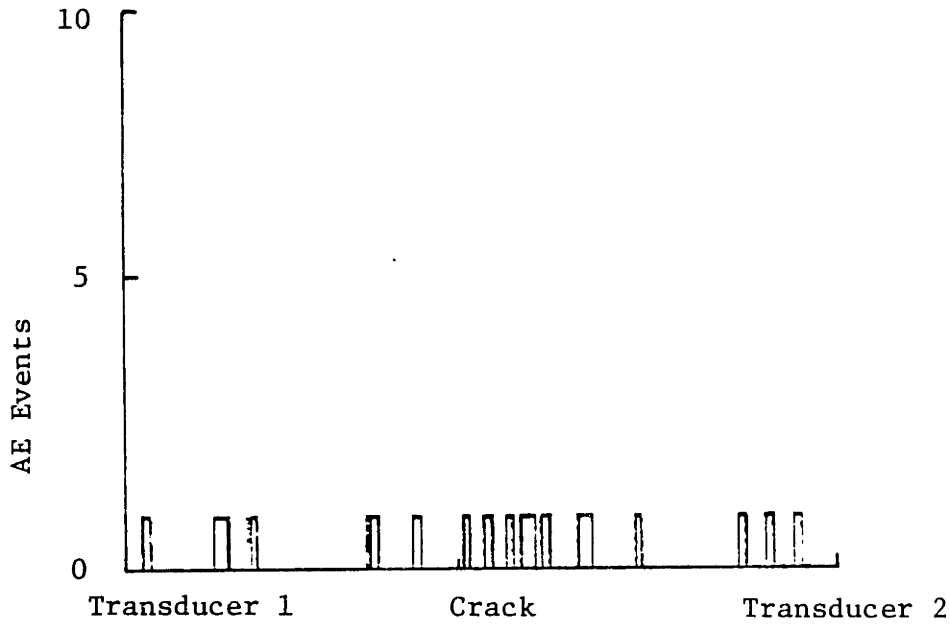

Fig. F-1 Distribution of AE events by location for A588 with crack growth rate of 5.1×10^{-5} mm/cycle, initial crack length of 22.5 mm, and maximum stress intensity factor of 49.5 $MN/m^{3/2}$.

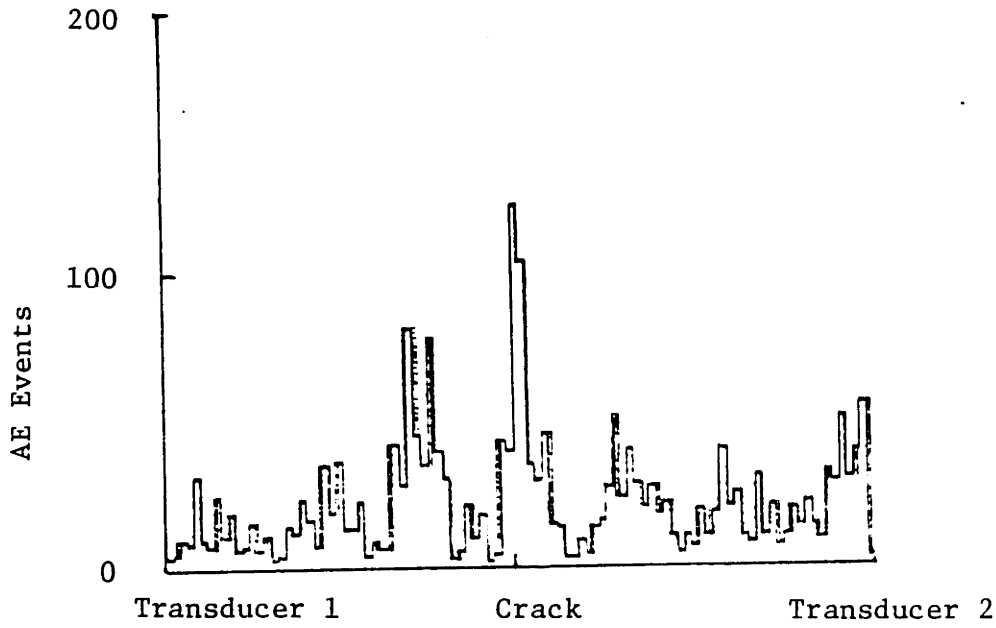

Fig. F-2 Distribution of AE events by location for A514, with crack growth rate of 1.5×10^{-3} mm/cycle, initial crack length of 22.5 mm, and maximum stress intensity factor of 71.4 $MN/m^{3/2}$.

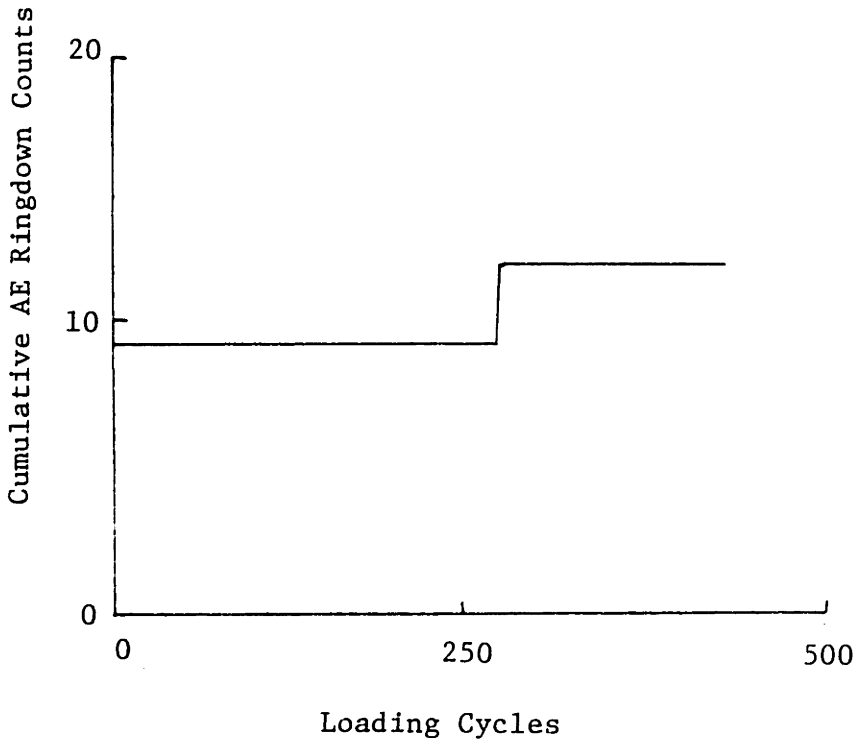

Fig. F-3 Cumulative AE ringdown counts versus loading cycles for A588 with crack growth rate of 5.1×10^{-5} mm/cycle, initial crack length of 22.5 mm, and maximum stress intensity factor of 49.5 $MN/m^{3/2}$.

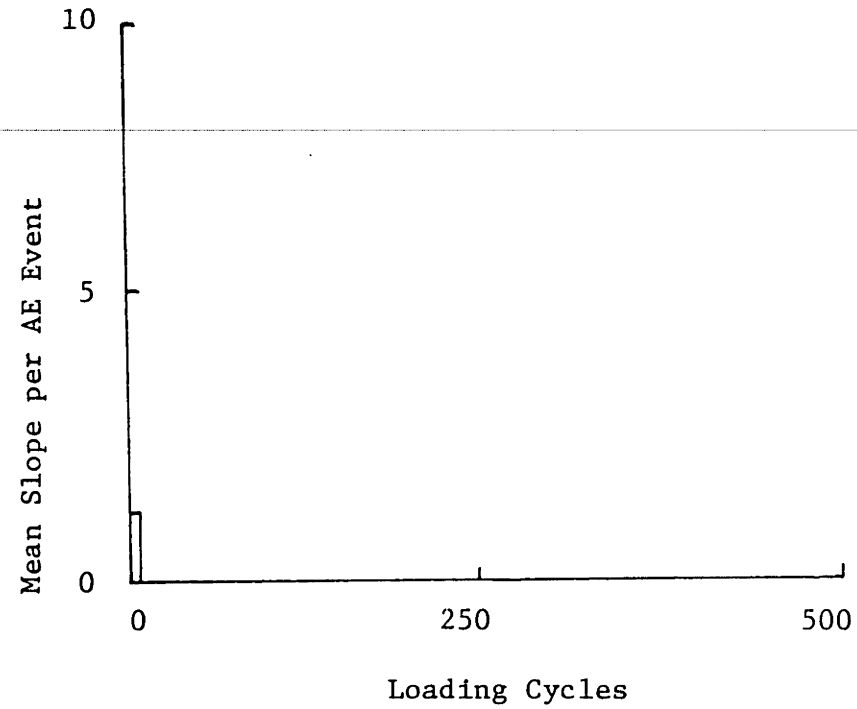

Fig. F-4 Mean slope per AE event versus loading cycles for A588 with crack growth rate of 5.1×10^{-5} mm/cycle, initial crack length of 22.5 mm, and maximum stress intensity factor of 49.5 $MN/m^{3/2}$.

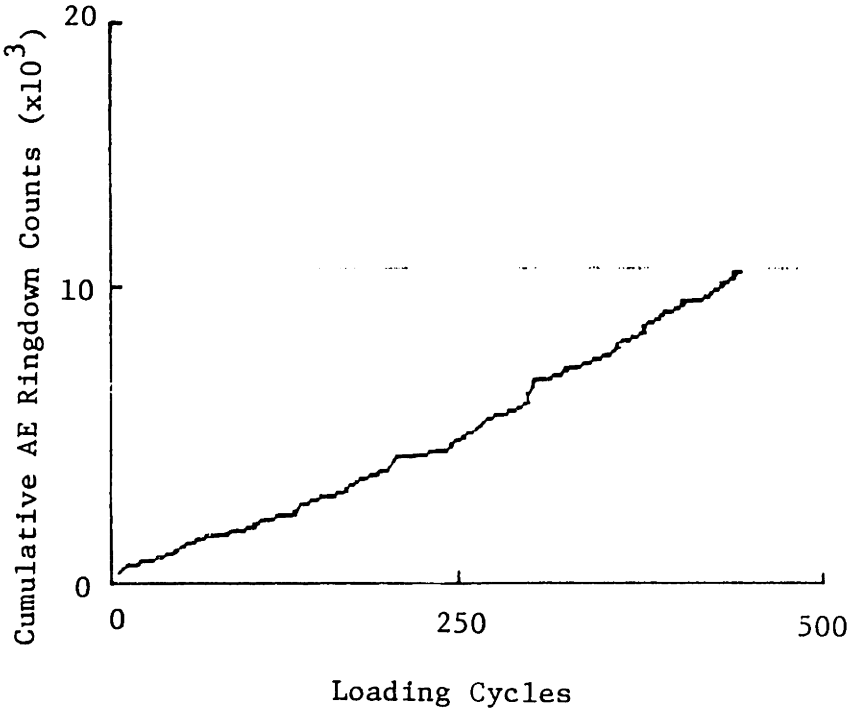

Fig. F-5 Cumulative AE ringdown counts versus loading cycles for A514 with crack growth rate of 1.5×10^{-3} mm/cycle, initial crack length of 22.5 mm, and maximum stress intensity factor of 71.4 $MN/m^{3/2}$.

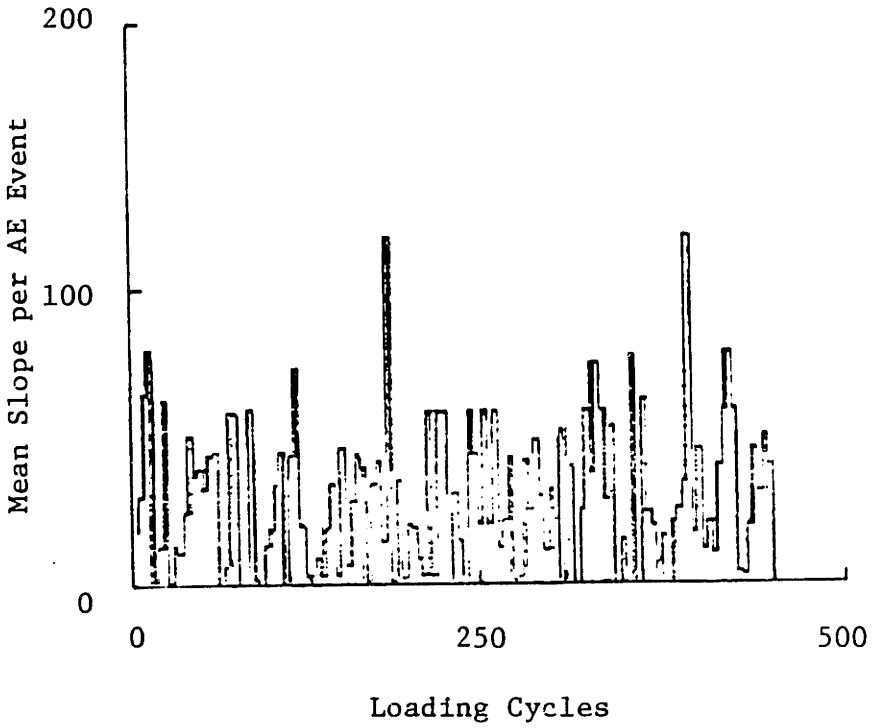

Fig. F-6 Mean slope per AE event versus loading cycles for A514 with crack growth rate of 1.5×10^{-3} mm/cycle, initial crack length of 22.5 mm, and maximum stress intensity factor of 71.4 $MN/m^{3/2}$.

APPENDIX G

INTERACTION OF PLASTIC ZONE SIZE WITH ACOUSTIC EMISSION EXPERIMENTS

A potential problem existed during the acoustic emission testing due to the use of the spatial discrimination capability of the AET-5000. Because of the proximity of the loading pin holes to the crack, a relatively small "region of acceptance" had to be set in the acoustic emission system to eliminate potential pin noise. The region of acceptance was about 10% of the specimen length, or about 6 mm wide. Plastic zone sizes for each material at the different K_{max} values are shown in Table G-1 for plane stress and plane strain. These were computed using the equations [18]:

$$r_p = \frac{1}{2\pi}\left(\frac{K_{max}}{Y}\right)^2 \quad \text{for plane stress} \tag{G1}$$

$$r_p = \frac{1}{6\pi}\left(\frac{K_{max}}{Y}\right)^2 \quad \text{for plane strain} \tag{G2}$$

where:

r_p = plastic zone size

K_{max} = maximum stress intensity factor

Y = yield strength

Fig. G-1 illustrates a possible situation in which the plastic zone of the growing fatigue crack extends beyond the region of

acceptance. This might result in a loss of AE data if, in fact, acoustic emission is due to either the elastic-plastic boundary or the volume of the growing plastic zone.

The issue arises as to whether the specimens are subjected to plane stress or plain strain conditions. One criterion that can be used is to evaluate the ratio of plastic zone size to the specimen thickness. If this ratio is on the order of unity, plane stress predominates. If the ratio is below about 0.025, plane strain predominates [17]. Since the specimen thickness was equal to 12.7 mm, it is apparent from examining Table G-1 that almost all tests were conducted in a condition somewhere between plane stress and plane strain.

Using a plastic zone size that is an approximate average of the plane stress and plane strain values suggests that the plastic zone extended beyond the region of acceptance for several tests. This introduces some question as to the validity of the AE data that were obtained in those cases.

TABLE G-1 Plastic Zone Size.

Material	K_{max} ($MN/m^{3/2}$)	Plastic zone size, r_p (mm)	
		Plane stress	Plane strain
A36	49.5	6.3	2.1
	60.4	9.4	3.1
	71.4	13.2	4.4
A514	49.5	0.8	0.3
	60.4	1.2	0.4
	71.4	1.7	0.5
A588	49.5	3.3	1.1
	60.4	4.9	1.6
	71.4	6.8	2.3

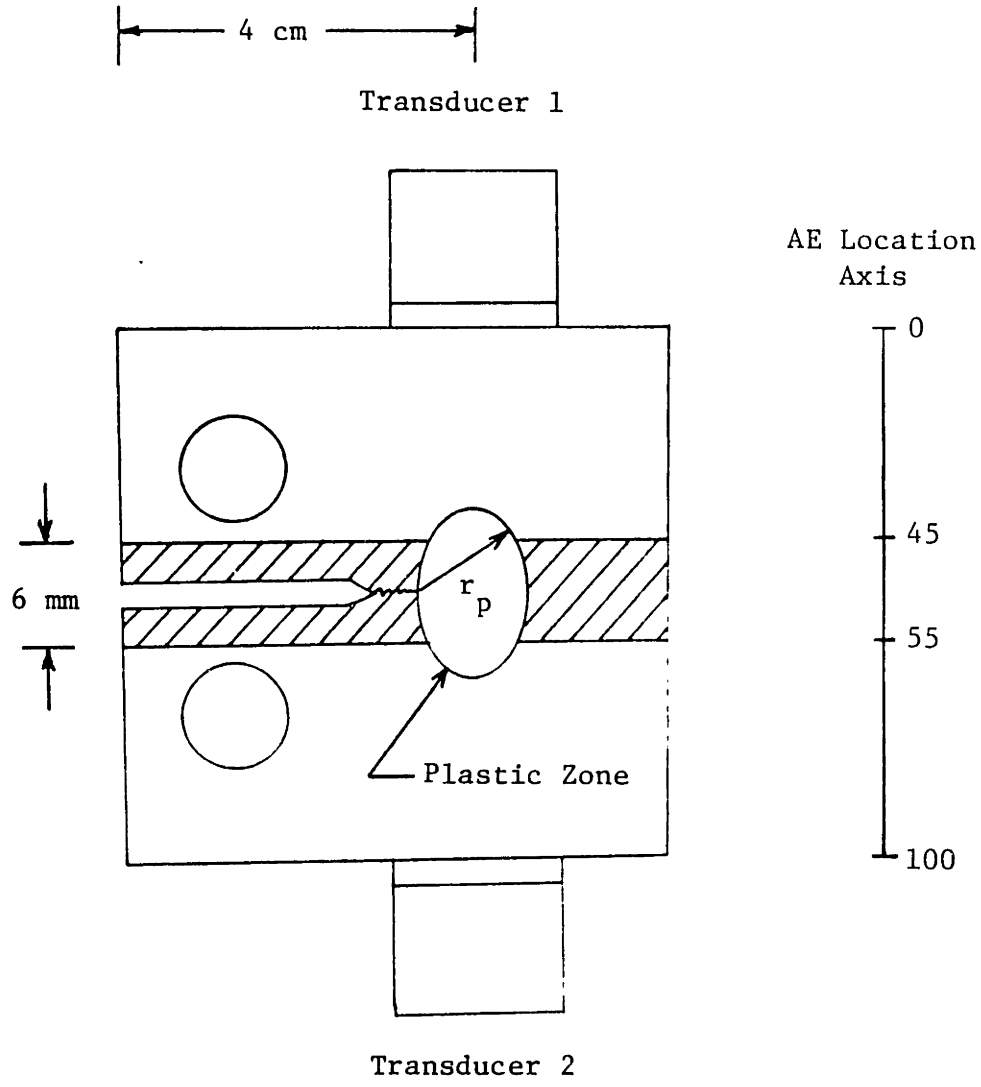

Fig. G-1 Schematic of region of acceptance, crack-tip plastic zone and location of AE transducers.

APPENDIX H

PROCEDURE TO FIT PROPOSED EQUATIONS TO OBSERVED DATA

The proposed equation is of the form

$$\dot{N} \alpha \dot{a}^n \tag{H1}$$

where

$\dot{N}$ = ringdown counts per loading cycle

$\dot{a}$ = crack growth rate

$n = f(K_{max}, a_o, Y)$

K_{max} = maximum stress intensity factor

a_o = initial crack length

Y = material yield strength

For simplicity, the exponent n is assumed to be a linear function of K_{max}, a_o, and Y. Thus,

$$n = C_1 K_{max} + C_2 a_o + C_3 Y + C_4 \tag{H2}$$

where C_1, C_2, C_3, and C_4 are constants. Note that the value of n is known for each loading condition from a plot of $\dot{N}$ versus $\dot{a}$ for that set of loading parameters.

An approximate value for the constant C_1 was determined by plotting the known value of n versus K_{max} for all values of a_o and Y, as shown in Fig. H-1. C_1 was set equal to the slope, determined

by linear regression, of this plot. Similarly, C_2 was taken as the slope of the n versus a_o graph, for all K_{max} and Y, as shown in Fig. H-2. Then C_3 was obtained from the slope of the n versus Y plot, for all K_{max} and a_o, as illustrated in Fig. H-3. Thus, C_4 remains as the only undetermined constant in eqn. (H2).

C_4 is determined by substituting known values of n into eqn. (H2) for all the different loading conditions. These values of C_4 obtained are then averaged. This average becomes the value of C_4 used in the equation.

A proposed equation of the form

$$\dot{N}\alpha\dot{a}^{C_1 K_{max} + C_2 a_o + C_3 Y + C_4} \tag{H3}$$

is therefore obtained, with the values for the constants given in Table H-1. Experimental values for maximum stress intensity factor, initial crack length, and yield strength can be substituted into this equation to predict the effect of crack growth rate on the number of ringdown counts per loading cycle. Further, by using the fracture mechanics relationship, $\dot{a}\alpha\Delta K^P$ [17], eqn. (H3) can be put into the form

$$\dot{N}\alpha\,\Delta K^{P^{(C_1 K_{max} + C_2 a_o + C_3 Y + C_4)}} \tag{H4}$$

where P is an empirical material dependent constant.

A similar analysis can be performed for a single material

(constant yield strength) by assuming an equation of the form

$$\dot{N}\alpha\dot{a}^{C_1 K_{max} + C_2 a_o + C_3} \tag{H5}$$

C_1 is the clope of the known n versus K_{max} for all values of a_o, as shown in Fig. H-4. C_2 is taken as the slope of the known n versus a_o (for all K_{max}) curve, illustrated in Fig. H-5. C_3 is determined by substituting known values of n into the equation

$$n = C_1 K_{max} + C_2 a_o + C_3 \tag{H6}$$

for all different loading conditions. The values of C_3 obtained are then averaged. This average becomes the value of C_3 used in the proposed equation. Values for the constants obtained from the A588 data are given in Table H-2.

As before, this equation can be rewritten in the form

$$\dot{N}\alpha\,\Delta K^{P\,(C_1 K_{max} + C_2 a_o + C_3)} \tag{H7}$$

using the fracture mechanics relationship: $\dot{a}\alpha\,\Delta K^P$ [17].

TABLE H-1 Values of Constants C_1, C_2, C_3, and C_4 for all Steel Types.

Constant	Value
C_1	-.058
C_2	-.092
C_3	-.0009
C_4	7.874

TABLE H-2 Values of Constants C_1, C_2, and C_3 for A588.

Constant	Value
C_1	-.084
C_2	-.214
C_3	12.640

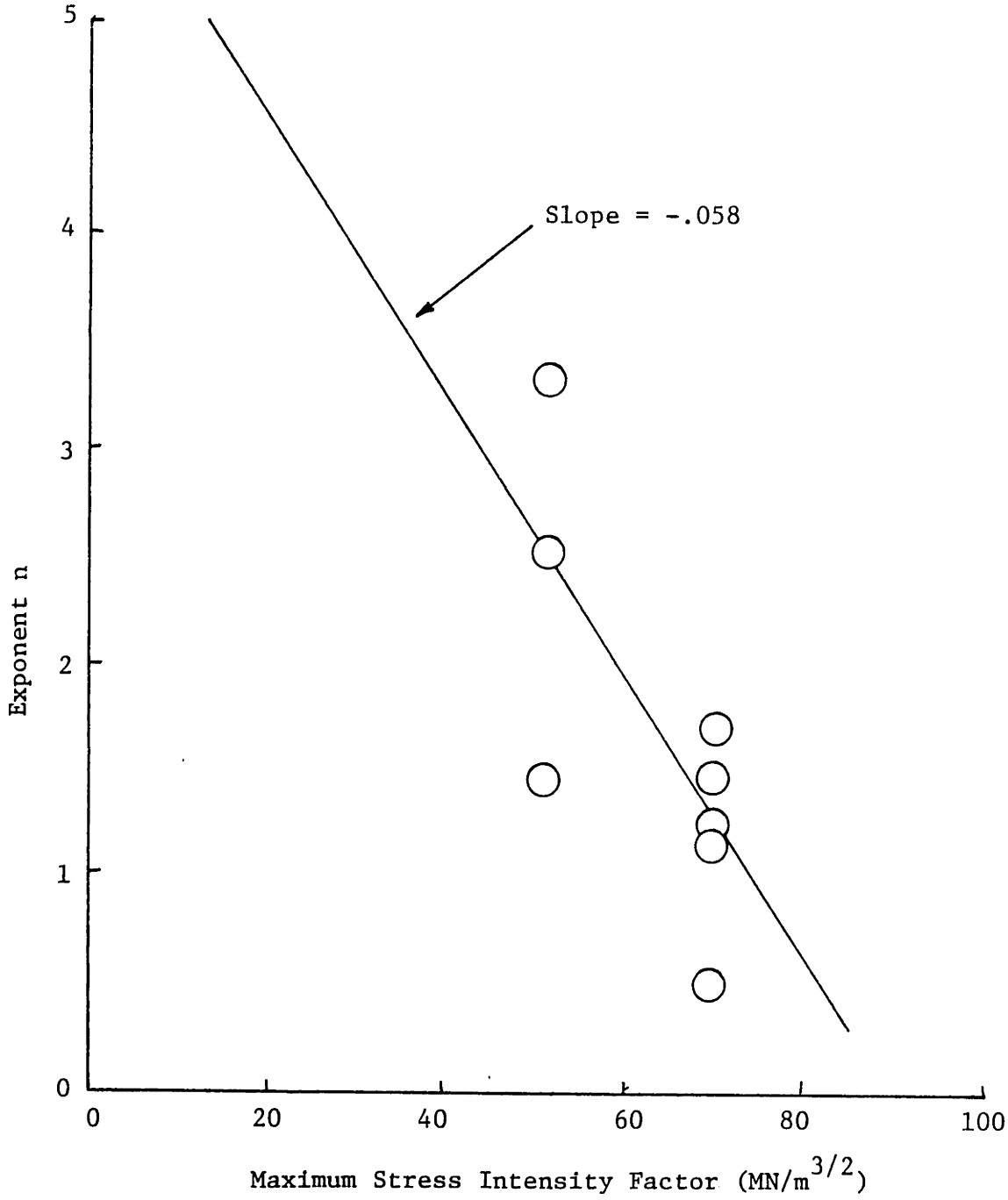

Fig. H-1 Exponent n versus maximum stress intensity factor for all materials.

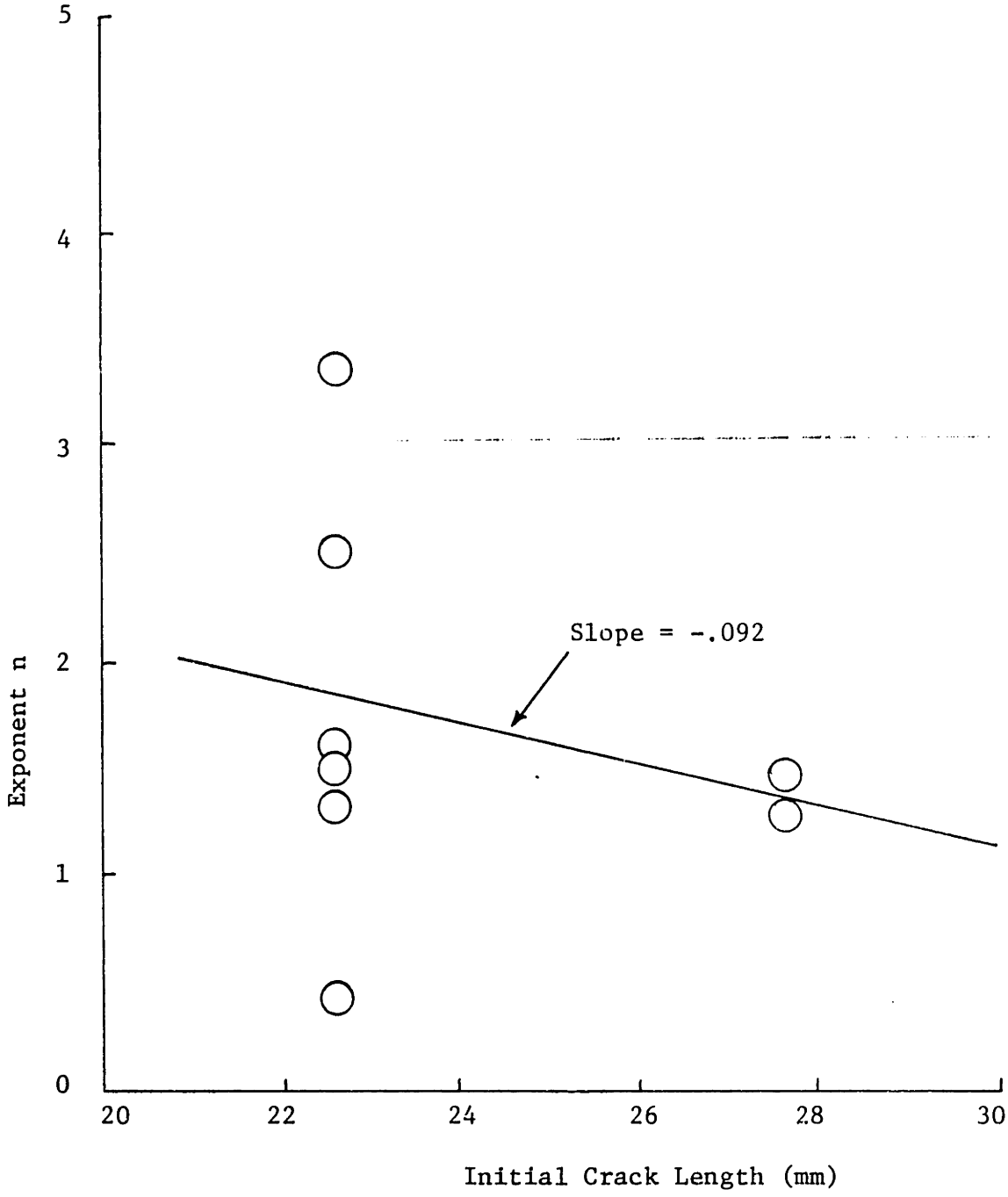

Fig. H-2 Exponent n versus initial crack length for all materials.

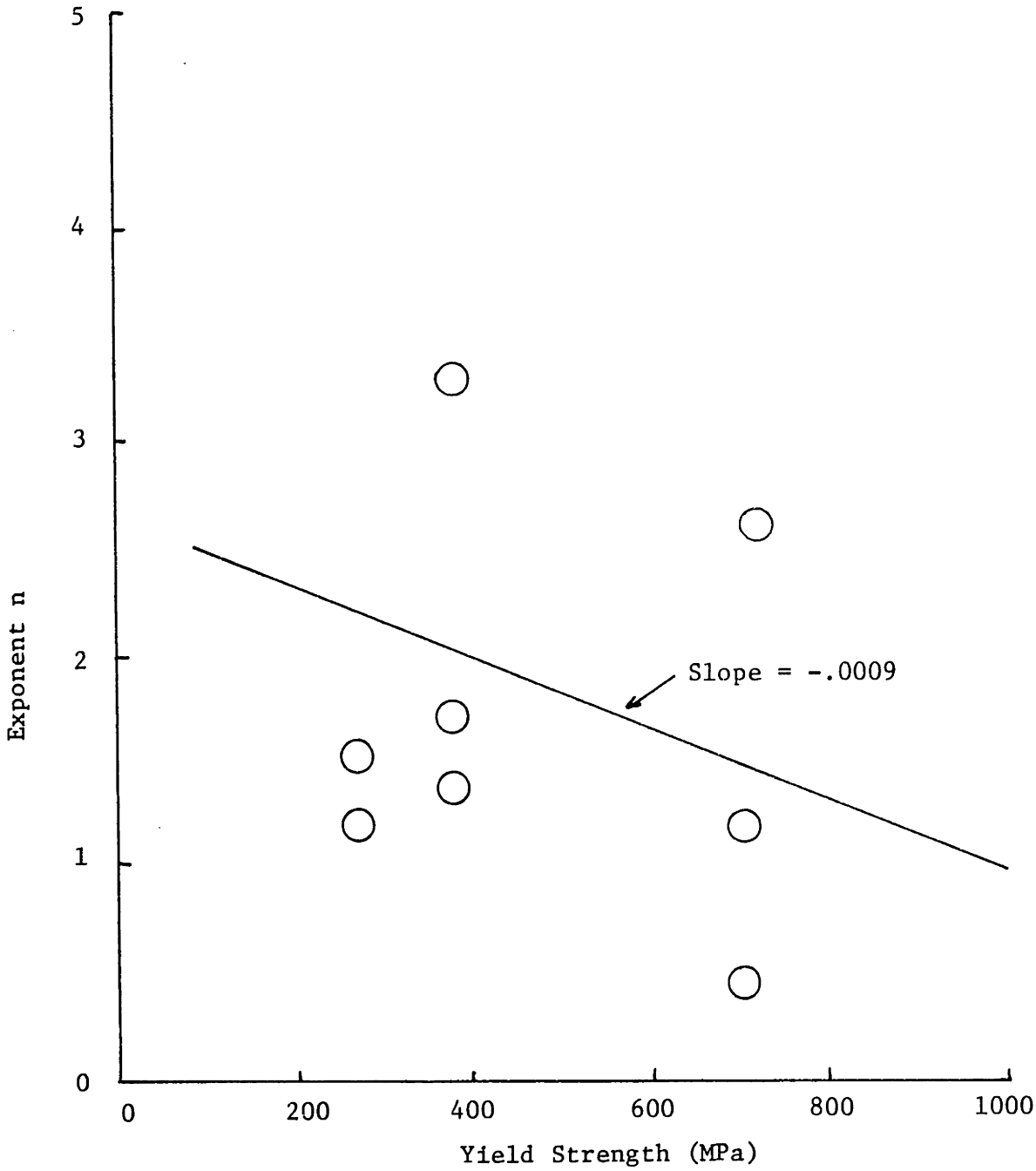

Fig. H-3 Exponent n versus yield strength for all steel types.

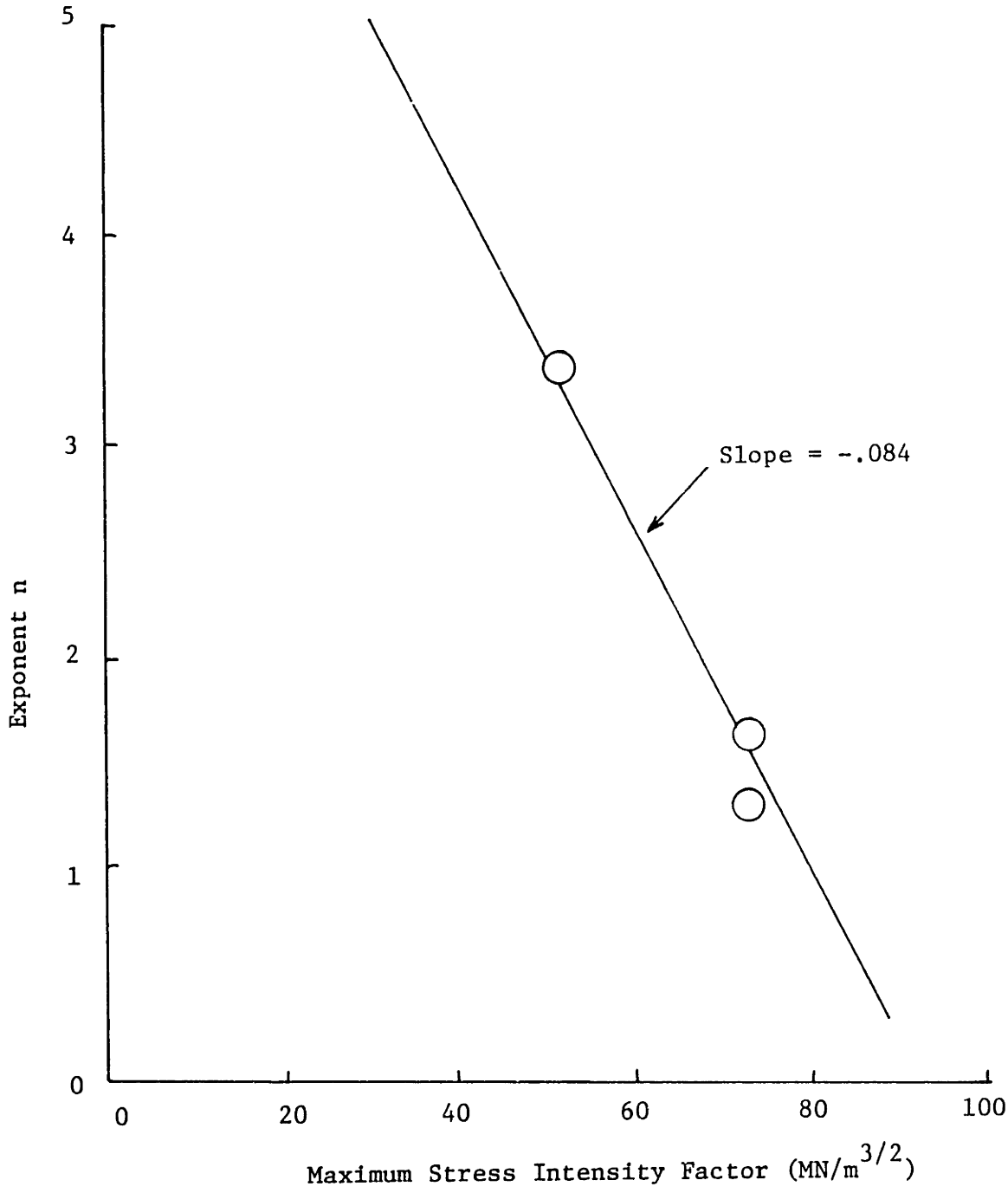

Fig. H-4 Exponent n versus maximum stress intensity factor for A588.

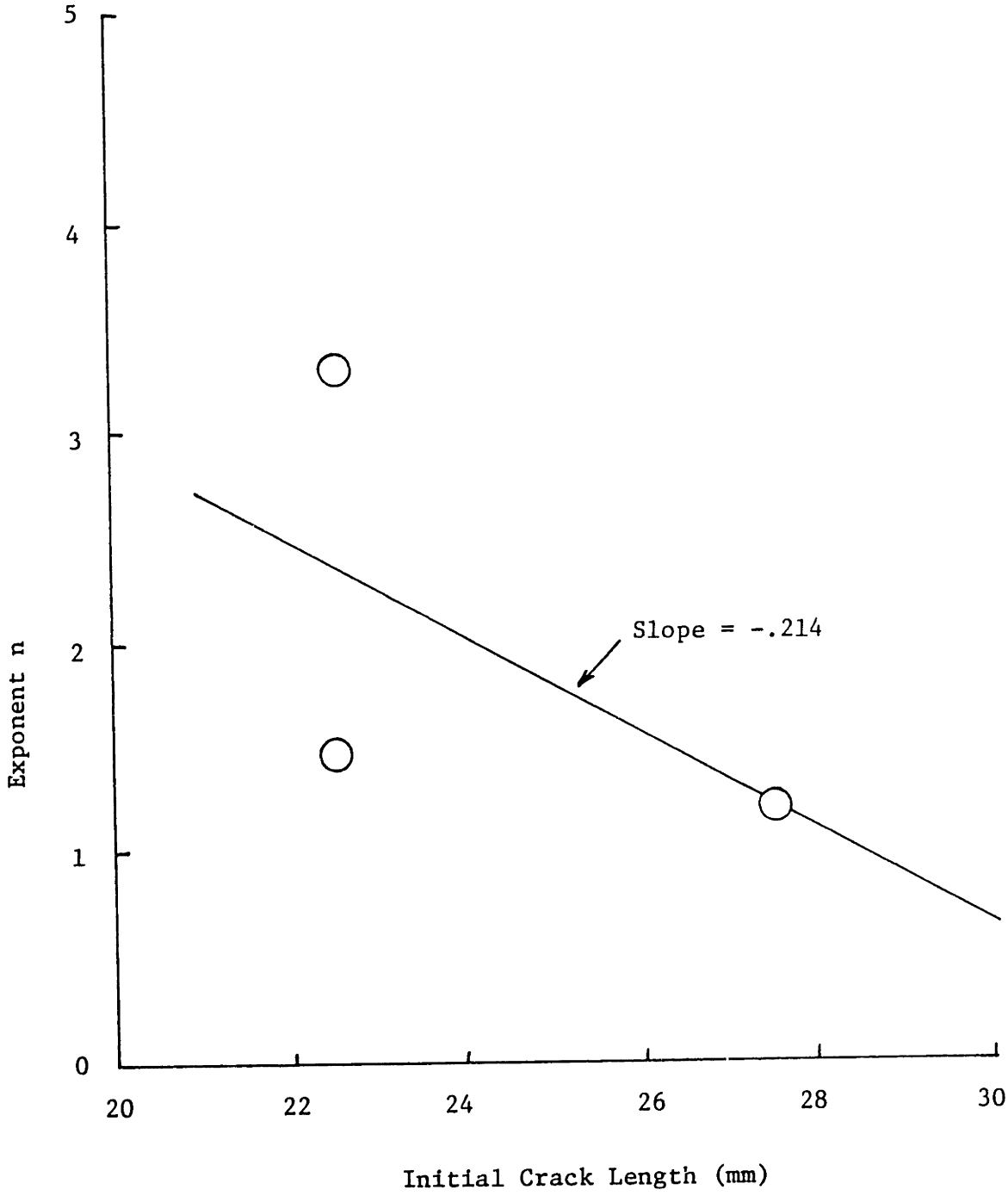

Fig. H-5 Exponent n versus initial crack length for A588.